2007-03

# Through-the-wall imaging from electromagnetic scattered field measurements

Kim, Jerry.

Monterey California. Naval Postgraduate School

# NAVAL POSTGRADUATE SCHOOL
## Monterey, California


# THESIS

**THROUGH-THE-WALL IMAGING FROM ELECTROMAGNETIC SCATTERED FIELD MEASUREMENTS**

by

Jerry Kim

March 2007

| | |
|---|---|
| Thesis Advisor: | Brett Borden |
| Second Reader: | Gamani Karunisiri |

THIS PAGE INTENTIONALLY LEFT BLANK

# REPORT DOCUMENTATION PAGE

Form Approved OMB No. 0704-0188



| 1. AGENCY USE ONLY (*Leave blank*) | 2. REPORT DATE | 3. REPORT TYPE AND DATES COVERED |
|---|---|---|
| | March 2007 | Master's Thesis |

4. TITLE AND SUBTITLE
Through-the-Wall Imaging from Electromagnetic Scattered Field Measurements

5. FUNDING NUMBERS

6. AUTHORS Kim, Jerry

7. PERFORMING ORGANIZATION NAME(S) AND ADDRESS(ES)
Naval Postgraduate School
Monterey CA 93943-5000

8. PERFORMING ORGANIZATION REPORT NUMBER

9. SPONSORING/MONITORING AGENCY NAME(S) AND ADDRESS(ES)

10. SPONSORING/MONITORING AGENCY REPORT NUMBER

11. SUPPLEMENTARY NOTES The views expressed in this thesis are those of the author and do not reflect the official policy or position of the Department of Defense or the U.S. Government.

12a. DISTRIBUTION/AVAILABILITY STATEMENT
Approved for public release; distribution is unlimited.

12b. DISTRIBUTION CODE

13. ABSTRACT(*maximum 200 words*)

We investigate an inverse imaging problem for TWI (Through-the-wall Imaging) using frequencies between 500 GHz and 1 THz. Starting from first principles, this thesis uses Maxwells equations to develop a model for the transmission Greens function. This simplified model is then used in a Lippman-Schwinger integral equation to predict the scattered field associated with interrogating THz waves. We investigate the effects of wave propagation through isotropic media, and present methods for creating images from the scattered field. These methods are examined using simulated data.

14. SUBJECT TERMS Inverse Problem, Terahertz, Imaging, Singlular Value Decomposition

15. NUMBER OF PAGES 125

16. PRICE CODE

| 17. SECURITY CLASSIFICATION OF REPORT | 18. SECURITY CLASSIFICATION OF THIS PAGE | 19. SECURITY CLASSIFICATION OF ABSTRACT | 20. LIMITATION OF ABSTRACT |
|---|---|---|---|
| Unclassified | Unclassified | Unclassified | UL |

NSN 7540-01-280-5500

Standard Form 298 (Rev. 2-89)
Prescribed by ANSI Std. 239-18 298-102

THIS PAGE INTENTIONALLY LEFT BLANK

**Approved for public release; distribution is unlimited**

# THROUGH-THE-WALL IMAGING FROM ELECTROMAGNETIC SCATTERED FIELD MEASUREMENTS

Jerry Kim
Lieutenant, United States Navy
Bachelor of Science in Mathematics, US Naval Academy 2000

Submitted in partial fulfillment of the
requirements for the degree of

**MASTER OF SCIENCE IN PHYSICS**

from the

**NAVAL POSTGRADUATE SCHOOL**
**March 2007**

Author: Jerry Kim

Approved by: Brett Borden
Thesis Advisor

Gamani Karunasiri
Co-Advisor

James Luscombe
Chairman, Department of Physics

THIS PAGE INTENTIONALLY LEFT BLANK

# ABSTRACT

We investigate an inverse imaging problem for TWI (Through-the-wall Imaging) using frequencies between 500 GHz and 1 THz. Starting from first principles, this thesis uses Maxwells equations to develop a model for the transmission Greens function. This simplified model is then used in a Lippman-Schwinger integral equation to predict the scattered field associated with interrogating THz waves. We investigate the effects of wave propagation through isotropic media, and present methods for creating images from the scattered field. These methods are examined using simulated data.

THIS PAGE INTENTIONALLY LEFT BLANK

# DISCLAIMER

"The views expressed in this thesis are those of the author and do not reflect the official policy or position of the Department of Defense or the U.S. Government."

THIS PAGE INTENTIONALLY LEFT BLANK

# TABLE OF CONTENTS

THIS PAGE INTENTIONALLY LEFT BLANK

# LIST OF FIGURES

# LIST OF TABLES

THIS PAGE INTENTIONALLY LEFT BLANK

# ACKNOWLEDGMENTS

In this world, we all can live a chaotic life. Bearing the burden of higher education, the weight of wisdom and greater responsibility that ensues from a pursuit of understanding have been goals of many that had walked ahead of me. It is a privilege to be enlightened by the pursuit of gaining knowledge in the Physics discipline. I have been blessed, but it would not have been possible for me to be here to express the results had it not been for the support and the faithfulness of great people in my life. First, I have to give nothing but a great acknowledgement of the Creator that breathed life into me, and for providing great health and opportunities that brought me to this place. Second, my closest friend and confidant, my wife Tracy. I want to thank her for all the time she has given up so that I can spend hours pursuing this degree. The irretrievable time sacrificed and memories that could have been built were on the shelf so that I can successfully finish this degree. She has been the greatest darling to me, and has become ever more special than the paper I will be holding in my hands. The perspiration that comes and the fruits therefore, can only be used to serve and provide for a better life that can come from this. I love my wife for encouraging me through the difficult times and being there for me each day as I struggle through this work. I will not be here if it weren't for her.

I also want to thank Professor Brett Borden who provided me the support and encouragement needed when I was lacking the motivation or the confidence to finish up this daunting task. Many sleepless nights were spent in pensive writing and reading as my time here encroached quickly to its finale. Prof Borden has given me the tools to fulfill this task and has become a close mentor for this field. I have been quite touched by his willingness to share and encourage my misgivings and challenges as I made my way through this thesis. The mechanism for which this thesis was completed was by no means trivial–He was able to bridge a gap of knowledge and provide a direction that is both conceivable and rewarding. I have much to thank him

and his many insights to the physical world. He has been an instrumental person who contributed in developing a passion in me to seek a deeper and more perspicacious intuition of the physical world and solving problems. I know I must have frustrated him tremendously with lots of editing work and reading. I hope that I have not worn him out but that more aspiring students would follow, and I am very grateful for his prompt and clairvoyant responses to my work. I have learned the values of living as an erudite, and its importance in the marriage with the military profession.

Professor Margaret Cheney has been great in shedding light to a difficult problem. From the short discussion I had with her and the interim correspondence on email, I cannot thank her enough for providing me critical ideas and working with me on an outline that made the forging of this thesis possible. I am greatly indebted to her and am thankful for her time and assistance. She has indeed provided a way for me to safely get through the difficulty of the problem, and perhaps, even leading to the final conclusion of my thesis.

I want to thank Professor Gamani Karunasiri for making the infusion of theory set forth in this thesis with real life application. I will not have been able to go as far as I did without his support and his interests in helping me to succeed. His concern for his students, his passion for his work, and his thorough understanding of solid state physics coupled with his broad theoretical background have been an instrumental part of my understanding in physics. He has been a great mentor. His concern for my work led me to get networked with researchers in the field that are directly involved with this thesis. It is my hope that perhaps some of the work done in this thesis would contribute to further the experiments currently being conducted at the Argonne National Laboratory or others who are working on this technology.

I want to thank Professor Scott Davis who spent much time with me in close sessions in aiding me understand difficult concepts.

I also want to thank Professor Don Walters for guiding me and giving me profound insights to my problems. He has been a great encourager and have motivated

me in my research in this field. He provided great references of which I am greatly indebted to in writing this daunting thesis. His willingness and his open door policy has allowed me to ask hard questions and gave me insights to my problems that I may have never thought about, had it not been for the discussions we had – such things may include writing codes and attacking the problem from a certain perspective.

I want to thank Professor James Luscombe for sharing with me the pain and shedding light to some parts of my thesis. I appreciate all his efforts and his sincerest interest in my project. Thank you for providing me some thoughts and ideas and even teaching me some methods which I had never thought about. I would not have gotten the deep physical understanding of the branch integral, had he not done some work with me in this area. He has been more than helpful in my own physical understanding of this problem, and I am want to express my deepest thanks.

I want to thank the professors from the math departments that helped me with great earnesty. I would like to thank Professor Clyde Scandrett, who took his time to help me understand some difficult concepts in mathematics. His lucid ability to see through the math and having a practical application to my problem has been more than rewarding and insightful. His clear cut understanding and being able to explain very high level tools in mathematics to a layman like myself paid great dividends into my ability to explore the theory. His encouragement and willingness to listen through my frustration has been much welcoming. I am thankful for his time.

I would also like to thank Professor Chris Frenzen who shared with me some ideas and assistance in providing guidance, shedding light to my problem and giving me a new perspective to looking at problems in complex theory. I also wish to thank Professor Don Danielson who inspired me to get involved in the theory of Green's function early in my NPS career while taking his course. His recommendations have been very welcoming and quite insightful to my understanding of the higher level mathematics.

I want to thank Sami Gopalsami at ANL who sponsored me and gave me

a tour of his lab. I want to thank Tom Elmer, his lab assistant who showed me the equipment for radar imaging. I also want to thank Prof Xi-Cheng Zhang from Rensselaer Polytechnic Institute who so kindly accepted me and gave me full privileges to his lab and his staff. Their hospitality have been very heart-warming, and their receptiveness to my questions and concerns have been earnest and prompt. I send my deepest gratitude for taking me into their labs and exposing me to their front and leading edge technology.

I want to thank all the faculty of the Physics Department who have been nothing but professional to me. I have learned quite a bit, and I am deeply grateful for the experiences that I had with them. Some have been trying and some have been quite joyful, but in the end, the education here has truly been first class, and I applaud to all who have diligently worked to make that happen.

It is said that some of the greatest ideas a person gets come from your friends. I want to thank my officemates Armando Lucrecio, Zak Cole, and Lars Lone who were so patient with me and sat through hours of my complaints. But you guys gave me some of the most insightful comments that shed light to my problem. I am greatly indebted to their encouragement and support. Zak, I want to say keep pushing on those codes. I am sure it will work. And thanks for making the whole experience down there in the dungeon a pleasant one. It sure feels that way with all those fluorescent lighting with some glimpses of sun light. It is amazing how we are still sane. I appreciate your support and encouragement! I will see you out in the fleet.

Armando, keep the walk, and enough of all that digital processing already. I think I am just about done with MATLAB. Can I go back to some good old paper and pencil now? Thanks for all your help and encouragement. I would like to help you with all that Simulink stuff, but sorry I won't help you on that anymore. Find Eric. He seems to know everything. I appreciate the time and effort that you helped me in getting all my powerpoint stuff onto Key Note. That was key! Thanks for the

friendship.

Lars, you are probably off to your great Department Head tour by now, perhaps on your way to becoming the next CNO. Thanks for showing me how to use some MATLAB, and by the way, you are right, the reference book you gave me on MATLAB is great! So great, I am leaving it here in the office for others to get blessed. And thanks for giving me all the books that were your bane of existence. I always like to solve difficult problems....(well, at least the solvable ones anyways).

THIS PAGE INTENTIONALLY LEFT BLANK

# I. INTRODUCTION

> Far better an approximate answer to the right question, which is often vague, than an exact answer to the wrong question, which can always be made precise. *John W. Tukey, 1962*

X-ray computed tomography (CT) was created in the late 1960's to early 1970's. Since that time, this imaging system has come to be recognized as one of the greatest achievements in radiology[Ref. 3]. From this point in time to the present, solving inverse problems and ill-posed problems has become an exciting and significant field for research. As in reverse engineering approaches, an "inverse problem" is simply one which attempts to attain information about a "source" from available information.

Unlike a "direct problem" in which the descriptive parameters of the problem are known in advance of the solution, and the system of equations can be solved (subject to initial and boundary conditions), an inverse problem poses a special challenge because the parameters are not known up-front.

Suppose we want to measure the electromagnetic field at a given position caused by a signal $\boldsymbol{x}$, and the field data $\boldsymbol{d}$ can be written as

$$\boldsymbol{d} = \{\boldsymbol{A}\boldsymbol{x}\} \tag{I.1}$$

where $\boldsymbol{A}$ is an operator that describes the nature of the measurement system.

Now let us entertain the idea that the object $\boldsymbol{x} \in \mathbf{R^n}$ is mapped into the data space $\boldsymbol{d} \in \mathbf{R^m}$ via the operator $\boldsymbol{A}$ which would be a mapping of the object from the Hilbert space $\mathbf{X}$ into another Hilbert space $\mathbf{Y}$. This problem is considered well-posed if it meets the conditions in Table I:

Conditions 1 and 2 tell us that $\boldsymbol{A}$ is injective and spans all of $\mathbf{Y}$. The requirement of condition 3 is a necessary but not sufficient condition for the stability of the solution. The third condition is motivated by the fact that in all applications the data will be measured quantities. If the problem is well-posed, the error propagation is

| |
|---|
| 1. A solution exists |
| 2. The solution is unique |
| 3. The inverse mapping is continuous |

Table I. Conditions for well-posed problems

controlled by the condition number. For example, if there are $n$ variables, there must be $n$ independent equations [Ref. 30] in order to obtain a solution. Therefore the mapping of $n$ variables by the system of equations to the data space can be written as $\boldsymbol{A}\boldsymbol{x}_n = \boldsymbol{d}$ where $\boldsymbol{A}$ is a matrix defining the system of equations and $\boldsymbol{x}_n$ is a vector of $n$ variables. By condition 1 and 2, $A^{-1}$ exists.

Now let's say that there is a small error $\Delta d$ in the measured data. Then the corresponding uncertainty$\Delta\boldsymbol{x}_n$ for the object $\Delta\boldsymbol{x}_n$ obeys

$$\frac{||\Delta\boldsymbol{x}_n||}{||\boldsymbol{x}_n||} \leq \text{cond}(A)\frac{||\Delta\boldsymbol{d}||}{||\boldsymbol{d}||}$$

The condition number is defined as

$$\text{cond}(\boldsymbol{A}) = ||\boldsymbol{A}||\,||\boldsymbol{A}^{-1}||$$

where the norm $||\boldsymbol{A}||$ is

$$||\boldsymbol{A}|| = \sup_{\boldsymbol{x}_n \neq 0} \frac{||\boldsymbol{A}\boldsymbol{x}_n||}{||\boldsymbol{x}_n||}$$

If cond($\boldsymbol{A}$) is not large, then the problem is considered to be well-conditioned, and the solution will be stable with respect to small variations of data. If the condition number is large, we classify the problem as ill-conditioned. The difference between ill-posed and ill-conditioned is therefore somewhat vague. Hadamard defines a problem to be ill-posed if it does not satisfy all three conditions of Table I. An ill-posed problem is one where an inverse does not exist because $\boldsymbol{d} + \Delta\boldsymbol{d}$ is outside the range of $\boldsymbol{A}$. Generally, more than one image can map into the same data, or small changes in the data can result in large changes in the image.

Most inverse problems are ill-posed. Therefore, no unique answer exists. Let us consider the Fredholm integral equation, which we will discuss in depth later in this thesis. In real-world problems, the integral has a square-integrable (Hilbert-Schmidt) kernel and is of the form:

$$\int_a^b k(x,s)f(s)ds = d(x) \qquad a \leq x \leq b$$

If $f$ has a small variation, say of the form $\Delta f = \epsilon \sin(2\pi\omega s)$, $\omega = 1, 2, 3, \ldots$, $\epsilon \in \mathbf{R}$ and is small. Then the variation of data will be

$$\Delta d(x) = \epsilon \int_a^b k(x,s) \sin(2\pi\omega s)ds$$

In Appendix A, we show that as $\omega \to \infty$ then $\Delta d \to 0$. Therefore, the ratio $\frac{\Delta f}{\Delta d}$ heads to $\infty$ as $\omega$ heads to $\infty$. This problem is ill-posed, and the example demonstrates that Fredholm integral equations can be sensitive to high-frequency variations.

Because of this behavior much research has been done in solving these types of problems, and many methods and techniques have been developed. This thesis will explore some of these techniques and create a simple electromagnetic scattering model for application to an inverse problem for high frequency imaging, appropriate to frequencies ranging from 10 GHz - 1 THz.

# A. BACKGROUND

In recent years, terahertz technology has become an exciting field. Demands for further development have increased many fold for military, security, civilian and medical applications. As solid state physicists are coming up with equipment that can provide stable terahertz radiation, and as detectors are getting more sophisticated in measuring these data, scientists and engineers are now starting to focus on the terahertz region with excitement. This is largely due to the fact that: at these frequencies, there is great material penetration capability; unlike X-rays, the radiation is non-ionizing; unlike ultrasound, you can image without contact; and penetration

depth is generally greater than near-IR radiation[Ref. 8]. The most useful region of this electromagnetic spectrum is from 0.3 to 20 THz[Ref. 16].

## B. SOME PROPERTIES IN THE GIGA-TERAHERTZ FREQUENCIES

Frequencies of terahertz (a period of 1ps) have some important properties. Most electrons in highly excited atomic Rydberg states orbit at this frequency. Collisions between gas-phase molecules at room temperature last about 1 ps. Superconducting energy gaps are found at THz frequencies. Important collective modes of proteins are known to vibrate at THz frequencies [Ref. 16]. These are just a few examples of terahertz characteristics in the physical world. This region lies above the frequency range for most electronics but below the range of optical and infrared equipment; therefore, it has been difficult to explore until recent developments in solid state technology.

However, there are limitations in propagating at terahertz frequencies because they are highly susceptible to atmospheric absorption. Only a small window within this region is practicable.

> The Terahertz Imaging Focal Plane Technology (TIFT) program at DARPA (Arlington, VA) defines the upper limit of this window to be 557 GHz.

There are also certain frequencies beyond this optimum band that can provide good propagation behavior. These windows are centered on 650GHz, 850GHz and at 1.5THz. Anything above 1.5 THz results in absorption that is currently too high to gather any meaningful data[Ref. 8].

## C. MOTIVATION

As devices provide reliable radiation at THz frequencies, there is also a need for more sophisticated scattering models. There are many models already in place for other fields such as radar, and we have had much success in extracting superb

images in SAR, X-ray tomography, sonograms, etc. If these powerful methods can be carried over to the terahertz range, it may become both a rewarding and a worthwhile goal for development in the area. Recently, *through-the-wall* high frequency imaging has become a promising new technology that addresses many civilian and military problems. Much of the practical challenges lie in the reliability of the system, its portability, and its ability to sustain an acceptable level of performance.

One of the greatest challenges in imaging at these frequencies is that the system parameters are affected by the structured ambiguities in the walls, and this can cause difficulty in measurement. One has to account for diffraction and refraction effects, but the fact that we can image with relative success has shown that this area has a promising future.

There are other factors that make terahertz radiation an attractive area for research. Waves at this frequency can penetrate non-metallic and non-polar media; moreover, explosives, chemical agents, and many different biological agents return a unique spectra. Furthermore, this radiation is safe for the operator of the device, and is harmless to the biological life that it may scan.

Until the devices that generate terahertz signals can be made portable, practical applications are still over the horizon. Academic institutions such as Rensselaer Polytechnic Institute have demonstrated the reliabliity of these sources and are currently developing a more portable system for which identification, imaging, and various real world applications can be used.

However, there are few other devices that are already in place that are small and reliable. Argonne National Laboratory (ANL) is currently investigating whether such penetration capability can be achieved at lower frequencies (in the $10 - 500$ Ghz region). Such waves would be carried through a wave guide, and the return fields are measured via a waveguide. ANL demonstrated that these waves do have great penetrating capabilities, and they are able to form images. But imaging performance at these frequencies is an open question.

Though imaging can be done, most methods take advantage of imaging via bi-static transmission where the transmitter is on one end, and the receiver on its opposite end so that the image can be done via intensity strengths of field going through the media and the object of the image. However, imaging from the back-scattered field is more of a challenge because of the problems encountered not only in the perturbation caused by the object but also the interactions that occurs through the transmission medium.

This thesis will emphasize the modeling requirements using Maxwell's equations and will develop inversion techniques for image reconstruction. We will first discuss the basic Inverse Problem. Then we will derive (from Maxwell's equations) the theory for the simple model used in this thesis; derive the Green's function for each region in space; establish the scattered field equation (perturbation of the field due to the object); discuss the various different approximations that can be done to establish the Fredholm equations for the scattered field; use the Born approximation and parametize the equations; discuss the Singular Value Decomposition and the Least Square Method; establish the problems of error due to noise and discuss regularization; and finally conduct some image reconstruction using simulated data. The final chapter will summarize the results of this thesis and provide some ideas for a more in-depth model for image reconstruction.

# D. PRELIMINARY DISCUSSION

## 1. Material Effects

For our model, we assume that the wall characteristics are known with a linear, homogeneous, and isotropic dielectric constant. There are certain ranges of Terahertz that are not very useful. For example, ranges above 5 to 15 THz frequencies have highly strong phonon absorption in virtually all crystalline materials [Ref. 11]. Innately metallic targets cause full terahertz reflection. Skin, due to the high water content, absorbs the terahertz rays, and most of the energy is dissipated in the first 100

microns [Ref. 12]. One must balance between the image object and the frequency that would provide the optimum penetration of the medium while providing the optimum reflection of the object. If we are looking for metallic material, it is an easier case because the focus would then be penetrating the medium.

## 2. Atmospheric Effects

Another important consideration is how feasible is it to transmit the electromagnetic waves at these frequencies. There will be transmission losses in the field's strength through the material and reflection of the target, but if atmospheric absorption is too strong, one may just as well abandon the idea of imaging at these frequencies. Absorption and scattering in transmission occur largely due to the interactions of many different elements in the atmosphere. However, absorption is mainly caused by oxygen and water vapor: the greatest amount of absorption occurs when the frequencies match the natural resonances of oxygen and water vapor. As the frequencies deviate away from the natural resonant frequency of the elements, "windows" (frequencies at which absorption is minimal) are created. These are the areas in which we are especially interested. The Liebe model gives us a simple view of the attenuation and dispersive affects in the atmosphere [Ref. 14]. In Figure 1, we can see that frequencies between 0.7 THz to 1 THz have some great areas where attenuation would be small enough that we can neglect absorption effects.

If we work at frequencies $\leq$ 1 terahertz (such as 0.8 THz), we have almost no dispersive delay, and our attenuation is also quite small ($< 0.10$dB/km). Because atmospheric affects determine the type of devices and the methods of gathering data, we have to first determine which frequencies would give us: (1) the least attenuation; (2) the least dispersive effects; and (3) the most stable and common atmospheric configuration. In Figure 2, we see that absorption is too high for any frequencies higher than 1 THz, and it will remain so until we get into the infrared and visible range — we will not be able to get any meaningful data in this region. Therefore, most of the research and work should be within this limit.

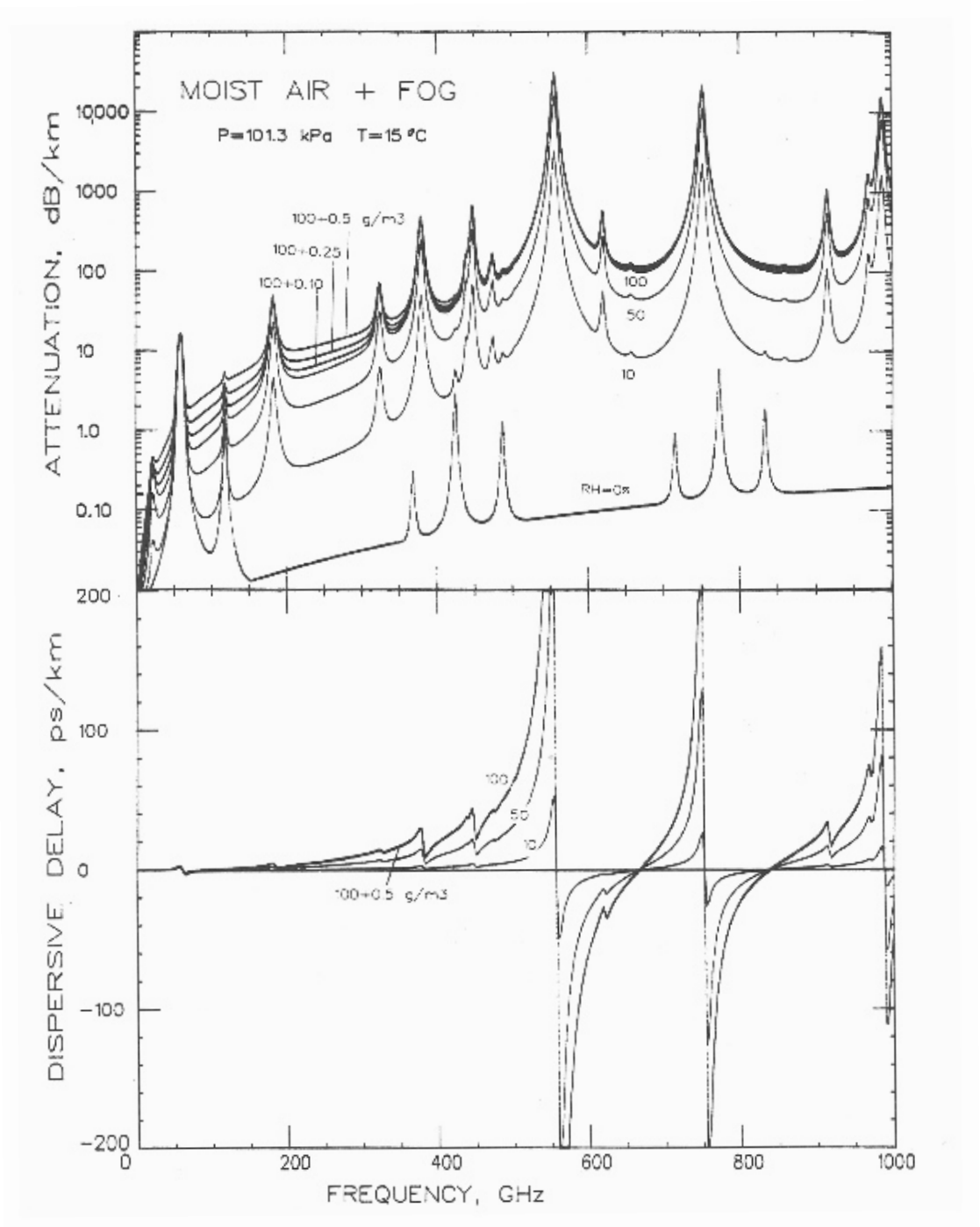


Figure 1. Attenuation $\alpha$ and delay $\beta$ rates for three fog events ($w = 0.10, 0.25, and 0.5 g/m^3$) added to a saturated air (RH=100%) sea level condition. This Figure is taken from [Ref. 14]

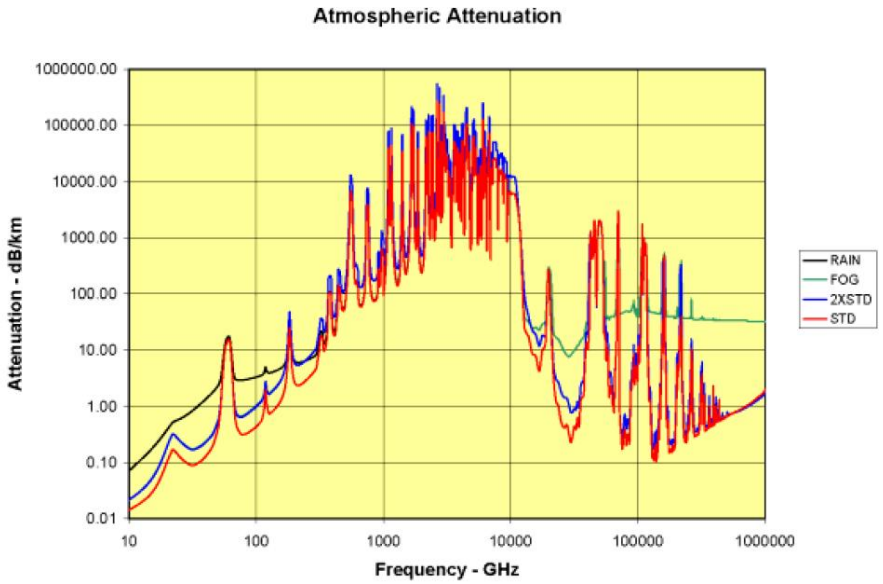


Figure 2. Atmospheric Attenuation from [Ref. 15]

## E. MODELING CRITERIA

Now that the unexplored electromagnetic spectrum is starting to become accessible, the areas of research are growing without bounds. For behind-the-wall imaging, the interest for us is to develop a model that could predict field information using the Green's function which, in turn, yields the system (PSF: Point Spread Function). The utility of having an analytical form for the PSF is that this is the kernel of the Fredholm Integral equation. Therefore, knowing the nature of the kernel which provides the mapping behavior from one Hilbert Space to the other, we can then find the source (object) of the perturbed fields. Since we can measure the fields, we can solve for the object $\boldsymbol{x}$ in equation I.1.

To solve for the PSF, we will make the following assumptions:

1. The waves are not dispersive: they each pass through the medium with speed $\frac{\mathrm{d}\omega}{\mathrm{dk}} = c$
2. The medium is linear and isotropic.
3. The medium is non-magnetic.
4. The medium is non-conductive.

Note that the last two conditions allow us to simplify Maxwell's equations. By making the transmission medium non-conductive, we allow the index of refraction to stay real and no damping will take place. This is a rather simple model, but one that can be adjusted in the future to implement this very real effect. Making the medium non-magnetic will make the slowing of the wave to be only dependent on the dielectric constant. And lastly to prevent the coupling of Maxwell's equations, we are going to make the medium linear and isotropic.

# II. THE INVERSE PROBLEM

This chapter is intended to be a basic overview of the inverse problem that this thesis will cover. We will review the basic ideas of ill-posed problems and regularization methods for forming stable approximate solutions. We will confine ourselves to linear equations with compact operators in Hilbert space. We will base our reconstruction algorithm design on the Singular Value Decomposition and the Tikhonov regularization method. There are many regularization methods for which the inverse problem for this imaging criteria could be done. The intention of this thesis would limit the scope of the most basic Tikhonov regularization method and the optimum methods for imaging would be achieved stochastically. For more in-depth discussion of ill-posed problems and different regularization techniques to enhance imaging, refer to Tikhonov and Arsenin [Ref. 26].

## A. CONCEPTS OF ILL-POSEDNESS REVISITED

In the last chapter, we saw that a well-posed problem must meet the three conditions listed in Table I. We now examine the data model equation in the form of a Fredholm integral equation:

$$\int_a^b A(x_i, s) f(s) ds = d(x_i) \quad a \leq s \leq b \quad c \leq x_1 < x_2 < \ldots < x_N \leq d$$

The interval [c,d] is partitioned into N parts for convenience to represent discrete measurements. This integral can be simplified into the following matrix problem:

$$d(x_i) = \left\{ \lim_{M \to \infty} \sum_{j=1}^{M} A(x_i, a + j\Delta s) f(a + j\Delta s) \Delta s \right\}, \quad \text{where } \Delta s = (b-a)/M \quad \text{(II.1)}$$

or

$$\boldsymbol{d} = \lim_{M \to \infty} \boldsymbol{A}\boldsymbol{f}$$

where

$$\mathbf{d} = \begin{bmatrix} d(x_1) \\ d(x_2) \\ \vdots \\ d(x_N) \end{bmatrix}, \quad \mathbf{A} = \begin{bmatrix} A(x_1, a+\Delta s) & A(x_1, a+2\Delta s) & \cdots & A(x_1, a+M\Delta s) \\ A(x_2, a+\Delta s) & A(x_2, a+2\Delta s) & \cdots & A(x_2, a+M\Delta s) \\ \vdots & \vdots & \ddots & \vdots \\ A(x_N, a+\Delta s) & A(x_N, a+2\Delta s) & \cdots & A(x_N, a+M\Delta s) \end{bmatrix} \Delta s$$

$$\mathbf{f} = \begin{bmatrix} f(a+\Delta s) \\ f(a+2\Delta s) \\ \vdots \\ f(a+M\Delta s) \end{bmatrix}$$

$\boldsymbol{A}$ will define the kernel which is to operate on $\boldsymbol{f} \in \mathbf{X}$ where $\mathbf{X}$ belongs to the Hilbert space. From the three conditions of Table I, we say that the mapping of $\boldsymbol{A}$ is therefore one-to-one and spans all of the vector space $\mathbf{Y}$. Because we are dealing with compact operators [Ref. 27], $\mathbf{Y}$ will also be a member of the Hilbert Space. This tells us that the inverse $\boldsymbol{A}^{-1}$ must be continuous and bounded. A well behaved problem requires that $\boldsymbol{f} \in \mathbf{X}$ and the data $\boldsymbol{d} \in \mathbf{Y}$ are well controlled by the norms of the vectors in $\mathbf{X}$ and $\mathbf{Y}$. But in most real life applications, we do not have this continuous inverse mapping, which suggests the contamination of the data space with elements not belonging to $\boldsymbol{A}(\mathbf{X}) \subset \mathbf{Y}$. This results in the instability of the solution for $\boldsymbol{f}$ which, as discussed in the previous chapter, is caused by the condition number. Colton [Ref. 27] proves that $\boldsymbol{Af} = \boldsymbol{d}$ is improperly posed if $\boldsymbol{f} \in \mathbf{X}$ is not of finite dimension. In everything we encounter in the real world, $\boldsymbol{f}$ is infinite in dimension, and therefore, ill-posedness of the equation II.1 is unavoidable.

Straightforward solutions of ill-posed problems often result in non-physical answers. For this reason, one must be very careful in the discretization of equation II.1. One may think that making the operator $\boldsymbol{A}$ more refined would make the solution more reliable, but the opposite is true [Ref. 27]. Therefore, techniques must be introduced to construct stable solutions.

## B. METHOD OF LEAST SQUARES

A standard technique in mathematical and statistical modeling is to find a "least squares" curve fit to a set of data points. This technique was first developed independently by Carl Friedrich Gauss and A. M. Legendre. Whenever we measure data, we are going to get errors in measurements or inaccuracies. Therefore, we cannot expect the curve to perfectly fit through all the data points. Instead we want the best approximation in the sense that the sum of squares of the range between the data point and its corresponding curve is minimized. A least squares problem is generally formulated for overdetermined systems. For example, suppose $\boldsymbol{x} \in \mathbb{R}^n$ and $\boldsymbol{b} \in \mathbb{R}^m$ are related by the system of equations $\boldsymbol{b} = \boldsymbol{H}\boldsymbol{x}$. In general, we may or may not find a vector $\boldsymbol{x} \in \mathbb{R}^n$ to find $\boldsymbol{b} \in \mathbb{R}^m$. We can, however, find a vector $\boldsymbol{x}'$ whose transformation by $\boldsymbol{H}$ would result in the minimum distance between $\boldsymbol{b}$ and $\boldsymbol{H}\boldsymbol{x}'$.

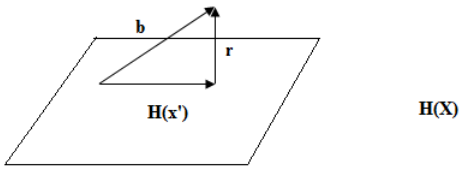


Figure 3. $\boldsymbol{b} \in \mathbb{R}^m$ while $\boldsymbol{x}' \in \boldsymbol{X}$ and $\boldsymbol{X} \equiv \mathbb{R}^n$

We form the residual:

$$\boldsymbol{r} = \boldsymbol{b} - \boldsymbol{H}\boldsymbol{x}'$$

and we minimize the distance

$$||\boldsymbol{r}|| = ||\boldsymbol{b} - \boldsymbol{H}\boldsymbol{x}'||$$

From the geometry, we see that the minimum distance between $\boldsymbol{b}$ and $\boldsymbol{H}\boldsymbol{x}'$ has to be orthogonal to the plane. It can be shown by using Pythagorean Law that this will result in the least squares solution [Ref. 7]. From Figure 3, one can see that $\boldsymbol{H}\boldsymbol{x}'$ is

the projection of $\boldsymbol{b}$ onto the $\boldsymbol{H}(\boldsymbol{X})$. Due to orthogonality, $\boldsymbol{r}$ must lie in the nullspace of $\boldsymbol{H}$, where a null space is defined as the set of all vectors $\boldsymbol{x} \in \mathbb{R}^n$ such that for a given operator $\boldsymbol{A}$, $\boldsymbol{A}\boldsymbol{x} = 0$. In set-builder's notation we have:

$$Null(\boldsymbol{H}) = \{\boldsymbol{x} \in \mathbb{R}^{\,n} : \boldsymbol{H}\boldsymbol{x} = 0\} \tag{II.2}$$

By the Fundamental Subspaces Theorem [Ref. 29] which says if $\boldsymbol{A}$ is an $m \times n$ matrix, then $Null(\boldsymbol{A}) = Range(\boldsymbol{A}^{\mathrm{T}})^{\perp}$ and $Null(\boldsymbol{A}^{\mathrm{T}}) = Range(\boldsymbol{A})^{\perp}$ and equation II.2, $\boldsymbol{H}^{\mathrm{T}}\boldsymbol{r} = 0$. Therefore, to solve the least squares problem $\boldsymbol{H}\boldsymbol{x} = \boldsymbol{b}$, we must solve

$$\boldsymbol{r} = \boldsymbol{b} - \boldsymbol{H}\boldsymbol{x}'$$

$$\boldsymbol{H}^{\mathrm{T}}\boldsymbol{r} = \boldsymbol{H}^{\mathrm{T}}(\boldsymbol{b} - \boldsymbol{H}\boldsymbol{x}')$$

$$0 = \boldsymbol{H}^{\mathrm{T}}\boldsymbol{b} - \boldsymbol{H}^{\mathrm{T}}\boldsymbol{H}\boldsymbol{x}'$$

$$\boldsymbol{H}^{\mathrm{T}}\boldsymbol{b} = \boldsymbol{H}^{\mathrm{T}}\boldsymbol{H}\boldsymbol{x}'$$

$$\boldsymbol{x}' = (\boldsymbol{H}^{\mathrm{T}}\boldsymbol{H})^{-1}\boldsymbol{H}^{\mathrm{T}}\boldsymbol{b}$$

and $(\boldsymbol{H}^{\mathrm{T}}\boldsymbol{H})^{-1}\boldsymbol{H}^{\mathrm{T}}$ is a *projection matrix* of $\boldsymbol{b}$ (otherwise known as the Moore Penrose Inverse). We will apply this method of model fitting using regularization technique in the next section.

## C. BRIEF DISCUSSION OF REGULARIZATION METHODS

In our previous discussion, we saw that the residual falls nicely into the nullspace of $\boldsymbol{H}^{\mathrm{T}}$, but unfortunately in "real life" problems, this residual will not completely fall under the null space because it will be contaminated by some other element that we now include as noise. Methods for constructing a stable approximate solution of an ill-posed problem caused by the effects mentioned are called regularization methods. If error/noise is introduced into the equation $\boldsymbol{d} = \boldsymbol{A}\boldsymbol{f}$ such that $\boldsymbol{d}' = \boldsymbol{A}\boldsymbol{f} + \boldsymbol{n}$, then the perturbation would be:

$$||\boldsymbol{d}' - \boldsymbol{d}|| \leq ||\boldsymbol{n}|| \tag{II.3}$$

$\boldsymbol{d}$ will belong in the range of $\boldsymbol{A}$, but $\boldsymbol{d}'$ may or maynot be in the range of $\boldsymbol{A}$. From functional analysis, we introduce a linear compact operator $\boldsymbol{R}$ such that:

$$\lim_{\alpha \to 0} \boldsymbol{R}_\alpha \boldsymbol{A} \boldsymbol{f} = \boldsymbol{f} \qquad \alpha > 0 \tag{II.4}$$

This is called a regularization scheme for the operator A [Ref. 27]. $\alpha$ is considered the regularization parameter. For example, equation II.4 implies

$$\lim_{\alpha \to 0} \boldsymbol{R}_\alpha \boldsymbol{d} \to \boldsymbol{A}^{-1} \boldsymbol{d}$$

As $\alpha$ goes to 0, $\boldsymbol{R}_\alpha$ converges to $\boldsymbol{A}^{-1}$.

Colton [Ref. 27] points out that the regularization schemes for compact operators are not uniformly convergent. Because physical objects are generally infinite in dimension, $\boldsymbol{R}_\alpha \boldsymbol{A}$ cannot converge to its norm as $\alpha \to 0$. For this reason, we must search for a good regularization parameter. The regularization scheme approximates $\boldsymbol{f}$ of the data model $\boldsymbol{A}\boldsymbol{f} = \boldsymbol{d}$ with a regularized object $\boldsymbol{f}'$ satisfying

$$\boldsymbol{f}' = \boldsymbol{R}_\alpha \boldsymbol{d}' \tag{II.5}$$

Including measurements, we have:

$$\boldsymbol{f}' - \boldsymbol{f} = \boldsymbol{R}_\alpha \boldsymbol{d}' - \boldsymbol{f}$$

$$\boldsymbol{f}' - \boldsymbol{f} = \boldsymbol{R}_\alpha \boldsymbol{d}' - \boldsymbol{R}_\alpha \boldsymbol{d} + \boldsymbol{R}_\alpha \boldsymbol{d} - \boldsymbol{f}$$

$$\boldsymbol{f}' - \boldsymbol{f} = \boldsymbol{R}_\alpha \boldsymbol{d}' - \boldsymbol{R}_\alpha \boldsymbol{d} + \boldsymbol{R}_\alpha \boldsymbol{A} \boldsymbol{f} - \boldsymbol{f}$$

$$\boldsymbol{f}' - \boldsymbol{f} = \boldsymbol{R}_\alpha (\boldsymbol{d}' - \boldsymbol{d}) + \boldsymbol{R}_\alpha \boldsymbol{A} \boldsymbol{f} - \boldsymbol{f} \tag{II.6}$$

where $\boldsymbol{d}' - \boldsymbol{d} = \boldsymbol{n}$, the (unknown) measurement noise. By the triangle inequality, we get

$$||\boldsymbol{f}' - \boldsymbol{f}|| \leq ||\boldsymbol{n}||\,||\boldsymbol{R}_\alpha|| + ||\boldsymbol{R}_\alpha \boldsymbol{A} \boldsymbol{f} - \boldsymbol{f}|| \tag{II.7}$$

The error in object estimation depends on two terms of equation II.7 [Ref. 27]: The first term demonstrates how the error is propagated by the measurement limitation

and the noise of the system; the second term shows that error comes from the inverse mapping $\boldsymbol{A}^{-1}$ from specific elements in $\mathbf{Y}$ mapped by $\boldsymbol{A}$ to $\mathbf{X}$, and the linear operator $\boldsymbol{R}$ that maps all elements in $\mathbf{Y}$ to $\mathbf{X}$. We desire that as the regularization parameter $\alpha$ goes to 0, so will the term $||\boldsymbol{R}_\alpha \boldsymbol{A}\boldsymbol{f} - \boldsymbol{f}||$. Unfortunately, this destabilizes the first term of eqn II.7. Since $\boldsymbol{R}_\alpha \rightarrow \boldsymbol{A}^{-1}$, $||\boldsymbol{R}_\alpha||$ becomes larger (and thus the condition number). This behavior rapidly increases the reconstruction error. The first term in eqn II.7 therefore requires a larger regularization parameter for stabilization, and the second term requires the parameter to go to 0 for accuracy. Therefore, a method must be reached to optimize the right hand side of equation II.7.

One way to accomplish this is to make a choice that the regularization parameter $\alpha$ be dependent on the noise level, that is, $\alpha = \alpha(n)$. From equation II.3, we see that $\boldsymbol{d}' \rightarrow \boldsymbol{d}$ as $\boldsymbol{n} \rightarrow 0$, and so

$$\boldsymbol{R}_{\alpha(n)}\boldsymbol{d}' \rightarrow \boldsymbol{A}^{-1}\boldsymbol{d} = \boldsymbol{f}$$

There are many approaches to accomplish this behavior. In practice, $\alpha$ has to be determined via *a priori* or *a posteriori* criteria. In most of the cases for TWI (Through-the-Wall-Imaging), we are not certain what we are looking for, which makes *a priori* less practical than the *a posteriori* choice. For proof of concept, this thesis will generate data with point scatterers (series of Dirac Delta functions), which we would then use the analytic form of the kernel to determine the point scatters themselves. We assume we have some prior knowledge of the model, which would not likely be the case in a "real world" type application. We will not cover a more detailed Bayesian statistical analysis of the model in this thesis, which is required for *a posteriori* criteria, but we leave it for future research to improve on the model.

## D. TIKHONOV REGULARIZATION

We note from the previous section that as the regularization parameter goes to 0, we have an instability of $||\boldsymbol{R}_\alpha||$ as $\alpha \rightarrow 0$. This is primarily due to the fact that the noise contamination of the data is related to the (nonzero) eigenvalues of

$\boldsymbol{R}_\alpha$. As we try to get a more accurate solution, the first term of the error in equation II.4 grows like $\frac{1}{2\sqrt{\alpha}}$ (for proof refer to Colton [Ref. 27]). This is what some refer to as the *penalty* term where we punish the equality for a large norm. This form of regularization is due to Tikhonov [Ref. 26].

There are a few things we can do to minimize this effect. We seek to minimize equation II.7 in the least square sense.

$$\boldsymbol{f}_\alpha = \arg\min_{\text{all}\boldsymbol{f}}\{||\boldsymbol{n}||^2\,||\boldsymbol{R}_\alpha||^2 + ||\boldsymbol{R}_\alpha\boldsymbol{A}\boldsymbol{f} - \boldsymbol{f}||^2\} \tag{II.8}$$

Using the fact that $\alpha$ is a function of noise, we can introduce this regularization parameter into equation II.8. Consequently with this and equations II.6 and II.7, we can arrive at the Least Square solution for $\boldsymbol{R}_\alpha$ via Newton's Method [Ref. 27].

$$\boldsymbol{R}_\alpha = (\alpha\boldsymbol{I} + \boldsymbol{A}^{\mathrm{T}}\boldsymbol{A})^{-1}\boldsymbol{A}^{\mathrm{T}} \tag{II.9}$$

Note that as $\alpha \to 0$, equation II.9 gives us the Moore Penrose inverse, the simple least-squares solution. From SVD, we know that $\boldsymbol{A}$ can be written in terms of right singular vectors ($\boldsymbol{V}$ matrix) and left singular vectors ($\boldsymbol{U}$ matrix) with common singular values $\sigma_i$ such that

$$\boldsymbol{A} = \boldsymbol{U}\boldsymbol{S}\boldsymbol{V}^{\mathrm{T}}$$

where $\boldsymbol{S}$ is a diagonal matrix with shared singular values (see Appendix C). Because $\boldsymbol{U}$ and $\boldsymbol{V}$ matrices are formed from eigenvectors of symmetric matrices of $\boldsymbol{A}\boldsymbol{A}^{\mathrm{T}}$ and $\boldsymbol{A}^{\mathrm{T}}\boldsymbol{A}$ respectively, $\boldsymbol{U}$ and $\boldsymbol{V}$ are orthogonal matrices.

$$\boldsymbol{A}^{\mathrm{T}} = (\boldsymbol{U}\boldsymbol{S}\boldsymbol{V}^{\mathrm{T}})^{\mathrm{T}} = \boldsymbol{V}\boldsymbol{S}^{\mathrm{T}}\boldsymbol{U}^{\mathrm{T}}$$

Now we make the subsitution of $\boldsymbol{A}$ and $\boldsymbol{A}^{\mathrm{T}}$ into equation II.9:

$$\boldsymbol{R}_\alpha = (\alpha\boldsymbol{V}\boldsymbol{I}\boldsymbol{V}^{\mathrm{T}} + \boldsymbol{V}\boldsymbol{S}\boldsymbol{U}^{\mathrm{T}}\boldsymbol{U}\boldsymbol{S}^{\mathrm{T}}\boldsymbol{V}^{\mathrm{T}})^{-1}\boldsymbol{V}\boldsymbol{S}^{\mathrm{T}}\boldsymbol{U}^{\mathrm{T}}$$

Because $\boldsymbol{U}$ and $\boldsymbol{V}$ matrices are formed from eigenvectors of symmetric matrices of $\boldsymbol{A}\boldsymbol{A}^{\mathrm{T}}$ and $\boldsymbol{A}^{\mathrm{T}}\boldsymbol{A}$ respectively, $\boldsymbol{U}$ and $\boldsymbol{V}$ are orthogonal matrices. Therefore, we get

the following:

$$\boldsymbol{R}_\alpha = (\alpha \boldsymbol{V}\boldsymbol{I}\boldsymbol{V}^{\mathrm{T}} + \boldsymbol{V}\boldsymbol{S}^2\boldsymbol{V}^{\mathrm{T}})^{-1}\boldsymbol{V}\boldsymbol{S}^{\mathrm{T}}\boldsymbol{U}^{\mathrm{T}}$$

$$\boldsymbol{R}_\alpha = \left[\boldsymbol{V}(\alpha \boldsymbol{I} + \boldsymbol{S}^2)\boldsymbol{V}^{\mathrm{T}}\right]^{-1}\boldsymbol{V}\boldsymbol{S}^{\mathrm{T}}\boldsymbol{U}^{\mathrm{T}}$$

$$\boldsymbol{R}_\alpha = \boldsymbol{V}(\alpha \boldsymbol{I} + \boldsymbol{S}^2)^{-1}\boldsymbol{V}^{\mathrm{T}}\boldsymbol{V}\boldsymbol{S}^{\mathrm{T}}\boldsymbol{U}^{\mathrm{T}}$$

$$\boldsymbol{R}_\alpha = \boldsymbol{V}\underbrace{(\alpha \boldsymbol{I} + \boldsymbol{S}^2)^{-1}\boldsymbol{S}^{\mathrm{T}}}_{\boldsymbol{D}}\boldsymbol{U}^{\mathrm{T}} \tag{II.10}$$

If $\lambda_i$ is an eigenvalue of $\boldsymbol{A}^{\mathrm{T}}\boldsymbol{A}$, then $\sigma_i^2 = \lambda_i$ (see Appendix C). We find that the eigenvalues $\tilde{\lambda}_i$ of the modified matrix $\boldsymbol{A}^{\mathrm{T}}\boldsymbol{A} + \alpha\boldsymbol{I}$ in equation II.9 are

$$\tilde{\lambda}_i = \lambda_i + \alpha$$

where $\lambda_i$ are the eigenvalues of $\boldsymbol{A}^{\mathrm{T}}\boldsymbol{A}$. We still have $\sigma_i = \sqrt{\lambda_i}$ and so the diagonal elements of $D$ become

$$D_{ii} = \frac{\sqrt{\lambda_i}}{\lambda_i + \alpha}$$

When $\lambda_i \gg \alpha$ it's clear that $D_{ii} \approx 1/\sqrt{\lambda_i}$ (as before). When $\lambda_i \ll \alpha$, however, the $D_{ii} \approx \sqrt{\lambda_i}/\alpha$ will not become arbitrarily large and the noise problem will be controlled.

## E. TRUNCATED SVD REGULARIZATION

Another way to control the ill-posed behavior is to simply truncate the SVD representation: pick a small threshold value $\alpha$ and compare this value with a given singular value, which you will determine. Once this threshold is reached you replace the corresponding $D_{ii}$ by 0. This method is called the *truncation filter.* There are many ways to determine where the threshold would lie. In this thesis, we will look for where the steepest changes in singular value occurs and will truncated at that point, most of which would be trial and error.

Both methods—Truncation filtering and Tikhonov regularization—are effective at reducing or minimizing the effects of noise. However, neither technique can independently offer a "best" threshold value $\alpha$.

THIS PAGE INTENTIONALLY LEFT BLANK

# III. WAVES IN MEDIA

## A. PRELIMINARY DISCUSSION

In this chapter, we will set the foundations for applying Maxwell's Equations to predict field perturbations in space located behind a transmission medium. We will work primarily with the time independent wave equations, particularly for the electric field. In free-space, the usual approach applies the free space Green's function to the source term of the inhomogenous electromagnetic wave equation. This source is otherwise known as the scattering potential.

If there is a source of perturbation that occurs in region III in Figure 4 and we have a receiver or measuring device in region I, generally the free-space Green's function would work if region II is of the same medium of region I and III, that is free-space. However, if region II is a wall, the free space Green's function does not satisfy the conditions determined by the boundaries of the wall. This will be explained in the following sections where we break the spherical waves into half space expansions and apply the appropriate boundary conditions. We must also consider the effects of refraction and diffraction in the media. The Green's function therefore needs to be solved either analytically or be measured. In real world situations, this function (also known as the System Transfer Function (STF)) cannot usually be determined analytically and is often measured. Such measurements are limited by the accuracy of the device. As discussed in chapter 2, noise contamination can result in catastrophic image reconstruction artifacts when null-space noise components contaminate the data. Furthermore, the reconstruction becomes more unstable as the condition number increases. Robust and powerful techniques of regularization will be generally required.

In the next chapter, we will create a simple model where we approximate this transfer function by imposing the appropriate boundary conditions. These results will then be applied (in the spatial frequency regime) to the development of an imaging

algorithm.

## B. PARAMETERS

Electromagnetic waves through matter are governed by three properties of the material: the permittivity $\epsilon$, the permeability $\mu$ and the conductivity $\sigma$. In our model, we assume the material to be non-magnetic with constant permittivity and no conductivity, which means the index of refraction is going to be constant and real-valued. We will discuss some of the effects of the model and shortcomings due to this simplification.

### *a. Maxwell's Equations*

Maxwell's equations for stationary media are of the following form[Ref. 6]:

$$\nabla \cdot \boldsymbol{E} = \frac{\rho_{total}}{\epsilon_0} = \frac{\rho_{true} - \nabla \cdot \boldsymbol{P}}{\epsilon_0} \tag{III.1}$$

$$\nabla \cdot \boldsymbol{B} = 0 \tag{III.2}$$

$$\nabla \times \boldsymbol{E} = -\frac{\partial \boldsymbol{B}}{\partial t} \tag{III.3}$$

$$\nabla \times \boldsymbol{B} = \mu_0 \left( \boldsymbol{j}_{true} + \frac{\partial \boldsymbol{P}}{\partial t} + \nabla \times \boldsymbol{M} + \epsilon_0 \frac{\partial \boldsymbol{E}}{\partial t} \right) \tag{III.4}$$

where $\rho_{total}$ is the total charge density composed of the charges that are free to move $\rho_{true}$ and those charges that are bounded $\rho_{bounded} = -\nabla \cdot \boldsymbol{P}$, and $\boldsymbol{P}$ is the polarization of the medium. $\boldsymbol{j}_{true}$ is considered the true or the free current. And if we introduce

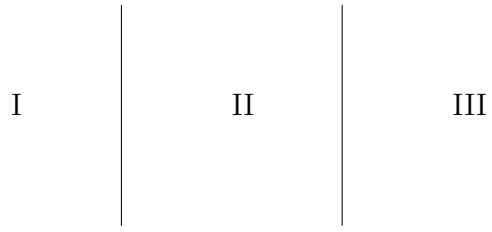


Figure 4. Region

the field vectors $\boldsymbol{D}$ and $\boldsymbol{H}$ by

$$\begin{aligned} \boldsymbol{D} &= \epsilon_0 \boldsymbol{E} + \boldsymbol{P} \\ \boldsymbol{H} &= \frac{\boldsymbol{B}}{\mu_0} - \boldsymbol{M} \end{aligned}$$

then the Maxwell equations simplify to

$$\nabla \cdot \boldsymbol{D} = \rho_{true} \tag{III.5}$$

$$\nabla \cdot \boldsymbol{B} = 0 \tag{III.6}$$

$$\nabla \times \boldsymbol{E} = -\frac{\partial \boldsymbol{B}}{\partial t} \tag{III.7}$$

$$\nabla \times \boldsymbol{H} = \boldsymbol{j}_{true} + \frac{\partial \boldsymbol{D}}{\partial t} \tag{III.8}$$

## 1. Anisotropic Media

For anisotropic media, the permittivity and/or permeability is not a scalar-valued parameter. Since most materials in the walls are non-magnetic, we can safely conclude that permeability will remain isotropic. However, most "real" problems may have anisotropic permittivity. Therefore $\boldsymbol{D}$ cannot be represented by a simple constant of proportionality to $\boldsymbol{E}$. Instead a tensor equation is necessary so that [Ref. 32]

$$\boldsymbol{D} = tensor(\epsilon) \cdot \boldsymbol{E} \tag{III.9}$$

where

$$\begin{aligned} \boldsymbol{D}_x &= \epsilon_{xx}\boldsymbol{E}_x + \epsilon_{xy}\boldsymbol{E}_y + \epsilon_{xz}\boldsymbol{E}_z \\ \boldsymbol{D}_y &= \epsilon_{yx}\boldsymbol{E}_x + \epsilon_{yy}\boldsymbol{E}_y + \epsilon_{yz}\boldsymbol{E}_z \\ \boldsymbol{D}_z &= \epsilon_{zx}\boldsymbol{E}_x + \epsilon_{zy}\boldsymbol{E}_y + \epsilon_{zz}\boldsymbol{E}_z \end{aligned}$$

and

$$tensor(\epsilon) = \begin{bmatrix} \epsilon_{xx} & \epsilon_{xy} & \epsilon_{xz} \\ \epsilon_{yx} & \epsilon_{yy} & \epsilon_{yz} \\ \epsilon_{zx} & \epsilon_{zy} & \epsilon_{zz} \end{bmatrix}$$

Since $\boldsymbol{D}$ may not be parallel to $\boldsymbol{E}$, the permittivity tensor is a function of nine numbers. If we are considering a homogeneous media, then $\epsilon_{ij}$ will be independent of position. Otherwise, they too can be varying. For most of the common cases, we expect the permittivity tensor to be symmetric [Ref. 32]. This means that only 6 different constants are needed to define the $3 \times 3$ matrix. Furthermore, because the matrix is symmetric, its eigenvectors will be orthogonal. Therefore, if you choose the coordinate systems such that it is aligned to these eigenvectors, you can reduce the tensor to a diagonal tensor whose elements are its eigenvalues such that

$$tensor'(\epsilon) = \begin{bmatrix} \epsilon'_x & 0 & 0 \\ 0 & \epsilon'_y & 0 \\ 0 & 0 & \epsilon'_z \end{bmatrix} \tag{III.10}$$

This coordinate system is called the principal system. When the electric field lies along one of these principal axis (eigenvector), then $\boldsymbol{D} \parallel \boldsymbol{E}$,and thus the mathematical analysis can be simplified.

For simplicity, our model will neglect this effect (that exists in materials such as crystals). We will restrict ourselves to a linear media where the polarization of the media is directly proportional to the field.

$$\boldsymbol{D} = \epsilon_0 \boldsymbol{E} + \epsilon_0 \chi \boldsymbol{E} = \epsilon_0 (1 + \chi) \boldsymbol{E} = \epsilon_0 \epsilon_r \boldsymbol{E} = \epsilon \boldsymbol{E} \tag{III.11}$$

where $\chi$ is the electric susceptibility, $\epsilon_0$ is the permittivity of free space, $\epsilon_r$ is the relative permittivity, and $\epsilon$ is the dielectric constant.

## 2. Conductive Materials

In a conductive media, which largely obeys Ohm's Law, and assuming the material is linear, we write

$$\boldsymbol{j} = \sigma \boldsymbol{E} = \frac{\sigma}{\epsilon} \boldsymbol{D} \tag{III.12}$$

By the equation of continuity

$$\nabla \cdot \boldsymbol{j} + \frac{\partial \rho}{\partial t} = 0 \tag{III.13}$$

we see that

$$\begin{aligned} \nabla \cdot \left( \boldsymbol{j} + \frac{\partial \boldsymbol{D}}{\partial t} \right) &= 0 \\ \boldsymbol{j} + \frac{\partial \boldsymbol{D}}{\partial t} &= \boldsymbol{j}_{stationary} \end{aligned}$$

so that $\nabla \cdot \boldsymbol{j}_{stationary} = 0$

Substituting equation III.12 into this last result yields

$$\begin{aligned} \boldsymbol{j} + \frac{\epsilon}{\sigma} \frac{\partial \boldsymbol{j}}{\partial t} &= \boldsymbol{j}_{stationary} \\ \boldsymbol{j} &= \boldsymbol{j}_{stationary} + \boldsymbol{j}_0 e^{-\frac{\sigma}{\epsilon} t} \end{aligned} \tag{III.14}$$

where $\tau_{rel} = \frac{\epsilon}{\sigma}$ is the characteristic or the relaxation time [Ref. 6].
Taking the curl of equation III.7, we obtain the following

$$\nabla \times (\nabla \times \boldsymbol{E}) = -\frac{\partial}{\partial t} (\nabla \times \boldsymbol{B}) \tag{III.15}$$

We also restrict our model to be non-magnetic. Most wall materials are indeed non-magnetic, and we are safe to employ this approximation. Therefore, the relative permeability $\mu_r \approx 1$ and so the material permeability is approximately the magnetic constant in vacuum $\mu \approx \mu_0$. This allows us to write $\boldsymbol{B} = \mu_0 \boldsymbol{H}$. With Equation III.8, Equation III.15 then can be simplified to

$$\nabla(\nabla \cdot \boldsymbol{E}) - \nabla^2 \boldsymbol{E} = -\mu_0 \frac{\partial}{\partial t} \left( \boldsymbol{j}_{true} + \epsilon \frac{\partial \boldsymbol{E}}{\partial t} \right) \tag{III.16}$$

For most cases, we will be dealing with charge free regions. Hence $\nabla \cdot \boldsymbol{E} = 0$. Now for conductive material, we may substitute Equation III.12 into III.16 for further simplification. We arrive at the following with the given assumptions:

$$\nabla^2 \boldsymbol{E} - \mu_0 \epsilon \frac{\partial^2 \boldsymbol{E}}{\partial^2 t} - \mu_0 \sigma \frac{\partial \boldsymbol{E}}{\partial t} = 0 \tag{III.17}$$

Harmonic solutions are of the form:

$$\boldsymbol{E}(x,y,z,t) = \boldsymbol{E}(x,y,z)_\omega e^{-i\omega t}$$

From this point, we shall work with time independent wave equations, and will refer all vectors in the frequency domain. and Equation III.17 becomes:

$$\begin{aligned} \nabla^2\boldsymbol{E} + \mu_0\epsilon\omega^2\boldsymbol{E} + i\mu_0\sigma\omega\boldsymbol{E} &= 0 \qquad \text{(III.18)} \\ \nabla^2\boldsymbol{E} + \left(1 + \frac{i\sigma}{\epsilon\omega}\right)\mu_0\epsilon\omega^2\boldsymbol{E} &= 0 \qquad \text{(III.19)} \end{aligned}$$

Since $\epsilon = \epsilon_0\epsilon_r$, $c = \frac{1}{\sqrt{\mu_0\epsilon_0}}$, and $n \approx \sqrt{\epsilon_r}$, we can simplify the above equation to

$$\begin{aligned} \nabla^2\boldsymbol{E} + \left(1 + \frac{i\sigma}{\epsilon\omega}\right)\frac{n^2}{c^2}\omega^2\boldsymbol{E} &= 0 \\ \nabla^2\boldsymbol{E} + \left(1 + \frac{i\sigma}{\epsilon\omega}\right)n^2k^2\boldsymbol{E} &= 0 \qquad \text{(III.20)} \end{aligned}$$

where $\omega/k = c$. With the relaxation time derived earlier $\tau_{rel} = \epsilon/\sigma$, we get

$$\nabla^2\boldsymbol{E} + \left(1 + \frac{i}{\tau_{rel}\omega}\right)n^2k^2\boldsymbol{E} = 0 \qquad \text{(III.21)}$$

From Equation III.18 we define a complex wave number $\tilde{k} = k + i\kappa$ so that

$$\tilde{k}^2 = \mu_0\epsilon\omega^2 + i\mu_0\sigma\omega \qquad \text{(III.22)}$$

and

$$\begin{aligned} k &\equiv \omega\sqrt{\frac{\epsilon\mu_0}{2}}\left[\sqrt{1 + \left(\frac{\sigma}{\epsilon\omega}\right)^2} + 1\right]^{1/2} \\ \kappa &\equiv \omega\sqrt{\frac{\epsilon\mu_0}{2}}\left[\sqrt{1 + \left(\frac{\sigma}{\epsilon\omega}\right)^2} - 1\right]^{1/2} \end{aligned}$$

Note that for all pure metals, the relaxation time is $\approx 10^{-14}$ [Ref. 6], which is on the same order as the collision time of the electrons. At the frequency that we propose to use (500GHz to 1THz), the relaxation time will be of the order $\frac{10^{14}}{10^{12}} \approx 10^2$ if the

material is fully conductive. This means that the diffusion part of the equation would dominate and therefore the attenuation would be quite high. The penetration depth governed by $d = 1/\kappa$ will be quite short, and the waves will not be able to penetrate. Usually for a good dielectric the relaxation time is of the order of days[Ref. 33], and hence the imaginary term of Equation III.21 vanishes, and thus there will be no damping in the media. For such frequencies, we maybe able to generalize to certain conductive materials with larger relaxation times, but such an analysis would require a large database of material effects and is beyond the scope of the thesis. For this reason, the model also assumes that the walls are non-conductive and we will deal with just the wave equation portion of Equation III.17

## 3. Frequency Dependence and the Dispersion Relation

Dispersive media have values of $\mu$, $\epsilon$, or $\sigma$ that are functions of frequency. It can be shown that for a dielectric $\epsilon$ as a function of frequency is well-modeled by[Ref. 33]:

$$\begin{aligned}
\epsilon(\omega) &= \epsilon'(\omega) - i\epsilon''(\omega) \\
\epsilon'(\omega) &= \epsilon_0 + \frac{\epsilon_0\omega_p^2(\omega_0^2 - \omega^2)}{(\omega^2 - \omega_0^2)^2 + \alpha^2\omega^2} \\
\epsilon''(\omega) &= \frac{\epsilon_0\omega_p^2\omega\alpha}{(\omega^2 - \omega_0^2)^2 + \alpha^2\omega^2}
\end{aligned}$$

where $\alpha = 1/\tau$ and $\tau$ is the collision times of the electrons, $\omega_0$ is the resonant frequency.

$$\omega_p^2 = \frac{Ne^2}{\epsilon_0 m} \qquad \text{plasma frequency,}$$

$N$ are the number of dipoles per unit volume, and $m$ is the mass of the electron. The real part $\epsilon'(\omega)$ defines the refractive index $n(\omega) = \sqrt{\epsilon'(\omega)/\epsilon_0}$, and the imaginary part $\epsilon''(\omega)$ is the loss tangent of the material $\tan\theta(\omega) = \epsilon''/\epsilon'(\omega)$, and it is related to the attenuation constant (absorption coefficient) of the electromagnetic wave [Ref. 33]. In Figure 5, we see that around the resonant frequency $\omega_0$, the dielectric behaves in a strange manner and the material absorption becomes quite high. Therefore, one

has to be careful that the radiation frequency we transmit would not be in resonance with the dielectric, and further material analysis might be required.

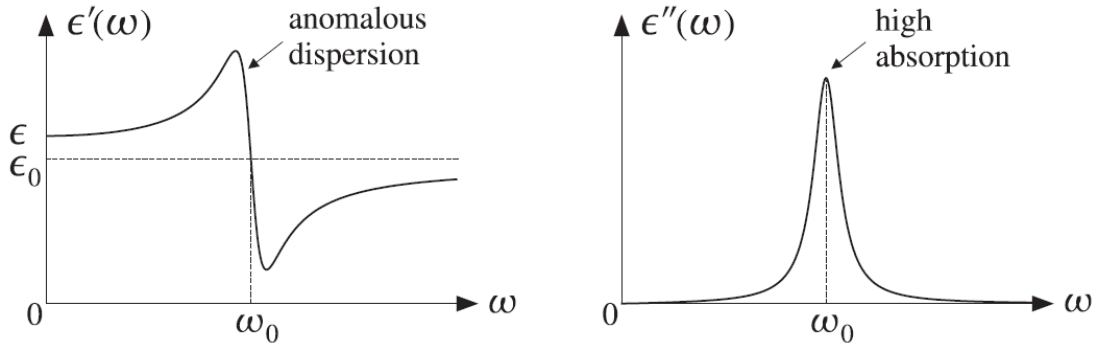


Figure 5. Real and Imaginary parts of dielectric constant. Figure taken from [Ref. 33]

For metals, charges are unbounded, so $\omega_0 = 0$, and from Ohm's Law, we find [Ref. 33]

$$\sigma(\omega) = \frac{\epsilon_0 \omega_p^2}{\alpha + i\omega} \tag{III.23}$$

In "real" phenomena, we know that from optics that $n$ is a function of frequency (See Figure 6). Therefore, it can be seen that different wavelengths of light refract differently. This is largely due to dispersion $\mathrm{d}\omega/\mathrm{dk} \neq$ constant. Because waves of different frequency travel at different speeds in a dispersive medium, one would have to find methods and ways to isolate these frequencies for application. The waves as a whole or the "envelope" of the waves travel at group velocity:

$$\nu_g = \frac{\mathrm{d}\omega}{\mathrm{dk}}$$

Because the velocity depends on the frequency and $\omega = \omega(k)$, the field is of the form:

$$\psi(x,t) = \int_{-\infty}^{\infty} A(k) e^{i(kx - \omega(k)t)} \mathrm{dk} = \int_{-\infty}^{\infty} \mathrm{A(k)e^{it(kx/t - \omega(k))}dk} \tag{III.24}$$

The amplitude $A(k)$ is related to the initial condition of $\psi(x,0)$ by:

$$\psi(x,0) = \int_{-\infty}^{\infty} A(k) e^{ikx} \mathrm{dk} \tag{III.25}$$

Analysis of the system typically requires a numerical approach (such as the the Method of Stationary Phase [Ref. 5]). The motivation for this is that we know that for all wave numbers $k$, wave component disperse for any initial conditions. All the waves will travel with the group velocity, and all of the energy maybe concentrated in one wave number [Ref. 5]. For this reason, using the Method of Stationary phase can provide us a very good prediction of the system. These are all physical realities we will have to face in dispersive mediums, for which case a large database of various different material will be required. It is beyond the scope of this thesis to analyze the effects of the waves for each different media. For this reason, this thesis will set the criteria that we are working with non-dispersive mediums.

## C. FOUNDATIONS OF THE SCALAR THEORY

From our Maxwell equations listed in Equations (III.5), (III.6), (III.7), (III.8), we get our wave equations by taking the curl of Equation III.7 and Equation III.8. Since the vector wave equation is obeyed by both $\boldsymbol{E}$ and $\boldsymbol{H}$, an identical scalar wave equation is obeyed by all components of those vectors provided we are in a cartesian

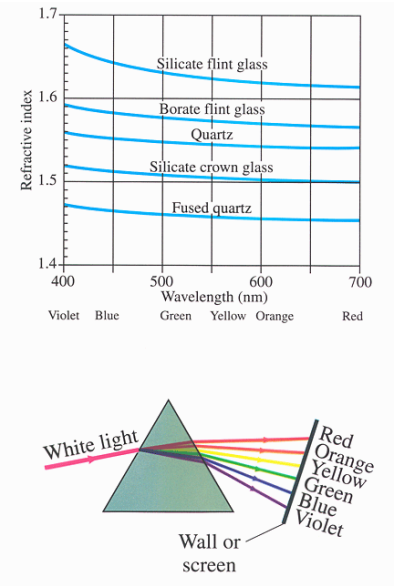


Figure 6. Index of Refraction vs Wavelength. This Figure is taken from [Ref. 31]

coordinate system. Thus, the component $\boldsymbol{E}_x$ will, for example, obey the equation:

$$\nabla^2 \boldsymbol{E}_x + n^2 k^2 \boldsymbol{E}_x = 0$$

Therefore, it is possible to summarize the behavior of all components of $\boldsymbol{E}$ and $\boldsymbol{H}$ through scalar equations of the form:

$$\nabla^2 \psi + n^2 k^2 \psi = 0 \tag{III.26}$$

If we take from Equations (III.7) and (III.8) and compare component by component, we will get 6 equations, and if we orient the coordinate system so that one component vanishes, then the equations will simplify to two equations with the $\boldsymbol{E}$ and $\boldsymbol{B}$ field. These equations can be uncoupled and reduced to a single scalar wave equation, which describes either a Transverse Magnetic Polarization (TM) or Transverse Electric Polarization (TE). When, all the medium parameters $\epsilon$, $\sigma$, and $\mu$ are independent of one of the space dimensions, then the corresponding electromagnetic field components are also independent of that same dimension. Then one can write the vector Maxwell equations as a superposition of the TE and TM fields.

If there is variation of permitivity as in the case of anisotropic media, the wave equation becomes

$$\nabla(\boldsymbol{E} \cdot \nabla(\ln \epsilon)) + \nabla^2 \boldsymbol{E} + \mathrm{n^2 k^2} \boldsymbol{E} = 0 \tag{III.27}$$

In this case, the extra term couples the x, y and z components. The scalar representation would fail in the conductor case where the boundary conditions are that there is a jump of $\sigma$ in the electric field perpendicular to the surface, and a jump with the magnitude of the free current in the magnetic field parallel to the surface. In these cases, the components of the Electric and Magnetic fields will be further restricted, and would require a more robust model such as the Stratton-Chu model for vector wave equations [Ref. 27].

If the waves are spherical in nature, one can still formulate the problem as a scalar wave in terms of the Debeye potentials [Ref. 6]. In either case, our model criteria gives us the flexibility for using the scalar model. Although there are faults in using the scalar model, our model criteria allow us to decouple the Maxwell equations and reasonably capture the essential behavior of the wave propagation.

Furthermore, we have to impose the conditions at infinity. In the vector case, the electric and magnetic fields must go to zero at infinity, and thus must satisfy the Silver-Müller conditons:

$$\lim_{r\to\infty}(\boldsymbol{H}\times\boldsymbol{x}-r\boldsymbol{E}) = 0 \tag{III.28}$$

$$\lim_{r\to\infty}(\boldsymbol{E}\times\boldsymbol{x}+r\boldsymbol{H}) = 0 \tag{III.29}$$

where $r=|\boldsymbol{x}|$ and where the limit is assumed to hold uniformly in all directions. The corresponding radiation condition for Cartesian components is the Sommerfeld radiation condition

$$\lim_{r\to\infty} r(\frac{\partial E}{\partial r}-ikE)=0 \tag{III.30}$$

For more complete discussion and proof, refer to [Ref. 27].

For the reasons mentioned above, we shall attack the problem for the scalar case with the Sommerfeld conditions imposed at infinity.

THIS PAGE INTENTIONALLY LEFT BLANK

# IV. THE INHOMOGENEOUS WAVE EQUATION/TRANSFER FUNCTION

To develop the transfer function, consider a field that emanates towards an infinite flat slab (Figure 7). We take this wave to be directed in the positive $z$ direction, and $y$ axis is positive downwards, and $x$ is positive outwards. The isotropic media has an index of refraction $n_m$ that is independent of frequency, and the location of the source is at $\boldsymbol{r_0} = -z_0\hat{\boldsymbol{k}}$.

For a field with source $s(\boldsymbol{r}, t)$, the wave equation becomes

$$\nabla^2\mathcal{E} - \frac{n^2}{c^2}\frac{\partial\mathcal{E}}{\partial t} = s(\boldsymbol{r}, t) \tag{IV.1}$$

where $\mathcal{E}$ is in the time domain for $E$. The source function can be written in terms of the Fourier integral:

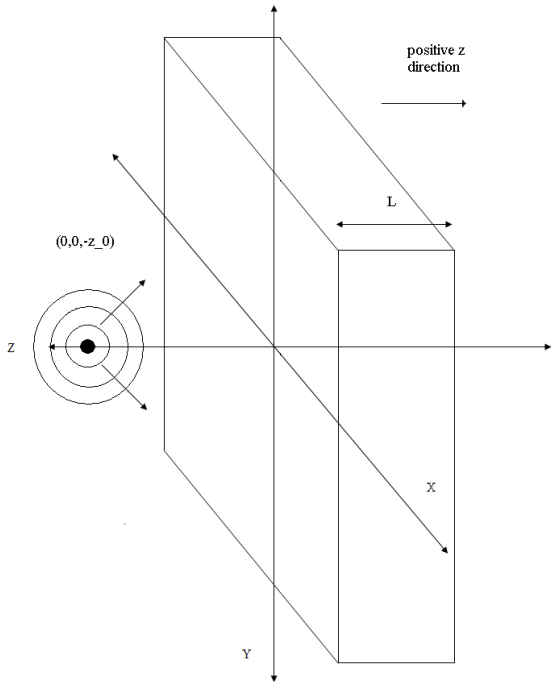


Figure 7. Point Source emanating waves through a constant dielectric medium (Infinitely large slab)

$$s(\boldsymbol{r},t)=\int_{-\infty}^{\infty}S(f,\boldsymbol{r})e^{i2\pi ft}\mathrm{df}$$

Thus the time independent wave equations reduces to

$$\nabla^2E+n^2k^2E=S(f,\boldsymbol{r}) \tag{IV.2}$$

We can construct the solution of Equation IV.2 by superposition of unit point solutions corresponding to a source at the point $\boldsymbol{r}_0=-z_0\hat{\boldsymbol{k}}$, and we placed this source on the $z$ axis for reasons to be discussed below.

The Green's function due to a source at $\boldsymbol{r}_0$ will satisfy equation:

$$(\nabla^2+k^2n^2(z))G(\boldsymbol{x},\boldsymbol{r_0})=\delta(\boldsymbol{x}+\boldsymbol{r_0}) \tag{IV.3}$$

where $k=2\pi/\lambda$, $\lambda$ is the wavelength in free-space

$$\delta(\boldsymbol{x}+\boldsymbol{r_0})=\delta(x)\delta(y)\delta(z+z_0) \tag{IV.4}$$

and

$$n(z)=\begin{cases}1 & \text{for} \quad z<0\\ n & \text{for} \quad 0\le z\le L\\ 1 & \text{for} \quad L<z\end{cases} \tag{IV.5}$$

Therefore, the particular solution for $E$ is

$$E=\int_{V_0}G(\boldsymbol{x},\boldsymbol{r}_0)S(f,\boldsymbol{r})\mathrm{d}^3\boldsymbol{r}_0 \tag{IV.6}$$

and, in the time domain, we have

$$\mathcal{E}(\boldsymbol{r},t)=\int_{-\infty}^{\infty}E(\boldsymbol{r},f)e^{-i2\pi ft}\mathrm{df} \tag{IV.7}$$

Since the media is non-conductive, the wave number remains real valued. Therefore, there will be no dampening term, and the media will become a wave guide

composed of TE and TM waves. Using Bracewell's notation, we take the Fourier transform of Equation IV.3 in the $x$ and $y$ coordinate to obtain

$$\hat{G}(f_x, f_y, z, \boldsymbol{r_0}) \equiv \int_{-\infty}^{\infty}\int_{-\infty}^{\infty} G(x, y, z, \boldsymbol{r_0}) e^{-i(2\pi f_x x + 2\pi f_y y)} \mathrm{dxdy} \tag{IV.8}$$

$$G(x, y, z, \boldsymbol{r_0}) \equiv \int_{-\infty}^{\infty}\int_{-\infty}^{\infty} \hat{G}(f_x, f_y, z, \boldsymbol{r_0}) e^{i(2\pi f_x x + 2\pi f_y y)} \mathrm{df_x df_y} \tag{IV.9}$$

This transform will reduce the three dimensional Laplacian to a single ODE. We are allowed to make this substitution because there is no slowing or changing of the media in the $x$ and $y$ direction: the media remains constant in these directions, and the index of refraction only changes in the $z$ direction. Application of Equation IV.3 yields

$$[-(2\pi f_x)^2 - (2\pi f_y)^2 + \frac{\partial^2}{\partial z^2}]\hat{G}(f_x, f_y, z, \boldsymbol{r_0}) + k^2 n^2(z)\hat{G}(f_x, f_y, z, \boldsymbol{r_0}) = \delta(z + z_0) \tag{IV.10}$$

Define

$$\boldsymbol{F} \equiv 2\pi f_x \hat{\boldsymbol{\imath}} + 2\pi f_y \hat{\boldsymbol{\jmath}} \tag{IV.11}$$

so that $|\boldsymbol{F}|^2 = (2\pi f_x)^2 + (2\pi f_y)^2$.

The wave number is related as:

$$\begin{aligned} k^2 = k_x^2 + k_y^2 + k_z^2 &= (\frac{2\pi}{\lambda_x})^2 + (\frac{2\pi}{\lambda_y})^2 + (\frac{2\pi}{\lambda_z})^2 \\ &= (2\pi f_x)^2 + (2\pi f_y)^2 + (2\pi f_z)^2 \end{aligned} \tag{IV.12}$$

Consequently, the Bracewell notation chooses the spatial frequency to obey $f_x = 1/\lambda_x\,, f_y = 1/\lambda_y\,, f_z = 1/\lambda_z$ and we write $\hat{G} = \hat{G}(f_x, f_y, z, \boldsymbol{r_0})$

When $z \neq -z_0$, Equation IV.10 is the homogeneous wave equation with solution

$$\hat{G} = \underbrace{a e^{i\sqrt{k^2 n^2(z) - |\boldsymbol{F}|^2} z}}_{\text{right going wave}} + \underbrace{b e^{-i\sqrt{k^2 n^2(z) - |\boldsymbol{F}|^2} z}}_{\text{left going wave}} \tag{IV.13}$$

This solution must satisfy the boundary conditions, which will determine the coefficients of each component wave as they propagate through the medium. The wave and its derivatives must be continuous at any boundaries. Consequently, the following conditions must be true (see Figure 8):

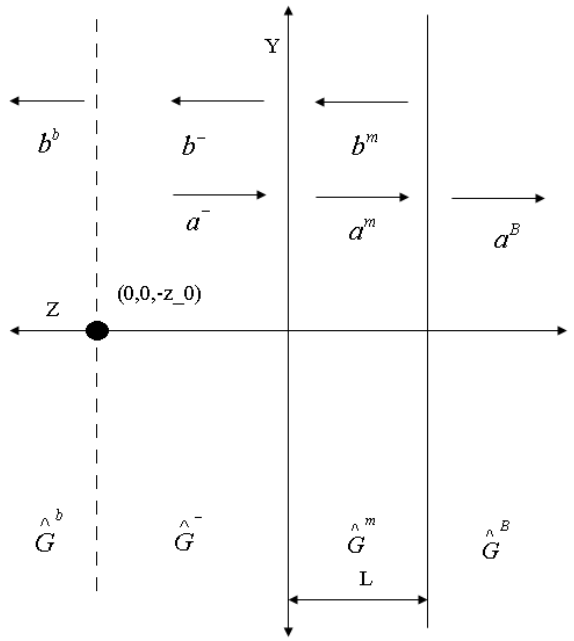


Figure 8. Cross sectional view of the wavefront

$$\hat{G}^-|_{z=0} = \hat{G}^m|_{z=0} \quad \frac{\partial \hat{G}^-}{\partial z}\Big|_{z=0} = \frac{\partial \hat{G}^m}{\partial z}\Big|_{z=0} \tag{IV.14}$$

$$\hat{G}^m|_{z=L} = \hat{G}^B|_{z=L} \quad \frac{\partial \hat{G}^m}{\partial z}\Big|_{z=L} = \frac{\partial \hat{G}^B}{\partial z}\Big|_{z=L} \tag{IV.15}$$

$$\hat{G}^b|_{z=-z_0} = \hat{G}^-|_{z=-z_0} \quad \frac{\partial \hat{G}^-}{\partial z}\Big|_{z=-z_0} - \frac{\partial \hat{G}^b}{\partial z}\Big|_{z=-z_0} = 1 \tag{IV.16}$$

Imposing the Sommerfeld conditions and using the fact that the wave is outgoing from the source, the coefficient $a^b$ of the right going component (for $z < -z_0$), and the coefficient $b^B$ of the left going component for $(z > L)$ must vanish (see Figure 8).

The waves are traveling to the left when $z < -z_0$ and are traveling to the right when $z > L$. The boundary conditions are such that the Green's function is continuous with continuous derivatives — except at the source. Since the waves are continuous, the Green's function has to be continuous. But its first derivative is not very obvious. Let us integrate Equation IV.10 both sides.

$$\int \frac{\partial^2}{\partial z^2}\hat{G}(f_x, f_y, z, \boldsymbol{r}_0)\mathrm{dz} + \int (\mathrm{k^2 n^2(z)}) - (2\pi \mathrm{f_x})^2 - (2\pi \mathrm{f_y})^2)\hat{\mathrm{G}}(\mathrm{f_x}, \mathrm{f_y}, \mathrm{z}, \boldsymbol{r}_0)\mathrm{dz} = \int \delta(\mathrm{z}+\mathrm{z}_0)\mathrm{dz} \tag{IV.17}$$

The right hand side will become the Heaviside Function. The left hand side would be composed of the first derivative of the Green's function and an integral of the Green's function.

$$\frac{\partial}{\partial z}\hat{G}(f_x, f_y, z, \boldsymbol{r}_0) + \int (k^2 n^2(z) - (2\pi f_x)^2 - (2\pi f_y)^2)\hat{G}(f_x, f_y, z, \boldsymbol{r}_0)\mathrm{dz} = \mathrm{H(z + z_0)} \tag{IV.18}$$

Since, the Green's function is continuous, the middle term will vanish at any given boundary. However, the first derivatives will become continuous as long the boundaries are $z < -z_0$ or $z > -z_0$. As the first derivative crosses the source (where the Heaviside Function transitions from $0 \rightarrow 1$, the difference across will have a jump of 1). And imposing these boundary conditions specified above, we arrive to the following:

Let

$$\begin{aligned} n_T &\equiv n(z < 0) \\ n_m &\equiv n(0 \leq z \leq L) \\ n_B &\equiv n(L < z) \end{aligned}$$

At $z = 0$

$$a^- + b^- = a^m + b^m \tag{IV.19}$$

$$\sqrt{k^2n_T^2 - |\boldsymbol{F}|^2}a^- - \sqrt{k^2n_T^2 - |\boldsymbol{F}|^2} = a^m\sqrt{k^2n_m^2 - |\boldsymbol{F}|^2} - b^m\sqrt{k^2n_m^2 - |\boldsymbol{F}|^2} \tag{IV.20}$$

$$\underbrace{\begin{bmatrix} 1 & 1 \\ \sqrt{N_T} & -\sqrt{N_T} \end{bmatrix}}_{M1}\begin{bmatrix} a^- \\ b^- \end{bmatrix} = \underbrace{\begin{bmatrix} 1 & 1 \\ \sqrt{N_m} & -\sqrt{N_m} \end{bmatrix}}_{M2}\begin{bmatrix} a^m \\ b^m \end{bmatrix} \tag{IV.21}$$

where $N_T = k^2n_T^2 - |\boldsymbol{F}|^2$ and $N_m = k^2n_m^2 - |\boldsymbol{F}|^2$.

At $z = L$, we require

$$a^m e^{i\sqrt{k^2n_m^2 - |\boldsymbol{F}|^2}L} + b^m e^{-i\sqrt{k^2n_m^2 - |\boldsymbol{F}|^2}L} = a^B e^{i\sqrt{k^2n_B^2 - |\boldsymbol{F}|^2}L} \tag{IV.22}$$

$$\begin{aligned} a^m\sqrt{k^2n_m^2 - |\boldsymbol{F}|^2}e^{i\sqrt{k^2n_m^2 - |\boldsymbol{F}|^2}L} - b^m\sqrt{k^2n_m^2 - |\boldsymbol{F}|^2}e^{-i\sqrt{k^2n_m^2 - |\boldsymbol{F}|^2}L} \\ = a^B\sqrt{k^2n_B^2 - |\boldsymbol{F}|^2}e^{i\sqrt{k^2n_B^2 - |\boldsymbol{F}|^2}L} \end{aligned} \tag{IV.23}$$

$$\begin{aligned} &\underbrace{\begin{bmatrix} e^{i\sqrt{N_m}L} & e^{-i\sqrt{N_m}L} \\ \sqrt{N_m}e^{i\sqrt{N_m}L} & -\sqrt{N_m}e^{-i\sqrt{N_m}L} \end{bmatrix}}_{M3}\begin{bmatrix} a^m \\ b^m \end{bmatrix} \\ &\qquad = \underbrace{\begin{bmatrix} e^{i\sqrt{N_B}L} & e^{-i\sqrt{N_B}L} \\ \sqrt{N_B}e^{i\sqrt{N_B}L} & e^{-i\sqrt{N_B}L} \end{bmatrix}}_{M4}\begin{bmatrix} a^B \\ 0 \end{bmatrix} \end{aligned} \tag{IV.24}$$

where $N_m = k^2n_m^2 - |\boldsymbol{F}|^2$ and $N_B = k^2n_B^2 - |\boldsymbol{F}|^2$

And at $z = -z_0$, we require

$$b^b e^{i\sqrt{k^2n_T^2 - |\boldsymbol{F}|^2}z_0} = a^- e^{-i\sqrt{k^2n_T^2 - |\boldsymbol{F}|^2}z_0} + b^- e^{i\sqrt{k^2n_T^2 - |\boldsymbol{F}|^2}z_0} \tag{IV.25}$$

Now we apply the jump condition (see Equation (IV.16)) to obtain

$$
\begin{aligned}
a^- \sqrt{k^2 n_T^2 - |\boldsymbol{F}|^2} e^{-i\sqrt{k^2 n_T^2 - |\boldsymbol{F}|^2} z_0} \\
-b^- \sqrt{k^2 n_T^2 - |\boldsymbol{F}|^2} e^{i\sqrt{k^2 n_T^2 - |\boldsymbol{F}|^2} z_0} \\
= -b^b \sqrt{k^2 n_T^2 - |\boldsymbol{F}|^2} e^{i\sqrt{k^2 n_T^2 - |\boldsymbol{F}|^2} z_0} + 1
\end{aligned}
\tag{IV.26}
$$

$$
\begin{aligned}
\underbrace{\begin{bmatrix} e^{-i\sqrt{N_T} z_0} & e^{i\sqrt{N_T} z_0} \\ \sqrt{N_T} e^{-i\sqrt{N_T} z_0} & -\sqrt{N_T} e^{i\sqrt{N_T} z_0} \end{bmatrix}}_{M5} \begin{bmatrix} a^- \\ b^- \end{bmatrix} = \\
\underbrace{\begin{bmatrix} e^{i\sqrt{N_T} z_0} & e^{-i\sqrt{N_T} z_0} \\ -\sqrt{N_T} e^{i\sqrt{N_T} z_0} & e^{-i\sqrt{N_T} z_0} \end{bmatrix}}_{M6} \begin{bmatrix} b^b \\ 0 \end{bmatrix} + \begin{bmatrix} 0 \\ 1 \end{bmatrix}
\end{aligned}
\tag{IV.27}
$$

where $N_T = k^2 n_T^2 - |\boldsymbol{F}|^2$. We note that all the matrices are invertible, and therefore, we can have a closed form solution for the coefficients of the Green's function.

To solve for these coefficients, we first simplify our results to read

$$
M_1 \begin{bmatrix} a^- \\ b^- \end{bmatrix} = M_2 \begin{bmatrix} a^m \\ b^m \end{bmatrix} \tag{IV.28}
$$

$$
M_3 \begin{bmatrix} a^m \\ b^m \end{bmatrix} = M_4 \begin{bmatrix} a^B \\ 0 \end{bmatrix} \tag{IV.29}
$$

$$
M_5 \begin{bmatrix} a^- \\ b^- \end{bmatrix} = M_6 \begin{bmatrix} b^b \\ 0 \end{bmatrix} + \begin{bmatrix} 0 \\ 1 \end{bmatrix} \tag{IV.30}
$$

where the reflection and transmission amplitudes can be expressed in terms of $a^-$, the amplitude of the incident wave:

$$
\begin{bmatrix} a^- \\ b^- \end{bmatrix} = \underbrace{M_1^{-1} M_2 M_3^{-1} M_4}_{B} \begin{bmatrix} a^B \\ 0 \end{bmatrix} \tag{IV.31}
$$

or

$$a^- = B_{1,1}a^B \qquad b^- = B_{2,1}a^B \tag{IV.32}$$

$$b^- = \frac{B_{2,1}}{B_{1,1}}a^- \qquad a^B = \frac{a^-}{B_{1,1}} \tag{IV.33}$$

After much algebra, we obtain the reflectance:

$$r = \frac{b^-}{a^-} = \frac{(\sqrt{N_B}+\sqrt{N_m})(\sqrt{N_T}-\sqrt{N_m})+(-\sqrt{N_B}+\sqrt{N_m})(\sqrt{N_T}+\sqrt{N_m})e^{i2\sqrt{N_m}L}}{(\sqrt{N_B}+\sqrt{N_m})(\sqrt{N_T}+\sqrt{N_m})+(-\sqrt{N_T}+\sqrt{N_m})(\sqrt{N_B}-\sqrt{N_m})e^{i2\sqrt{N_m}L}} \tag{IV.34}$$

The Reflection coefficient then is $R = r * r$.

Similarly, the transmittance is

$$t = \frac{a^B}{a^-} = \frac{4\sqrt{N_T}\sqrt{N_m}e^{-i\sqrt{N_B}L}}{(\sqrt{N_T}+\sqrt{N_m})(\sqrt{N_B}+\sqrt{N_m})e^{-i\sqrt{N_m}L}+(\sqrt{N_T}-\sqrt{N_m})(-\sqrt{N_B}+\sqrt{N_m})e^{i\sqrt{N_m}L}} \tag{IV.35}$$

The Transmission is $T = t * t$.

We can also solve for the other coefficients. Inside the medium, we have

$$\begin{bmatrix} a^m \\ b^m \end{bmatrix} = \underbrace{M_3^{-1}M_4}_{C} \begin{bmatrix} a^B \\ 0 \end{bmatrix} \tag{IV.36}$$

$$a^m = C_{1,1}a^B = \frac{C_{1,1}}{B_{1,1}}a^- \qquad b^m = C_{2,1}a^B = \frac{C_{2,1}}{B_{1,1}}a^- \tag{IV.37}$$

$$\frac{a^m}{a^-} = \frac{2\sqrt{N_T}(\sqrt{N_m}+\sqrt{N_B})}{(\sqrt{N_B}+\sqrt{N_m})(\sqrt{N_T}+\sqrt{N_m})+(-\sqrt{N_T}+\sqrt{N_m})(\sqrt{N_B}-\sqrt{N_m})e^{i2\sqrt{N_m}L}} \tag{IV.38}$$

$$\frac{b^m}{a^-} = \frac{2\sqrt{N_T}(\sqrt{N_m}-\sqrt{N_B})}{(\sqrt{N_B}+\sqrt{N_m})(\sqrt{N_T}+\sqrt{N_m})+(-\sqrt{N_T}+\sqrt{N_m})(\sqrt{N_B}-\sqrt{N_m})e^{i2\sqrt{N_m}L}} \tag{IV.39}$$

Finally, at the source, we obtain

$$\begin{bmatrix} b^b \\ 0 \end{bmatrix} = M_6^{-1} \left( M_5 M_1^{-1} M_2 M_3^{-1} M_4 \begin{bmatrix} a^B \\ 0 \end{bmatrix} - \begin{bmatrix} 0 \\ 1 \end{bmatrix} \right) \tag{IV.40}$$

Writing $X = M_6^{-1} M_5 M_1^{-1} M_2 M_3^{-1} M_4$ and

$$S = M_6^{-1} \begin{bmatrix} 0 \\ 1 \end{bmatrix} = \begin{bmatrix} -\frac{1}{e^{i\sqrt{N_T} z_0}(1+\sqrt{N_T})} \\ \frac{1}{e^{-i\sqrt{N_T} z_0}(1+\sqrt{N_T})} \end{bmatrix} \tag{IV.41}$$

yields

$$b^b = X_{1,1} a^B - S_{1,1} = (X_{1,1}/B_{1,1}) a^- - S_{1,1} \tag{IV.42}$$

and

$$0 = X_{2,1} a^B - S_{2,1} \tag{IV.43}$$

We can simplify these results somewhat. Outside the medium, we assume $\sqrt{N_T} = \sqrt{N_B} \equiv \sqrt{N}$. We are interested in the amplitudes of the transmitted wave ($a^B$), the incident wave ($a^-$) and the reflected wave ($b^-$).

In the next chapter, we will show that we can consider the Green's function to be shift-invariant so that $G(\boldsymbol{x}, \boldsymbol{r_0}) \equiv G(x - x_0, y - y_0, z, z_0) = G(\boldsymbol{r} - \boldsymbol{r}_0)$.

$$a^- = \frac{e^{i\sqrt{N} z_0}}{2\sqrt{N}} \tag{IV.44}$$

$$b^- = r * a^- = \frac{(N - N_m) + (N_m - N) e^{i2\sqrt{N_m} L}}{(\sqrt{N_m} + \sqrt{N})^2 - (\sqrt{N_m} - \sqrt{N})^2 e^{i2\sqrt{N_m} L}} \frac{e^{i\sqrt{N} z_0}}{2\sqrt{N}} \tag{IV.45}$$

$$a^B = t * a^- = \frac{4\sqrt{N}\sqrt{N_m} e^{-i\sqrt{N} L}}{(\sqrt{N} + \sqrt{N_m})^2 e^{-i\sqrt{N_m} L} - (\sqrt{N_m} - \sqrt{N})^2 e^{i\sqrt{N_m} L}} \frac{e^{i\sqrt{N} z_0}}{2\sqrt{N}} \tag{IV.46}$$

We note that for $z < -z_0$, is free space. Since the free space Green's function is a solution to the Helmholtz equation and satisfies the radiation condition at infinity,

it must be the solution in this region. We will show this for $-z_0 < z < 0$ in the next chapter. For the regions of interest, we have the following:

$$\hat{G}(f_x, f_y, z, \boldsymbol{r_0}) = \begin{cases} \frac{e^{i\sqrt{N}z_0}}{2\sqrt{N}} e^{i\sqrt{k^2-|\boldsymbol{F}|^2}z} & \text{for } -z_0 < z < 0 \text{ right-going} \\ \frac{(N-N_m)+(N_m-N)e^{i2\sqrt{N_m}L}}{(\sqrt{N_m}+\sqrt{N})^2-(\sqrt{N_m}-\sqrt{N})^2 e^{i2\sqrt{N_m}L}} \frac{e^{i\sqrt{N}z_0}}{2\sqrt{N}} e^{-i\sqrt{k^2-|\boldsymbol{F}|^2}z} & \text{left-going} \end{cases} \tag{IV.47}$$

$$\hat{G}(f_x, f_y, z, \boldsymbol{r_0}) = \frac{4\sqrt{N}\sqrt{N_m}e^{-i\sqrt{N}L}}{(\sqrt{N}+\sqrt{N_m})^2 e^{-i\sqrt{N_m}L}-(\sqrt{N_m}-\sqrt{N})^2 e^{i\sqrt{N_m}L}} \frac{e^{i\sqrt{N}z_0}}{2\sqrt{N}} e^{i\sqrt{k^2-|\boldsymbol{F}|^2}z} \quad \text{for } z > L \text{ right-going} \tag{IV.48}$$

We solve the coefficients $a^m$ and $b^m$ by solving

$$\begin{bmatrix} a^m \\ b^m \end{bmatrix} = M_2^{-1} M_1 \begin{bmatrix} a^- \\ b^- \end{bmatrix}$$

For $0 \leq z \leq L$, we obtain

$$a^m = \underbrace{\frac{e^{i\sqrt{N}z_0}}{2\sqrt{N}}}_{a^-} \times \frac{2\sqrt{N}(\sqrt{N}+\sqrt{N_m})}{(\sqrt{N}+\sqrt{N_m})^2-(\sqrt{N_m}-\sqrt{N})^2 e^{i2L\sqrt{N_m}}} \tag{IV.49}$$

and

$$b^m = \underbrace{\frac{e^{i\sqrt{N}z_0}}{2\sqrt{N}}}_{a^-} \times \frac{2\sqrt{N}(\sqrt{N_m}-\sqrt{N})e^{i2L\sqrt{N_m}}}{(\sqrt{N}+\sqrt{N_m})^2-(\sqrt{N_m}-\sqrt{N})^2 e^{i2L\sqrt{N_m}}} \tag{IV.50}$$

Therefore, within the media, the Green's function behaves in the following way:

$$\hat{G}(f_x, f_y, z, \boldsymbol{r}_0) = a^m e^{i\sqrt{n^2k^2-|\boldsymbol{F}|^2}z} \quad \text{right going wave} \tag{IV.51}$$

$$\hat{G}(f_x, f_y, z, \boldsymbol{r}_0) = b^m e^{-i\sqrt{n^2k^2-|\boldsymbol{F}|^2}z} \quad \text{left going wave} \tag{IV.52}$$

# V. THE ANGULAR SPECTRUM

## A. WEYL'S INTEGRAL AND SPHERICAL WAVES

In this chapter, we will show that the right-going wave of Equation IV.47 is the planar expansion of the spherical wave by introducing the Weyl's integral. We will also discuss the properties of the Inverse Transform of the Green's function in the spatial domain, and demonstrate the shift-invariant form of the Green's Function.

What makes the problem very difficult is the reflection and refraction of a spherical wave on a planar media because the wave has spherical symmetry and the boundary is a plane. For this reason, we want a way to expand the spherical waves in terms of planes. In equation IV.47, we will first take the case for the right-going wave. The Inverse Fourier Transform defined as:

$$G(x,y,z,\boldsymbol{r_0}) = \int_{-\infty}^{\infty}\int_{-\infty}^{\infty} \hat{G}(f_x,f_y,z,\boldsymbol{r_0}) e^{i2\pi(f_x x+f_y y)} \mathrm{df_x df_y} \tag{V.1}$$

H. Weyl's expansion of the spherical waves into planar waves is [Ref. 24]:

$$\frac{e^{ik|\boldsymbol{r}-\boldsymbol{r'}|}}{|\boldsymbol{r}-\boldsymbol{r'}|} = \frac{ik}{2\pi}\int_{-\infty}^{\infty}\int_{-\infty}^{\infty} \frac{1}{s_z} e^{ik[s_x(x-x')+s_y(y-y')+s_z|z-z'|]} ds_x ds_y \tag{V.2}$$

where $r = x\hat{\boldsymbol{\imath}} + y\hat{\boldsymbol{\jmath}} + z\hat{\boldsymbol{k}}$, $r' = x'\hat{\boldsymbol{\imath}} + y'\hat{\boldsymbol{\jmath}} + z'\hat{\boldsymbol{k}}$ and

$$s_z = +\sqrt{1-s_x^2-s_y^2} \qquad \text{when } s_x^2+s_y^2 \le 1$$

$$s_z = +i\sqrt{s_x^2+s_y^2-1} \qquad \text{when } s_x^2+s_y^2 > 1$$

Therefore, the Inverse Fourier Transform for the right going wave becomes

$$G(x,y,z,\boldsymbol{r_0}) = \int_{-\infty}^{\infty}\int_{-\infty}^{\infty} \frac{e^{i\sqrt{k^2-(2\pi f_x)^2-(2\pi f_y)^2}(z+z_0)}}{2k\sqrt{1-(2\pi f_x/k)^2-(2\pi f_y/k)^2}} e^{i(2\pi f_x x+2\pi f_y y)} \mathrm{df_x df_y} \tag{V.3}$$

Under the change of variables:

$$s_x = \frac{2\pi f_x}{k} \qquad s_y = \frac{2\pi f_y}{k}$$
$$ds_x = \frac{2\pi \mathrm{df_x}}{k} \quad \mathrm{ds_y} = \frac{2\pi \mathrm{df_y}}{\mathrm{k}}$$

Equation V.3 becomes:

$$G(s_x, s_y, z, \boldsymbol{r_0}) = \int_{-\infty}^{\infty}\int_{-\infty}^{\infty} \frac{e^{i\sqrt{k^2-k^2s_x^2-k^2s_y^2}(z+z_0)}e^{i(ks_xx+ks_yy)}}{2k\sqrt{1-s_x^2-s_y^2}} \left(\frac{k}{2\pi}\right)\left(\frac{k}{2\pi}\right)\mathrm{ds_x ds_y} \tag{V.4}$$
$$= \frac{k}{8\pi^2}\int_{-\infty}^{\infty}\int_{-\infty}^{\infty} \frac{e^{i(k\sqrt{1-s_x^2-s_y^2}(z+z_0)+ks_xx+ks_yy)}}{\sqrt{1-s_x^2-s_y^2}}\mathrm{ds_x ds_y}$$

and, substituting equation V.4 into equation V.2, we arrive at the following:

$$G(x, y, z, \boldsymbol{r_0}) = \frac{1}{i4\pi}\frac{e^{ik|\boldsymbol{r}-\boldsymbol{r_0}|}}{|\boldsymbol{r}-\boldsymbol{r_0}|} \tag{V.5}$$

Operating at far field, this Green's function would then be simplified to

$$\frac{e^{ik|\boldsymbol{r}-\boldsymbol{r_0}|}}{i4\pi|\boldsymbol{r}-\boldsymbol{r_0}|} \sim \frac{e^{ikr}}{i4\pi r}e^{-ik\hat{r}\cdot\boldsymbol{r_0}} \tag{V.6}$$

where $\hat{r}$ is the unit vector pointing in the $\boldsymbol{r}$ direction [Ref. 25].

## B. GREEN'S FUNCTION IN MEDIA

We make a coordinate transformation of Equation IV.47 and Equation IV.48 for reasons to be explained in the following sections. Use the relationship in equation IV.12, and substitute the spatial frequencies in for the wave number such that we get the following (see Figure 9):

$$2\pi f_x = k\sin\theta\cos\phi \qquad 2\pi f_y = k\sin\theta\sin\phi \tag{V.7}$$
$$2\pi f_z = k\cos\theta$$

In equation IV.47, we notice that $\frac{e^{i\sqrt{N}z_0}}{2\sqrt{N}}e^{i\sqrt{k^2-|\boldsymbol{F}|^2}z}$ is the planar expansion of the spherical wave. We use this observation to see some physical similarities of

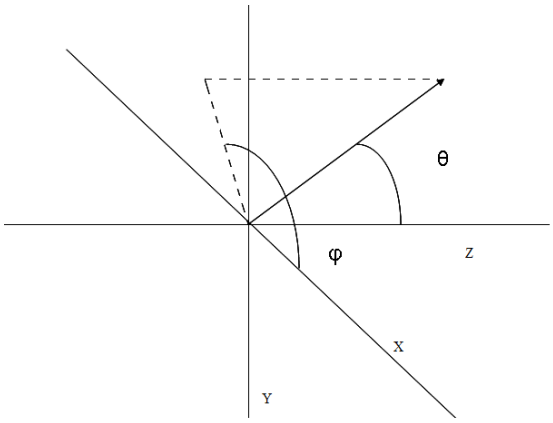


Figure 9. Coordinate Axis

the other waves. The reflection of the wave in Equation IV.47 can be written as $R\frac{e^{i\sqrt{N}z_0}}{2\sqrt{N}}e^{-i\sqrt{k^2-|\boldsymbol{F}|^2}z}$. And so the returning wave is also spherical in nature:

$$R = \frac{(N-N_m)+(N_m-N)e^{i2\sqrt{N_m}L}}{(\sqrt{N_m}+\sqrt{N})^2-(\sqrt{N_m}-\sqrt{N})^2e^{i2\sqrt{N_m}L}} \tag{V.8}$$

$$\sqrt{N_m} = \sqrt{n_m^2k^2-(2\pi f_x)^2-(2\pi f_y)^2} \quad \sqrt{N} = \sqrt{k^2-(2\pi f_x)^2-(2\pi f_y)^2} \tag{V.9}$$

From equation V.7, we rewrite equation V.9 as

$$\sqrt{N_m} = k\sqrt{n_m^2-\sin^2\theta} \quad \sqrt{N} = k\sqrt{1-\sin^2\theta} = k\cos\theta \tag{V.10}$$

Substituting equation V.10 into V.8, we get the following:

$$R(\theta) = \frac{(1-n^2)+(n^2-1)e^{i2kL\sqrt{n^2-\sin^2\theta}}}{(\sqrt{n^2-\sin^2\theta}+\sqrt{1-\sin^2\theta})^2-(\sqrt{n^2-\sin^2\theta}-\sqrt{1-\sin^2\theta})^2e^{i2kL\sqrt{n^2-\sin^2\theta}}} \tag{V.11}$$

$$= \frac{(1-n^2)+(n^2-1)e^{i2kL\sqrt{n^2-\sin^2\theta}}}{(\sqrt{n^2-\sin^2\theta}+\cos\theta)^2-(\sqrt{n^2-\sin^2\theta}-\cos\theta)^2e^{i2kL\sqrt{n^2-\sin^2\theta}}}$$

The Inverse Fourier Transform defined in equation V.1, with the following change of variables:

$$f_x = \frac{k}{2\pi}\sin\theta\cos\phi \quad f_y = \frac{k}{2\pi}\sin\theta\sin\phi$$

so that

$$\begin{vmatrix} \frac{\partial f_x}{\partial\theta} & \frac{\partial f_x}{\partial\phi} \\ \frac{\partial f_y}{\partial\theta} & \frac{\partial f_y}{\partial\phi} \end{vmatrix} = \begin{vmatrix} \frac{k}{2\pi}\cos\theta\cos\phi & -\frac{k}{2\pi}\sin\theta\sin\phi \\ \frac{k}{2\pi}\cos\theta\sin\phi & \frac{k}{2\pi}\sin\theta\cos\phi \end{vmatrix} = \left(\frac{k}{2\pi}\right)^2\cos\theta\sin\theta$$

The spatial reflected Green's function becomes

$$G(x,y,z,\boldsymbol{r_0}) = \iint \hat{G}(\theta,\boldsymbol{r_0})e^{i(kx\sin\theta\cos\phi+ky\sin\theta\sin\phi)}\left(\frac{k}{2\pi}\right)^2\cos\theta\sin\theta\mathrm{d}\theta\mathrm{d}\phi \quad \text{(V.12)}$$

where $\hat{G}(\theta,z,\boldsymbol{r_0}) = R(\theta)\frac{e^{ikz_0\cos\theta}}{2k\cos\theta}e^{-ikz\sqrt{1-\sin^2\theta}}$

It is easy to see that, under the coordinate transformation, Equation IV.47 can be made into Equation V.12, but the limits of integration are not very obvious. Because we are summing the contributions of all the waves from various propagation directions, we can see that $\phi$ varies from 0 to $2\pi$. The projection of the propagation vector onto the $x-y$ plane is symmetric for any given angle $\theta$ normal to the media. However, the $\theta$ coordinate requires more careful analysis. In its cartesian form (Equation V.1), the Inverse Fourier transform suggests that there will be an area of integration where $f_x$ and $f_y$, the projected components of the propagation vector onto the $x-y$ plane, will be large enough that the argument of the exponential of $z$ in the frequency domain of the Green's function is no longer complex-valued but instead, becomes exponentially decaying in the $z$ direction. In the following section, we shall discuss this effect, and discuss how $\theta$ will have to be adjusted to include this effect.

## C. ANGLE OF REFLECTION/INCIDENCE

Because the Green's functions are continuous at the boundaries, the total field at the interface between any two media must obey *incident wave + reflected wave = transmitted wave* for all the regions in space where there is a change in the index of

refraction. Since this requirement must hold true for all time, it must be frequency independent. Therefore

$$\omega(z<0)=\omega(0\le z\le L)=\omega(L<z) \tag{V.13}$$

Now, for the reflection at a surface, this requirement becomes

$$c(z<0)k_{right-going}=c(z<0)k_{left-going}\rightarrow k_{right-going}=k_{left-going} \tag{V.14}$$

Because the waves must be continuous at the interface, the projection of the propagation vector onto the $x-y$ plane will be the same at the boundaries($z=0$ and $z=L$). Therefore

$$k_x=2\pi f_x,\qquad k_y=2\pi f_y,\qquad \text{and } k\sin\theta$$

must the same at $z=0$ and $z=L$ for all the waves (incident, reflected, transmitted). From Equation IV.47, a single wave propagating to the right from the source can be written as

$$G_{incident}=\hat{G}(f_x,f_y,z,\boldsymbol{r_0})e^{i(2\pi f_x x+2\pi f_y y)} \tag{V.15}$$

$$=\frac{e^{i\sqrt{N}z_0}}{2\sqrt{N}}e^{i\sqrt{k^2-|\boldsymbol{F}|^2}z}e^{i(2\pi f_x x+2\pi f_y y)} \tag{V.16}$$

and the reflected wave (the left going wave) is written as

$$G_{reflected}=\frac{(N-N_m)+(N_m-N)e^{i2\sqrt{N_m}L}}{(\sqrt{N_m}+\sqrt{N})^2-(\sqrt{N_m}-\sqrt{N})^2e^{i2\sqrt{N_m}L}}\frac{e^{i\sqrt{N}z_0}}{2\sqrt{N}}e^{-i\sqrt{k^2-|\boldsymbol{F}|^2}z}e^{i(2\pi f_x x+2\pi f_y y)} \tag{V.17}$$

Comparing the exponents, we see that only the $z$-component of the propagation vector is different by a negative sign with the same magnitude. And seeing that the $k$ must be equal, we conclude

$$\underbrace{\sqrt{k^2-|\boldsymbol{F}|^2}}_{incident}=\underbrace{\sqrt{k^2-|\boldsymbol{F}^2|}}_{reflected} \tag{V.18}$$

$$k\cos\theta_{inc} = k\cos\theta_{ref} \tag{V.19}$$

$$\theta_{inc} = \theta_{ref} \tag{V.20}$$

This is the familiar Law of Reflection.

## D. SNELL'S LAW

For transmission, we can verify Snell's Law in the same manner: The frequencies and the projection of the propagation vector at the $x-y$ plane need to be the same due to the boundary conditions discussed earlier. This requirement means:

$$\begin{aligned} \omega(z<0) &= \omega(0\le z\le L) \\ ck_{inc} &= \frac{c}{n}k_{trans} \\ nk_{inc} &= k_{trans} \end{aligned}$$

If we measure $\theta_{trans}$ from the normal (see Figure 10), we can see from the geometry that

$$\sin\theta_{trans} = k_{inc}\sin\theta_{inc}/nk_{inc}$$

$$n\sin\theta_{trans} = \sin\theta_{inc} \tag{V.21}$$

This is Snell's Law. Equation V.21 suggests that there is a limit to the angle for transmission because the sine function has a range between $-1$ and 1. But if we need to integrate further into infinity, we cannot be restricted to real angles. Stratton [Ref. 34] introduces the complex angle of incidence through which the sine functions will become hyperbolic functions. This approach can be used to account for the evanescing waves, and is implicit in the Inverse Fourier Transform of Equations (IV.47), (IV.48), (IV.51),(IV.52). In the Cartesian form, we can see that $f_z \to i\infty$ as $f_x \to \pm\infty$ or $f_y \to \pm\infty$.

To see this in the spherical transformation, we examine at the $z$-component of Equation V.7: $\cos\theta = \frac{2\pi f_z}{k} = \frac{\sqrt{k^2-(2\pi f_x)^2-(2\pi f_y)^2}}{k}$. If the combination of $f_x^2$ and $f_y^2$ is larger than $k^2$, then

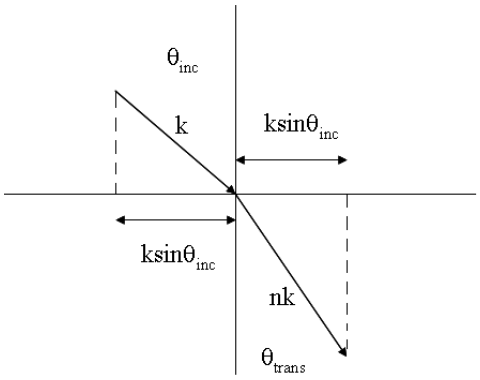


Figure 10. Snell's Law

$$\cos\theta = \frac{i\sqrt{(2\pi f_x)^2 + (2\pi f_y)^2 - k^2}}{k} \to i\infty \tag{V.22}$$

as either $f_x$ or $f_y$ approaches to infinity. From the geometry in Figure 9, $\theta$ must go from 0 to $\pi/2$, but which branch of $\theta$ should be used in the complex plane? A complex angle of incidence indicates that $\theta$ should be of the form $\theta = \alpha + i\beta$, and so by trig identity:

$$\cos(\theta) = \cos(\alpha + i\beta) = \cos(\alpha)\cos(i\beta) - \sin(\alpha)\sin(i\beta) \tag{V.23}$$

$$= \cos(\alpha)\cosh(\beta) - i\sinh(\beta)\sin(\alpha) \tag{V.24}$$

Our allowable angles $\theta \leq \pi/2$ and, in order for Equation V.22 to be true, $\beta$ must go towards $-\infty$ since $\sinh(\beta)$ is an odd function. Therefore, we choose a path for which $\theta = 0 \to \frac{\pi}{2} - i\infty$.

## E. EVANESCING WAVES

We consider the region $-z_0 < z < 0$. From Equations (IV.47) and (IV.51), we consider the reflection and the transmission for a single wave front.

$$G(x, y, z, \boldsymbol{r}_0) = \tilde{A}(f_x, f_y)e^{-i\sqrt{k^2-(2\pi f_x)^2-(2\pi f_y)^2}(z+z_0)}e^{i(2\pi f_x x + 2\pi f_y y)} \tag{V.25}$$

$$G(x, y, z, \boldsymbol{r}_0) = \tilde{A}'(f_x, f_y)e^{i\sqrt{n^2k^2-(2\pi f_x)^2-(2\pi f_y)^2}(z+z_0)}e^{i(2\pi f_x x + 2\pi f_y y)} \tag{V.26}$$

where $\tilde{A}(f_x, f_y)$ and $\tilde{A}'(f_x, f_y)$ can be complex or real-valued amplitudes.

Consider the reflected wave: the propagation vector of the reflected wave must be parallel to the $x-y$ plane before the wave can start to evanesce. Once this condition exists, we can see that the exponent in the z direction becomes real, and the only imaginary portion is the argument $2\pi f_x x + 2\pi f_y y \equiv \boldsymbol{F} \cdot x\hat{\boldsymbol{\imath}} + y\hat{\boldsymbol{\jmath}}$. Therefore, the wave propagation is parallel to the media before it can start to evanesce. But from a larger index of refraction to air (which is the case at $0 \leq z \leq L$) where the rays bend away from the normal, one can see from Equations (IV.48) and (IV.51) that there is an angle of incidence will result in a transmission angle that is parallel to the surface. This is the condition for total internal reflection, and the angle is the critical angle. From this view point as the $z$ component of the incident wave inside the medium decreases, the angle of incidence increases, and thus the transmitted wave will start to evanesce. As either $f_x$ or $f_y$ increases further, the conditions are met where the reflected waves will also evanesce in the medium. Since the nature of the Green's function changes at the boundary $z = 0$ and $z = L$, the energy of the evanescent wave would return back into the media pertinent to the appropriate region of the Green's function. For example, at $z < 0$ no energy from the evanescing waves from reflection would go into the medium, nor would any energy from the evanescing wave from transmission contribute into the air.

From this point on, we will ignore the effects of the evanescent waves because we will assume the transmitter and receiver are sufficiently far away from this region. But,we can see that in a half-space $z < 0$, the intensity $G^*G = A^*Ae^{2\sqrt{(2\pi f_x x)^2+(2\pi f_y y)^2-k^2}(z+z_0)}$ becomes smaller as $z$ gets increasingly negative. We expect therefore that the evanescent contribution will be small, and we should be able to neglect such effects.

## F. REDUCTION OF THE INTEGRAL

The motivation behind the coordinate transformations of Equations (IV.47), (IV.48),(IV.51),(IV.52) is twofold. First, they will allow us to reduce the double integral of Equation V.12 into a single integral, which is more tractible. But we

also do this transformation in conformity to Brekhovskikh's model. This approach will allow us to set up the contour integral which we will present in this section and perhaps be able to solve in the future. Since the method for which this transformation is the same for all the Green's functions, we will demonstrate it for the case of the reflected Green's function in this section.

The symmetry in the $\phi$ direction implies a switch to polar coordinates:

$$x = \rho\cos\phi' \quad y = \rho\sin\phi' \tag{V.27}$$

Substituting this equation into (V.12), yields

$$G(\rho, z, \boldsymbol{r_0}) = \int_0^{2\pi}\int_0^{\frac{\pi}{2}-i\infty} \hat{G}(\theta, z, \boldsymbol{r_0}) e^{i(k\rho\sin\theta\cos\phi'\cos\phi + k\rho\sin\theta\sin\phi'\sin\phi)} \left(\frac{k}{2\pi}\right)^2 \cos\theta\sin\theta \mathrm{d}\theta\mathrm{d}\phi$$

Since

$$2\pi J_0(k\rho\sin\theta) = \int_0^{2\pi} e^{ik\rho\cos(\phi-\phi')}\mathrm{d}\phi$$

We are left with a Bessel Transform:

$$G(\rho, z, \boldsymbol{r_0}) = \int_0^{\frac{\pi}{2}-i\infty} \hat{G}(\theta, z, \boldsymbol{r}_0) \left(\frac{k}{2\pi}\right)^2 2\pi J_0(k\rho\sin\theta)\cos\theta\sin\theta\mathrm{d}\theta \tag{V.28}$$

Because the Hankel functions are a linear combination of the Bessel series of the first and second order, Brekhovskikh [Ref. 2] writes the Bessel $J_0$ in the following way:

$$J_0(k\rho\sin\theta) = \frac{1}{2}\left[H_0^{(1)}(k\rho\sin\theta) + H_0^{(2)}(k\rho\sin\theta)\right] \tag{V.29}$$

and, using the Hankel function property

$$H_0^{(2)}(e^{-i\pi}x) = -H_0^{(1)}(x),$$

Equation V.28 becomes

$$G(\rho, z, \boldsymbol{r}_0) = \frac{k^2}{2\pi}\int_0^{\frac{\pi}{2}-i\infty} \hat{G}(\theta, z, \boldsymbol{r_0})\frac{1}{2}\left[H_0^{(1)}(k\rho\sin\theta) + H_0^{(2)}(k\rho\sin\theta)\right]\cos\theta\sin\theta\mathrm{d}\theta$$

$$= \frac{k^2}{4\pi}\left[\int_0^{\frac{\pi}{2}-i\infty} \hat{G}(\theta, z, \boldsymbol{r_0})\cos\theta\sin\theta H_0^{(1)}(k\rho\sin\theta)\mathrm{d}\theta + \int_0^{\frac{\pi}{2}-\mathrm{i}\infty} \hat{\mathrm{G}}(\theta, \mathrm{z}, \boldsymbol{r_0})\cos\theta\sin\theta \mathrm{H}_0^{(2)}(\mathrm{k}\rho\sin\theta)\mathrm{d}\theta\right]$$

$$= \frac{k^2}{4\pi}\left[\int_0^{\frac{\pi}{2}-i\infty} \hat{G}(\theta, z, \boldsymbol{r_0})\cos\theta\sin\theta H_0^{(1)}(k\rho\sin\theta)\mathrm{d}\theta + \int_{-(\frac{\pi}{2}-\mathrm{i}\infty)}^{0} \hat{\mathrm{G}}(\theta, \mathrm{z}, \boldsymbol{r_0})\cos\theta\sin\theta \mathrm{H}_0^{(1)}(\mathrm{k}\rho\sin\theta)\mathrm{d}\theta\right]$$

The reflection Green's function is therefore

$$G(\rho, z, \boldsymbol{r_0}) = \frac{k^2}{4\pi}\int_{-\frac{\pi}{2}+i\infty}^{\frac{\pi}{2}-i\infty} \hat{G}(\theta, z, \boldsymbol{r_0})\cos\theta\sin\theta H_0^{(1)}(k\rho\sin\theta)\mathrm{d}\theta$$

$$= \frac{k^2}{4\pi}\int_{-\frac{\pi}{2}+i\infty}^{\frac{\pi}{2}-i\infty} R(\theta)\frac{e^{ikz_0\cos\theta}}{2k\cos\theta}e^{-ikz\sqrt{1-\sin^2\theta}}\cos\theta\sin\theta H_0^{(1)}(k\rho\sin\theta)\mathrm{d}\theta$$

$$= \frac{k^2}{4\pi}\int_{-\frac{\pi}{2}+i\infty}^{\frac{\pi}{2}-i\infty} \frac{(1-n^2)+(n^2-1)e^{i2kL\sqrt{n^2-\sin^2\theta}}}{(\sqrt{n^2-\sin^2\theta}+\cos\theta)^2-(\sqrt{n^2-\sin^2\theta}-\cos\theta)^2 e^{i2kL\sqrt{n^2-\sin^2\theta}}} \tag{V.30}$$

$$\times \frac{e^{ikz_0\cos\theta}}{2k\cos\theta}e^{-ikz\sqrt{1-\sin^2\theta}}\cos\theta\sin\theta H_0^{(1)}(k\rho\sin\theta)\mathrm{d}\theta$$

## G. ANALYSIS

Performing the contour integration of Equation V.30 requires very advanced mathematical concepts. One has to approximate the integral by assuming certain conditions of the argument of the integrand — such as wave number being very large. By using the Method of Steepest Decent where one has to find the saddle points and determine the right saddle path, an analytical approximate solution can result from Equation V.30. We will not perform this integral in this thesis, but we will analyze the integral.

First, the limits of integration tell us that the summation goes from all the allowed real angles to the complex angles (which is the region of evanescent waves).

Let us examine the latter half of the integral. We saw earlier that Equation V.3 is the free space Green's function. Analogously

$$\frac{k^2}{4\pi}\int_{-\frac{\pi}{2}+i\infty}^{\frac{\pi}{2}-i\infty}\frac{e^{ikz_0\cos\theta}}{2k\cos\theta}e^{-ikz\sqrt{1-\sin^2\theta}}\cos\theta\sin\theta H_0^{(1)}(k\rho\sin\theta)\mathrm{d}\theta \tag{V.31}$$

would give us the free space Green's function (The only difference being that it is left going from the negative sign given as $e^{-ikz\sqrt{1-\sin^2\theta}}$). The stunning idea is that the reflected wave is spherical in nature after performing the Hankel Transform. This is the idea behind Huygen wavelets as shown in Figure 11. From the figure you can see that the returning waves are spherical, and they superpose with each other to create a wave front. The singularities of Equation V.30 are the trapped modes of either the TE or TM waves in the media (C. Scandrett, personal communication, December 2006), [Ref. 32]. This approach can be better seen when converting the Cartesian form into the polar form instead of the spherical form (See Appendix G). The branch cuts show the forbidden regions, and these are the regions of evanescing waves which Brekhovskikh describes in meticulous detail, and whch require a contour integration path that will account for these forbidden regions [Ref. 2].

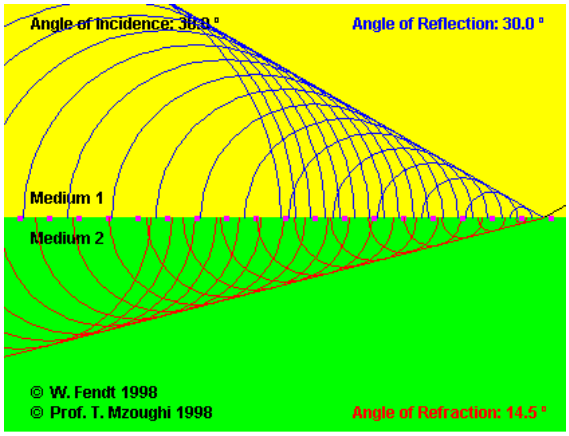


Figure 11. Huygen Wavelets. Figure was taken from [Ref. 35]

On the other side of the media ($z > L$), we can also use Huygen Wavelets. From its Cartesian form, we can demonstrate see this effect in a MATLAB simula-

tion(see Appendix F). In Figure 12, the observer is on the plane $z = 3$m, and we can see these wavelets.

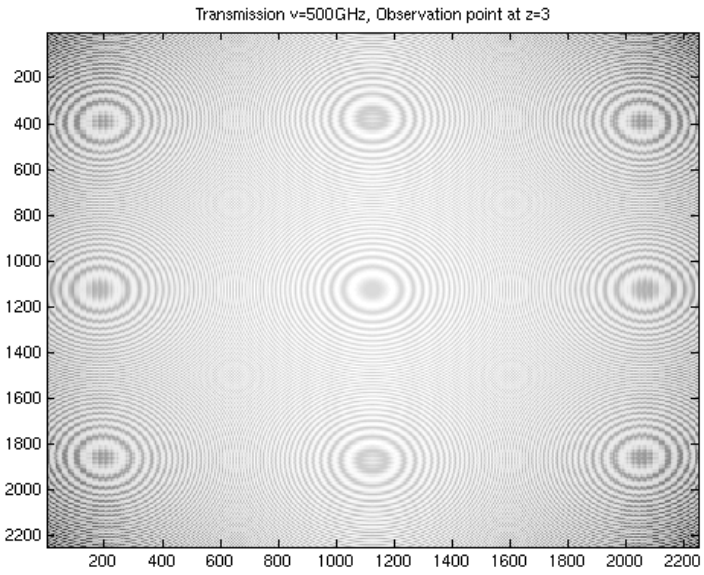


Figure 12. Huygen Wavelets. Observation at $z = 3$m

It maybe beneficial to perform the integral in Equation V.30 to obtain the Green's function in the spatial domain because it shows us the effects of all these spherical waves. However, this thesis will focus on an imaging algorithm, and we will work in the spatial frequency domain since we already have an analytical form. We will simulate the data and perform the transforms numerically.

## H. MATERIAL ANALYSIS

Listed in Table II are some common barrier materials. We will examine the reflection from the wall. As expected, the type of material will greatly affect the amount of reflection from the wall. And there are frequency windows at which we get minimal reflection. Figures 13, 14, and 15 show the reflectivity of materials listed in Table II, with barrier width of half a meter.

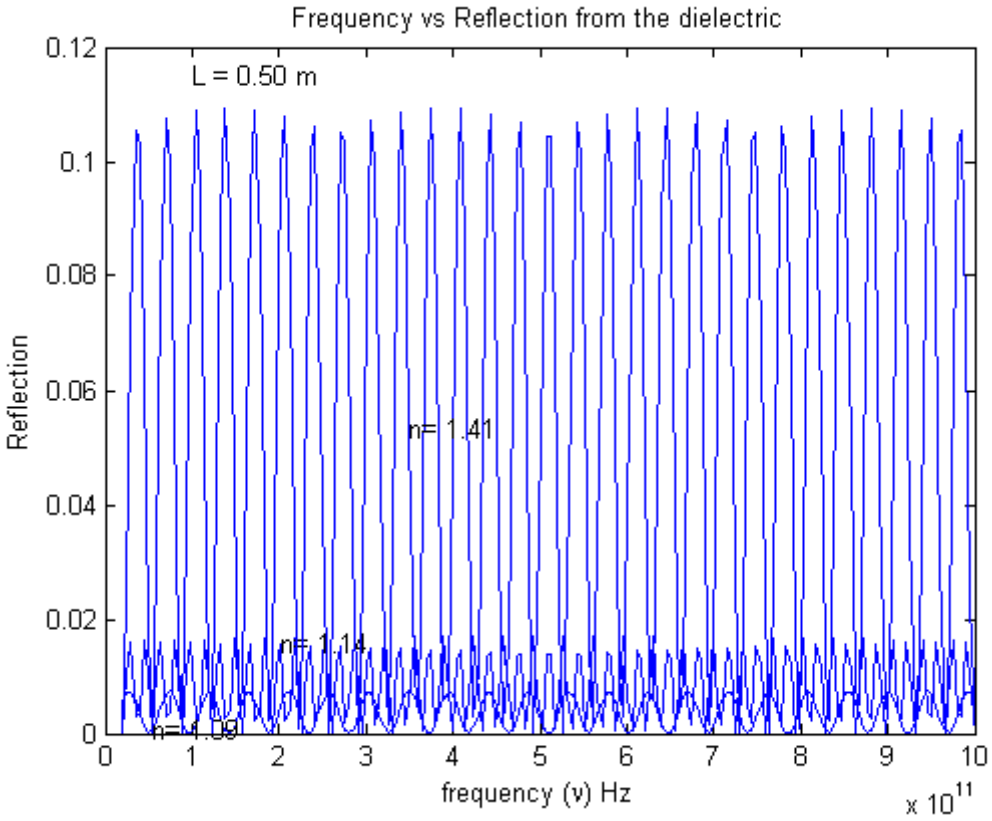


Figure 13. Reflection (Cloth, Balsa Wood, and Wooden Door)

The MATLAB code used to generate these results uses the reflection coefficient calculated in this thesis. The code is modeled for a plane wave parallel to the surface, and its interaction within the media.

We see from Figure 13 that the reflection from cloth and wood are very small at THz frequencies of current interest and so the material becomes almost transparent to these waves.

As the index of refraction increases, the reflections coming back from the medium become more significant as shown in Figure 14. But there are key frequencies where reflection can be minimized. For the case of Dry Concrete, a common material used in construction of most walls, the material essentially becomes transparent at 500 GHz. But a potential problem relates to the target you trying to image. At

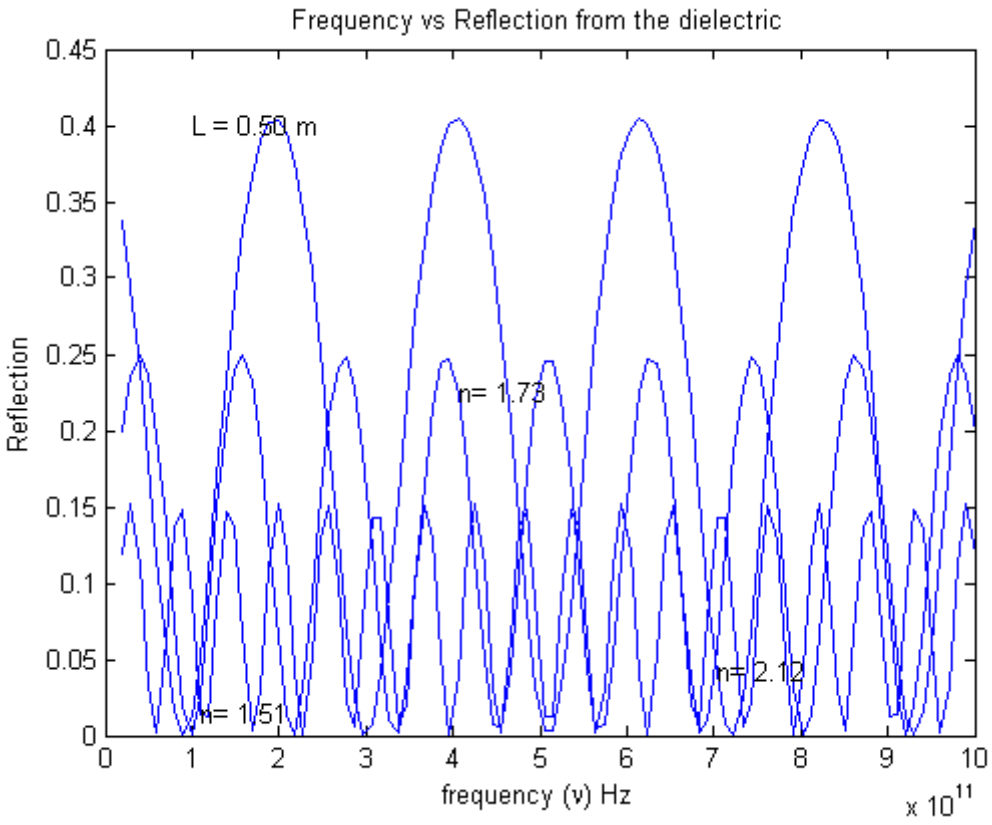


Figure 14. Reflection (Plexiglas, Paper, Dry Concrete)

500 GHz, plane waves will penetrate dry concrete with little loss (at one meter in depth). If you want to get information on people, this frequency would be great. If you look at Figure 15, muscle is not very reflective at this frequency, but blood is as high as 90% reflective. Thus, gathering data scattered from people at this frequency would be "ideal". In general, a balance must be achieved between wave penetration of the dielectric and return information from the object—unless the object is metallic (in which case the only concern then would be determining the best penetrating frequency).

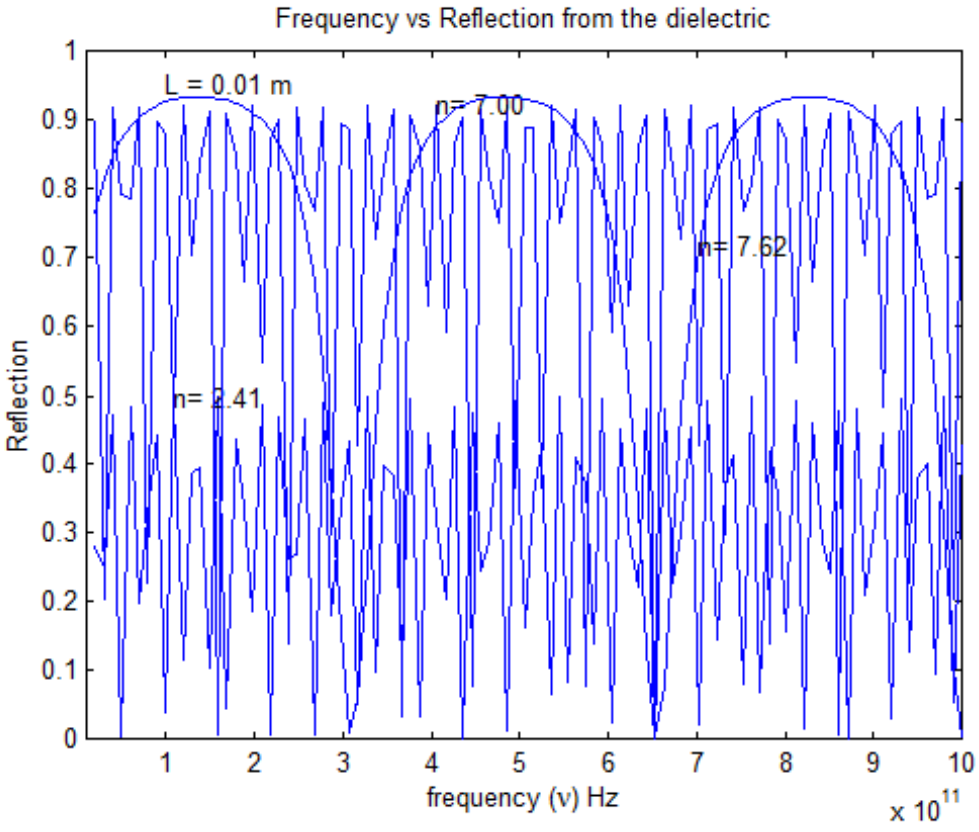


Figure 15. Reflection (Diamond, Muscle, Blood)

| Index of Refraction | |
|---|---|
| Cloth | 1.09 |
| Balsa Wood | 1.14 |
| Wooden Door | 1.41 |
| Plexiglas | 1.51 |
| Paper | 1.73 - 2.00 |
| Dry Concrete | 2.12 |
| Diamond | 2.41 |
| Muscle at 37 °C | 7.00 |
| Blood at 37 °C | 7.62 |

Table II. Typical index of refraction for common items

THIS PAGE INTENTIONALLY LEFT BLANK

# VI. INTEGRAL EQUATIONS

## A. WAVE EQUATION

The Electric field obeys the time independent Helmholtz equation. If we allow the index of refraction to vary so slowly with position that it is essentially constant over distances on the order of a wavelength, then we do not have to concern ourselves with the coupling of Maxwell's Equations [Ref. 25], and thus we may examine its scalar form:

$$\nabla^2 E(\boldsymbol{r}) + k^2 n_{obj}^2(\boldsymbol{r}) E(\boldsymbol{r}) = 0 \tag{VI.1}$$

We can re-write this equation as

$$\nabla^2 E(\boldsymbol{r}) + k^2 E(\boldsymbol{r}) = -\underbrace{k^2 (n_{obj}(\boldsymbol{r})^2 - 1)}_{U} E(\boldsymbol{r}) \tag{VI.2}$$

where $U$ denotes the "scattering potential" of the medium.

$$\nabla^2 E(\boldsymbol{r}) + k^2 E(\boldsymbol{r}) = -U(\boldsymbol{r}) E(\boldsymbol{r}) \tag{VI.3}$$

The the Green's function of the Helmholtz equation will be a solution of

$$(\nabla^2 + k^2) G(\boldsymbol{r} - \boldsymbol{r}_0) = -\delta(\boldsymbol{r} - \boldsymbol{r}_0) \tag{VI.4}$$

## B. LIPPMAN-SCHWINGER EQUATION

We see from Figure 16 that the Green's function is divided into three regions with solutions discussed in the previous chapter. We also know that the Green's function is symmetric so that the response at $\boldsymbol{r}$ due to a concentrated source at $\boldsymbol{r}_0$ is the same as the response at $\boldsymbol{r}_0$ due to a concentrated source at $\boldsymbol{r}$. We will use these ideas to derive the Lippman-Schwinger's Equation and apply the first Born Approximation in its solution. In Equation VI.3, $E(\boldsymbol{r})$ is the total field. If a transmitter is in region III and it emanates a planar wave $E_{inc}(\boldsymbol{r}) = Ae^{-ikz}$ into the media, then this incident wave will be planar inside the medium (region II), and comes out as a planar wave on

the other side into region I as $E'_{inc}(\boldsymbol{r}) = tAe^{-ikz}$ where $t$ is the transmittance. This field satisfies the homogeneous Helmholtz equation

$$\nabla^2 E'_{inc}(\boldsymbol{r}) + k^2 E'_{inc}(\boldsymbol{r}) = 0 \tag{VI.5}$$

$E(\boldsymbol{r})$ can be expressed as the sum of incident field and the scattered field so that

$$E(\boldsymbol{r}) = E'_{inc}(\boldsymbol{r}) + E_{sc}(\boldsymbol{r})$$

So where $E_{sc}(\boldsymbol{r})$ is the field scattered from the target. Equation VI.3 can be therefore simplified to

$$\nabla^2 E_{sc}(\boldsymbol{r}) + k^2 E_{sc}(\boldsymbol{r}) = -U(\boldsymbol{r})E(\boldsymbol{r}) \tag{VI.6}$$

Multiplying Equation VI.4 by $E_{sc}(\boldsymbol{r})$ and Equation VI.6 by $G$, and subtracting the two yields

$$E_{sc}(\boldsymbol{r})\nabla^2 G(\boldsymbol{r}-\boldsymbol{r}_0) - G(\boldsymbol{r}-\boldsymbol{r}_0)\nabla^2 E_{sc}(\boldsymbol{r}) = U(\boldsymbol{r})E(\boldsymbol{r})G(\boldsymbol{r}-\boldsymbol{r}_0) - E_{sc}(\boldsymbol{r})\delta(\boldsymbol{r}-\boldsymbol{r}_0) \tag{VI.7}$$

Using the fact that the Green's function is symmetric, we integrate with respect to $\boldsymbol{r}_0$ throughout the entire Volume $V_R$ and apply Green's Second Theorem to arrive at

$$\begin{aligned} E_{sc}(\boldsymbol{r}) = &\int_{V_R} U(\boldsymbol{r}_0)E(\boldsymbol{r}_0)G(\boldsymbol{r}_0-\boldsymbol{r})\mathrm{d}^3\boldsymbol{r}_0 \\ &- \int_{S_R} \left(E(\boldsymbol{r}_0)\nabla^0 G(\boldsymbol{r}_0-\boldsymbol{r}) - G(\boldsymbol{r}_0-\boldsymbol{r})\nabla^0 E_{sc}(\boldsymbol{r}_0)\right)\cdot \mathrm{d}\boldsymbol{S_R} \end{aligned} \tag{VI.8}$$

The Sommerfeld Radiation condition guarantees us that the fields go to 0 at infinity, and therefore, as the surface area increases with the radius $R$, the area integral vanishes. Furthermore, since the Scattering potential is 0 everywhere outside the scattering object, the volume integral of the entire volume $V_R$ is then shrunk down to just the volume of the scattering object. Therefore, the integral reduces to

$$E_{sc}(\boldsymbol{r}) = \int_{V_0} U(\boldsymbol{r}_0)E(\boldsymbol{r}_0)G(\boldsymbol{r}_0-\boldsymbol{r})\mathrm{d}^3\boldsymbol{r}_0 \tag{VI.9}$$

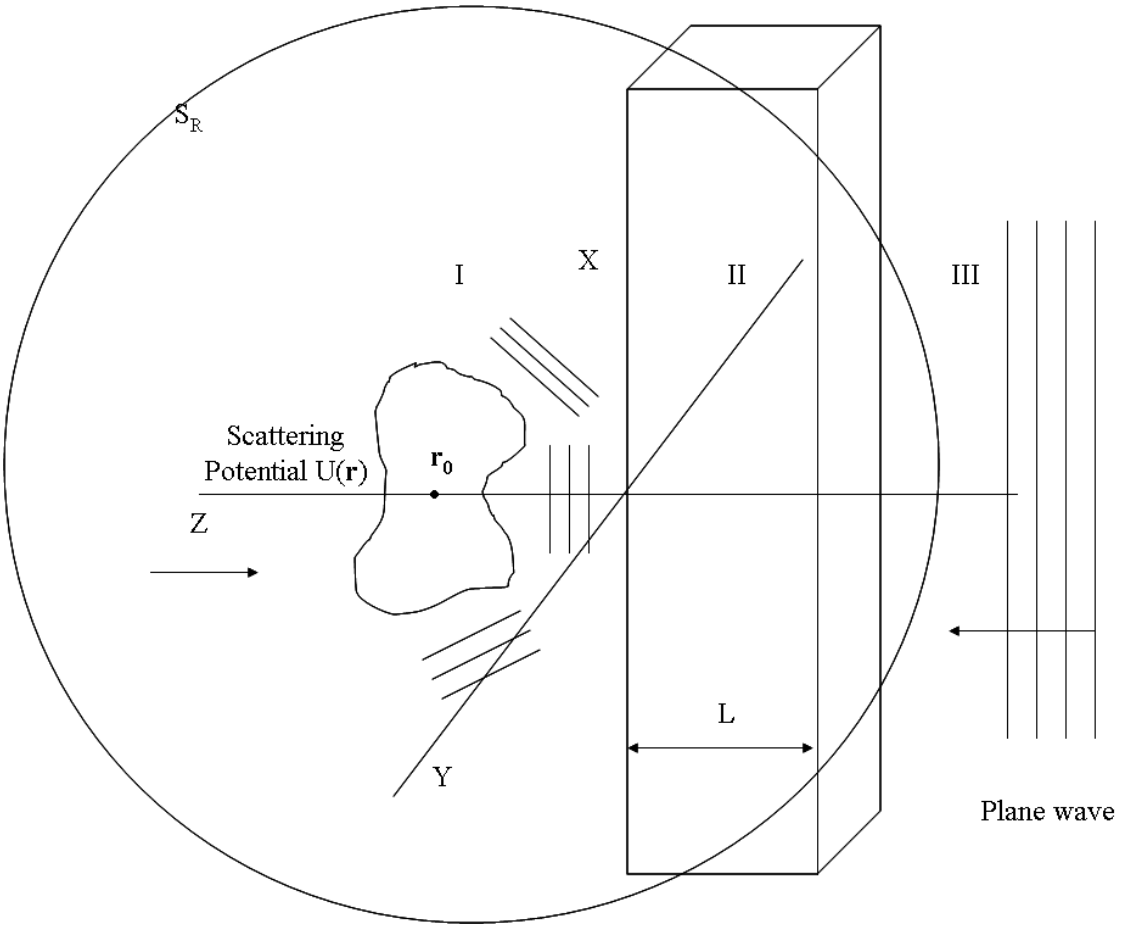


Figure 16. Illustration of a Scattering Medium occupying Volume $V_R$ bounded by a closed Surface $S_R$

This is the Lippman-Schwinger Equation. The Green's function is different for each region, depending on where the observation point is located, particularly along the z-axis:

$$G(\boldsymbol{r}-\boldsymbol{r}_0) = \begin{cases} G_I(\boldsymbol{r}-\boldsymbol{r}_0) & \text{for z} < 0 \\ G_{II}(\boldsymbol{r}-\boldsymbol{r}_0) & \text{for } 0 \leq \text{z} \leq \text{L} \\ G_{III}(\boldsymbol{r}-\boldsymbol{r}_0) & \text{for L} < \text{z} \end{cases} \tag{VI.10}$$

and $G_I$, $G_{II}$ and $G_{III}$ are the respective Inverse Fourier Transforms of Equations (IV.47), (IV.3), (IV.51), and (IV.52).

## C. BORN APPROXIMATION

Substituting Equation VI.9 into Equation Byields

$$E = E'_{inc} + \int_{V_0} U(\boldsymbol{r}_0)E(\boldsymbol{r}_0)G(\boldsymbol{r}_0 - \boldsymbol{r})\mathrm{d}^3\boldsymbol{r}_0 \tag{VI.11}$$

If we formally define the operator

$$(\boldsymbol{A}E)(\boldsymbol{r}) = \int_{V_0} G(\boldsymbol{r}_0 - \boldsymbol{r})E(\boldsymbol{r}_0)\mathrm{d}^3\boldsymbol{r}_0$$

$$\begin{aligned} E &= E'_{inc} + \underbrace{AE}_{E_{sc}} \\ &= E'_{inc} + A(E'_{inc} + AE) \\ &= E'_{inc} + AE'_{inc} + A^2(E'_{inc} + AE) \\ &= ... \end{aligned}$$

Then the Born approximation of Equation VI.11 becomes

$$E = E'_{inc} + \int_{V_0} U(\boldsymbol{r}_0)E'_{inc}(\boldsymbol{r}_0)G(\boldsymbol{r}_0 - \boldsymbol{r})\mathrm{d}^3\boldsymbol{r}_0 \tag{VI.12}$$

$$E_{sc} = \int_{V_0} U(\boldsymbol{r}_0)E'_{inc}(\boldsymbol{r}_0)G(\boldsymbol{r}_0 - \boldsymbol{r})\mathrm{d}^3\boldsymbol{r}_0 \tag{VI.13}$$

## D. THE MODELING SCHEME

In this thesis, we will only account for single scatter events, assuming the scattering from other points to be significantly smaller and so will not add any meaningful contributions. We shall now the Scattering Potential. For point scatterers, we can easily model this as a series of Dirac Delta Functions so that

$$U(\boldsymbol{r}) = \sum_i A_i\delta(\boldsymbol{r} - \boldsymbol{r}_i) \tag{VI.14}$$

where $A_i$ are (complex-valued) scatterer amplitudes. Substituting Equation VI.14 into Equation VI.13 and integrating, we get a summation of Green's functions. Since the receiver will be in region III, we use the Transmitted Green's function in region III.

$$E_{sc}(\boldsymbol{r}) = \sum_i A_i A t e^{-ikz_i} G_{III}(\boldsymbol{r} - \boldsymbol{r}_i) \tag{VI.15}$$

# VII. ALGORITHM

## A. SPATIAL DOMAIN VS FREQUENCY

The Green's function forms a kernel which operates on the Scattering Potential and the Electric field. It is also shift invariant, giving us the special characteristic of the convolution integral. Let us revisit and focus on the volume integral of Equation VI.8

$$E_{sc}(\boldsymbol{r}) = \int_{V_R} U(\boldsymbol{r}_0)E(\boldsymbol{r}_0)G(\boldsymbol{r}_0 - \boldsymbol{r})\mathrm{d}^3\boldsymbol{r}_0 \tag{VII.1}$$

When $R$ becomes infinitely large, the volume integral extends over all space.

$$E_{sc}(x,y,z) = \iiint_{-\infty}^{\infty} U(x_0,y_0,z_0)E(x_0,y_0,z_0)G(x-x_0,y-y_0,z-z_0)\mathrm{dx}_0\mathrm{dy}_0\mathrm{dz}_0 \tag{VII.2}$$

It is the scattering potential that limits this integration to the scattering volume. The first Born approximation of this integral yields

$$E_{sc}(x,y,z) = \iiint_{-\infty}^{\infty} U(x_0,y_0,z_0)E'_{inc}(x_0,y_0,z_0)G(x-x_0,y-y_0,z-z_0)\mathrm{dx}_0\mathrm{dy}_0\mathrm{dz}_0 \tag{VII.3}$$

Since we know the kernel in terms of its spatial frequencies, we perform the convolution integral in the Fourier domain. We reduce the 3D Fourier Transform to a 2D Fourier Transform by holding $z$ constant. The idea is that the receiver will be placed at a fixed $z$ measurement. The 2D Fourier Transform of this convolution integral will result in the 2D Fourier Transform of the Green's function, and a 2D Fourier Transform of the product of $U$ and $E'_{inc}$, which is $U$ convolved with $E'_{inc}$ in the frequency regime. Since our scattering model is a summation of Dirac Delta Functions, the 2D Fourier Transform of Equation VI.15 with respect to $x$ and $y$ is simplified to

$$\iint_{-\infty}^{\infty} E_{sc}(x,y)e^{-i(2\pi f_x x+2\pi f_y y)}\text{dxdy} = \tag{VII.4}$$
$$\iint_{-\infty}^{\infty} \sum_i A_i A t e^{-ikz_i} G_{III}(x-x_i, y-y_i)e^{-i(2\pi f_x x+2\pi f_y y)}\text{dxdy}$$

The scattered field in the spatial frequency domain for a given $z$ is then

$$E(f_x,f_y) = \sum_i A_i A t e^{-ikz} G_{III}(f_x,f_y)e^{-i(2\pi f_x x_i+2\pi f_y y_i)} \tag{VII.5}$$

The advantage of using the frequency domain is that we deal with only products in MATLAB, and therefore, no fancy coding will be required (simple element-to-element matrix multiplications are enough). We will also let the computer calculate the 2D Inverse Fourier Transform to the spatial regime and compare the results.

## B. MATLAB CODE IMPLEMENTATION

Equation VII.5 is the equation we shall use to create our simulated scattered field data. The total field at the transmitter will be composed of the transmitted field of the device, the reflected fields from the wall, the scattered field, and the lateral (evanescing) field. We assume that the evanescing waves will be minimal, and that we are purposely staying away from the evanescing regions. Therefore, the only factors we account for are the transmitted, reflected, and the scattered fields. For our simulation, we neglect the details of the transmitted fields and reflected fields as these will be known measurements in the real world. For image processing, we are interested in the scattered field information, and whether Tikhonov and/or SVD methods will work in mitigating noise corruption.

For simulation purpose, we reduce the propagation number so that the effects of the point scatterers will be amplified. The limitation of this model is that it is computation intensive, and we are limited to the sampling frequency and bandwidth.

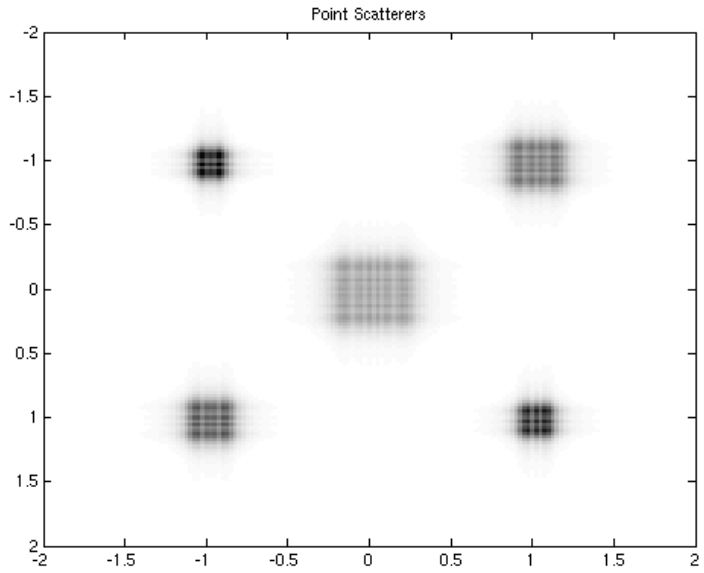


Figure 17. Amplitude of field measurements due to 5 Scattering Points

Figure D displays the noise-free field measurements, collected from 5 scattering points measured at $z = 2$m. To this data, we add Gaussian noise, and we will apply the method of Tikhonov and SVD filtering discussed in Chapter 2.

The code is presented in Appendix D. The idea is to do all the work in the spatial frequency and use a 2-D inverse FFT to bring the results back to the spatial domain.

## C. SIGNAL TO NOISE RATIO

The additive noise is Gaussian noise and applied in the frequency domain. The SNR is calculated by summing up the intensities of each element of the matrix for the signal and the noise, and taking the ratio of the two. This provides a way to gauge our data. We increased the Gaussian noise by multiplying it by a noise factor which gives us the desired SNR value.

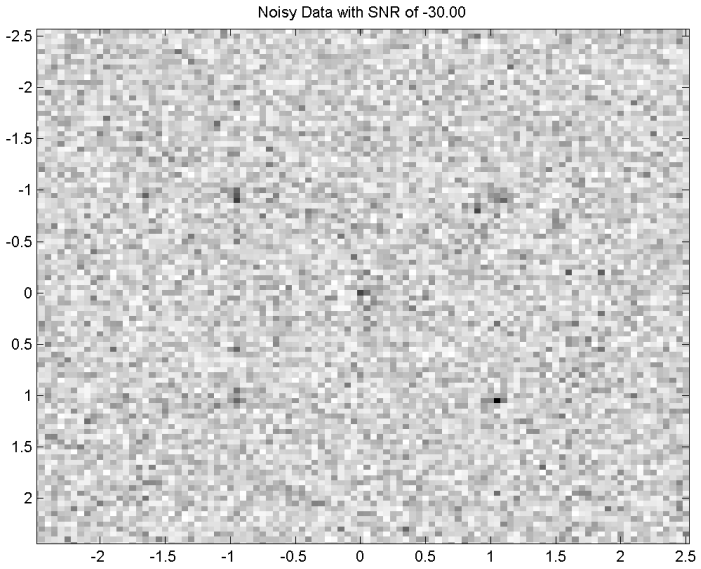


Figure 18. 5 Scattering Points under Gaussian Noise SNR=−30dB

## D. SPATIAL FREQUENCY DOMAIN

Consider the case of a two-point scatterer. For one scatterer, the frequency domain follows Figure 19. The second point scatterer, looks similar to the first one (see Figure 20). The phase shift is hard to observe.

However, when we add the two, we can see the effects of phase interference. (see Figure 21, and upon Fourier inversion, we get what we are supposed to get – two scattering points (see Figure 22).

## E. TIKHONOV REGULARIZATION

From Figure 18, the noise has almost completely masked the signal. Now we apply Tikhonov regularization, and the we will choose the regularization parameter by trial and error. We know that as the regularization parameter decreases, the linear compact operator $R_\alpha$ discussed in Chapter 2 will head towards the Least Squares solution to the problem — and thereby increase the condition number. Thus, we will see that the recovered image will become more unstable (see Figure 23).

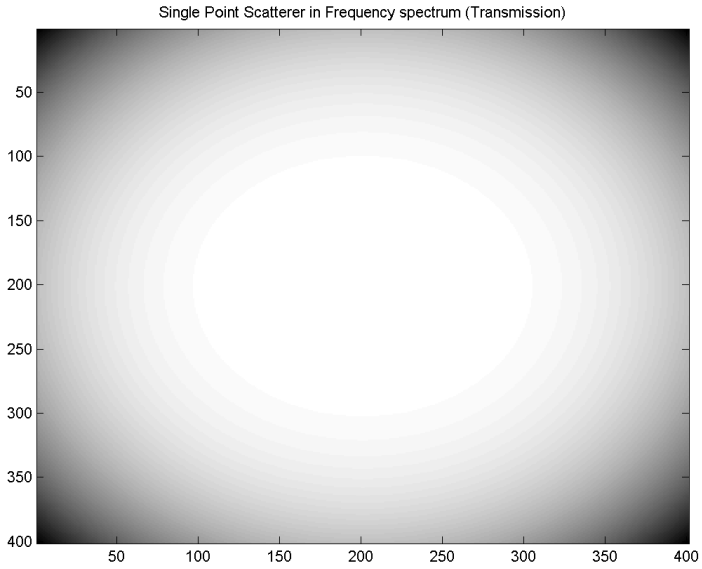


Figure 19. Single Point Scatterer (Spatial Frequency Domain)

This figure shows the ill-conditioned nature of the problem. When the regularization parameter is increased to $\alpha = 10$, we see how well the noise can be mitigated(see Figure 24). There is a trade-off between a large regularization parameter and a small one. A larger regularization parameter will dominate the inverse operator giving you optimization problems, while a small one will give you a least squares solution but a diverging condition number.

## F. TRUNCATION SVD

We now apply the SVD-truncation method. At first, the singular values were truncated at the very large value $\alpha = 10000$, and we see the ill-conditioned behavior (see Figure 25).

The idea is to compare the singular values, and try to locate where the rapid changes of singular values occur and truncate at that point. One parameter was determined to be at $\alpha = 1$, and the image is pulled out of the noise (see Figure 26).

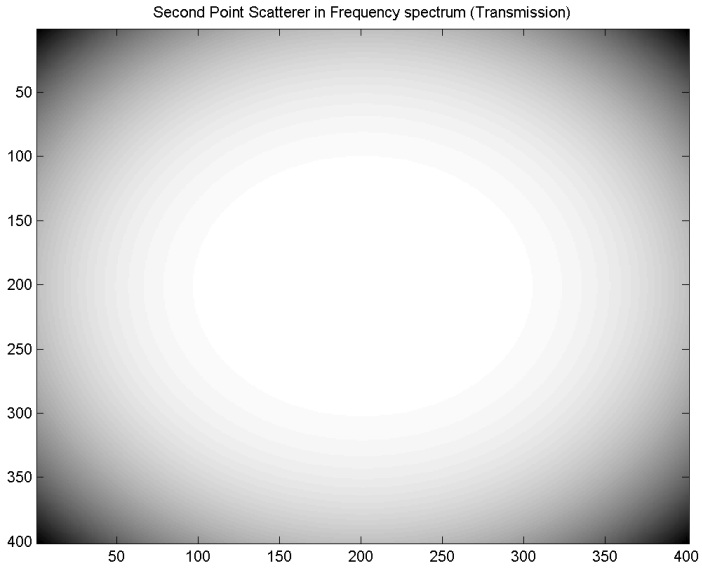


Figure 20. Second Point Scatterer (Spatial Frequency Domain)

One can see that the SVD method appears to do a visually better job in retrieving the signal from the noise, but this may not be generally true.

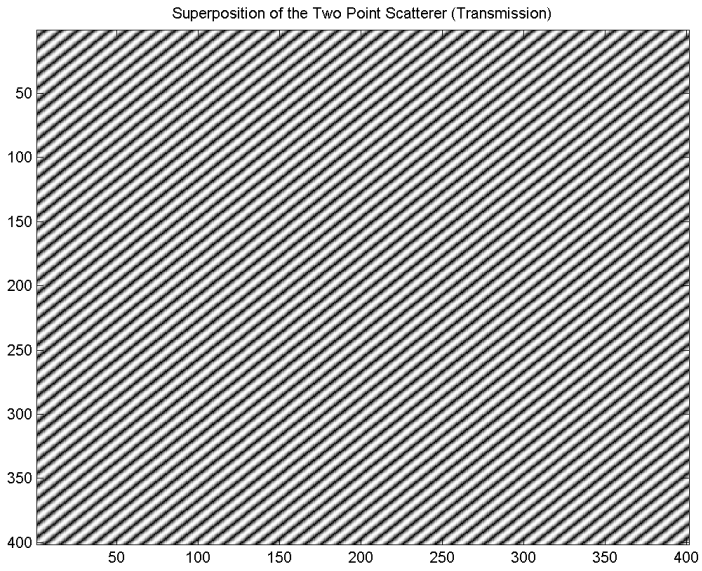


Figure 21. Two Scattering Points (Spatial Frequency Domain)

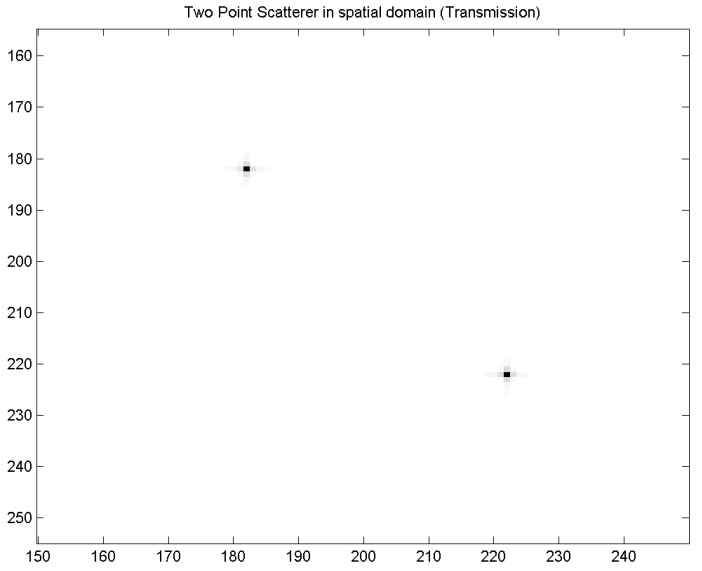


Figure 22. Two Scattering Points (Spatial Domain)

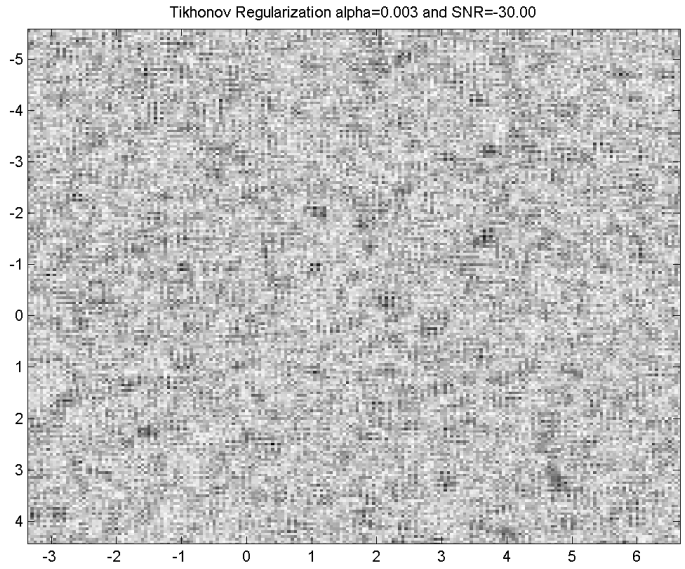


Figure 23. Tikhonov Regularization $\alpha = 0.003$ at SNR$=-30$ dB

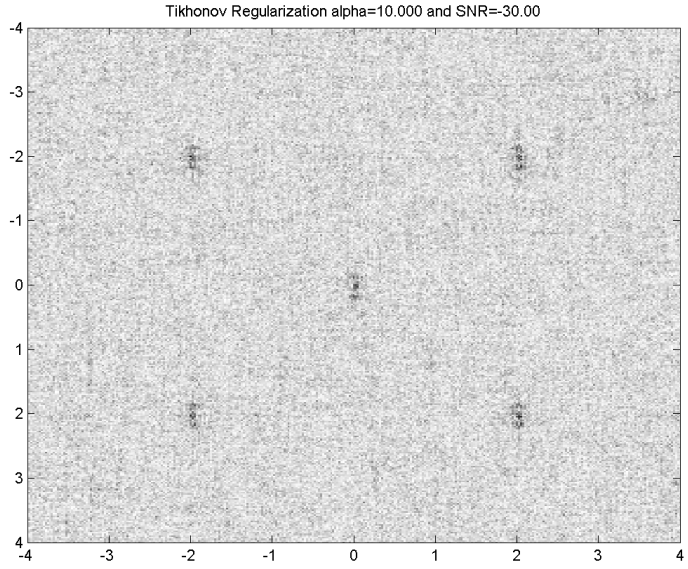


Figure 24. Tikhonov Regularization $\alpha = 10$ at SNR$=-30$ dB

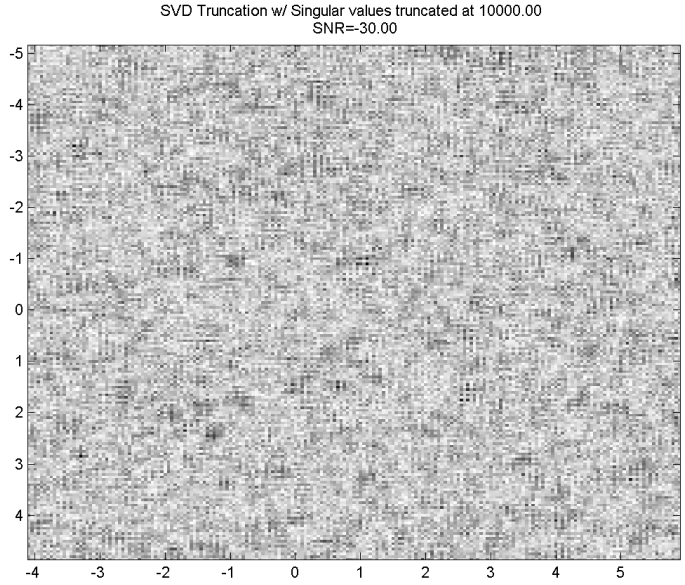


Figure 25. TSVD $\alpha = 10000$ at SNR$=-30$ dB

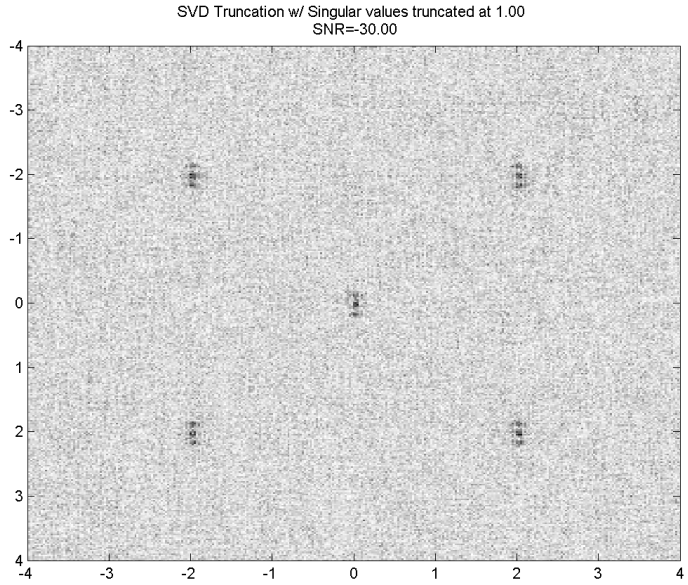


Figure 26. TSVD $\alpha = 1$ at SNR$=-30$ dB

THIS PAGE INTENTIONALLY LEFT BLANK

# VIII. CONCLUSION

Our model has assumed linearly polarizable media with unchanging permittivity. For non-linear materials, the polarization vectors will have to be accounted for separately. Though tedious, this extension would provide us with a more general model. In addition, the material we considered is not magnetizable. These assumptions are generally good, but cannot be true for all Through-the-Wall cases. It is important to note that when the media is both non-linear and magnetic, the Maxwell equations will be coupled and the scalar theory has to be readjusted to fit this model. A complementary examination of common wall materials will be required, and some of the future work is to see how well the model works in "real-life" applications, and how we can adjust the model to fit specific problems. We have demonstrated in this thesis that the scattered field can be modeled as simple summation of Green's functions because we applied the the *weak scatterer model*. When the Born approximation is not valid, we may have to consider other approximations, and we may also want to include multiple scattering in which case the Lippman-Schwinger equation may be extended to include for scatterers from nearby points.

The Rytov Approximation assumes that the wave perturbation is caused by objects through a phase change in the incident wave along the propagation path. It is derived similarly to the way we derived the Born approximation, except the field is comprised of the phases as functions of position. It is said that the Rytov approximation is a more accurate approximation than the standard Born model. In future work, one may take the Lippman-Schwinger Equation and apply Rytov and compare to the Born model. It may be worth applying this to "real" world problems along with the Born model for future work.

We discussed non-conductive dielectrics. For conductive media, the attenuation maybe too great for examining the scattered field. The attenuation of a signal through the media and back maybe masked by the Gaussian noise and the data may

be too noisy for any reasonable image reconstruction algorithm to work. For direct application to real world scenarios, the conductive case may be unlikely to be encountered. For imaging behind walls, most construction materials are not completely made of conductive materials. However, steel bars may pose a problem with back scatter inside the media, which we would have to deal with separately.

We also ignored dispersive effects that need to be examined for various materials for which *a priori* knowledge of the material characteristics must be known in order to make the appropriate approximations for the theory. It will be of interest in future work to make appropriate approximations and account for dispersion by using the Method of Stationary Phase. Such approximate analytical solutions can provide some understanding about how the waves behave in transit through the medium, but also can be much more efficient and accurate in the image reconstruction stage.

The Tikhonov regularization parameter was found by trial and error. There are much more effective ways to determine the regularization parameter such as the L-curve method [Ref. 30]. The Bayesian statistical approach [Ref. 30] to the problem can give us better image reconstruction and might be fruitful for future research.

Our code implementation has some limitations. Since MATLAB can be very memory hungry, the bandwidth examined could not be very wide, nor can one increase the sampling frequencies very high without sacrificing time (and patience). A more efficient computation scheme will be required. In this thesis, I have used short bandwidths with sampling frequencies at Nyquist frequencies to avoid aliasing. A dual core 2Ghz with 6GB of RAM would take $5-15$ minutes to do one full computations for a reasonable frequency bandwidth of $20\text{m}^{-1}$ for $f_x$ and $f_y$. This poses a problem in computation and analysis on systems requiring higher bandwidths. Efficient coding and higher computing power will be required for analysis of larger bandwidths.

# APPENDIX A. THE RIEMANN LEBESGUE LEMMA

$$\lim_{n\to\infty} \int_a^b K(\lambda, s) C \sin(ns) ds = 0 \tag{A.1}$$

Through integration by parts, we get the following and therefore conclude that as $n \to \infty$, the integral will then goes to 0.

$$\lim_{n\to\infty} -\frac{K(\lambda, s)\cos(ns)}{n}\Big|_a^b + \frac{1}{n^2}\int_a^b \frac{\partial K(\lambda, s)}{\partial s}\cos(ns) ds = 0 \tag{A.2}$$

THIS PAGE INTENTIONALLY LEFT BLANK

# APPENDIX B. CURRENT IMAGING METHODS (ANL)

At Argonne National Laboratory, A receiver and transmitter via waveguides are used for imaging. The wave guides are shown in the following diagram. The configuration is set to send electromagnetic waves from 10 Ghz to 200 Ghz, but it also has the ability to go to higher frequencies if necessary. Both the transmitter and receiver are of the same type and design, and they are adjacent to each other while in radar mode (i.e. data received from scattered fields). In the radar mode, both the transmitter and receiver are moved simultaneously in space in sequence.

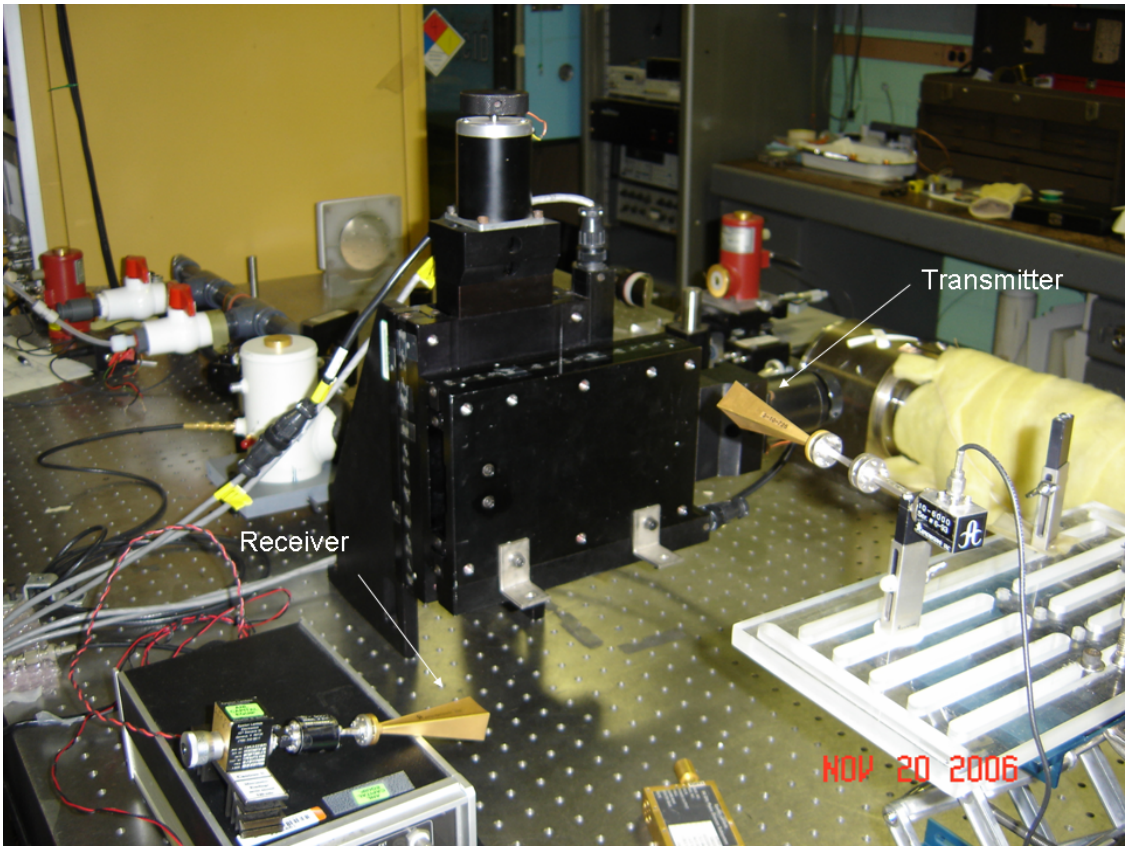


Figure 27. Waveguide for transmitter. Separate waveguide for receiver not presented

THIS PAGE INTENTIONALLY LEFT BLANK

# APPENDIX C. SINGULAR VALUE DECOMPOSITION

Let $\boldsymbol{A}$ be a linear operator that maps $\boldsymbol{X} \rightarrow \boldsymbol{Y}$, and to be more specific, let us say that $\boldsymbol{X} \subseteq \mathbb{R}^n$ and $\boldsymbol{Y} \subseteq \mathbb{R}^m$. So that $\boldsymbol{A}$ will have dimension $m \times n$. In this section we will discuss $\boldsymbol{A}^{\mathrm{T}}\boldsymbol{A}$ $(n \times n)$ and $\boldsymbol{A}\boldsymbol{A}^{\mathrm{T}}$ $(m \times m)$.

The eigen equation for $\boldsymbol{A}^{\mathrm{T}}\boldsymbol{A}$ is

$$\boldsymbol{A}^{\mathrm{T}}\boldsymbol{A}\boldsymbol{x}_i = \lambda_i \boldsymbol{x}_i \tag{C.1}$$

where $\lambda_i$ is the eigenvalue corresponding to the vector $\boldsymbol{x}_i$. Because $\boldsymbol{A}^{\mathrm{T}}\boldsymbol{A}$ is symmetric, the eigenvectors are orthogonal [Ref. 29]. Similarly, the eigen equation for $\boldsymbol{A}\boldsymbol{A}^{\mathrm{T}}$ is

$$\boldsymbol{A}\boldsymbol{A}^{\mathrm{T}}\boldsymbol{y}_j = \psi_j \boldsymbol{y}_j \tag{C.2}$$

where $\psi_j$ is the eigenvalue corresponding to $\boldsymbol{y}_j$. $\boldsymbol{A}\boldsymbol{A}^{\mathrm{T}}$ is also a symmetric matrix and therefore the eigenvectors $\boldsymbol{y}_i$are orthogonal.

Consider the eigenvector $\boldsymbol{x}_i$ of $\boldsymbol{A}^{\mathrm{T}}\boldsymbol{A}$, with nonzero eigenvalue $\lambda_i$. Then $\boldsymbol{A}\boldsymbol{x}_i \neq 0$ because $\boldsymbol{A}\boldsymbol{x}_i$ is an eigenvector of $\boldsymbol{A}\boldsymbol{A}^{\mathrm{T}}$:

$$(\boldsymbol{A}\boldsymbol{A}^{\mathrm{T}})\boldsymbol{A}\boldsymbol{x}_i = \boldsymbol{A}(\boldsymbol{A}^{\mathrm{T}}\boldsymbol{A})\boldsymbol{x}_i = \lambda_i(\boldsymbol{A}\boldsymbol{x}_i) \tag{C.3}$$

The same is true for an eigenvector $\boldsymbol{y}$ of $\boldsymbol{A}\boldsymbol{A}^{\mathrm{T}}$ with nonzero eigenvalue since $\boldsymbol{A}^{\mathrm{T}}\boldsymbol{y}$ is an eigenvector of $\boldsymbol{A}^{\mathrm{T}}\boldsymbol{A}$.

It follows that the non-zero eigenvalues of $\boldsymbol{A}^{\mathrm{T}}\boldsymbol{A}$ must also be eigenvalues of

$\boldsymbol{A}\boldsymbol{A}^{\mathrm{T}}$ and vice versa. If the rank of $\boldsymbol{A}^{\mathrm{T}}\boldsymbol{A}$ is $r$, then this means that

$$\begin{aligned}
\lambda_1 &= \psi_1 \\
\lambda_2 &= \psi_2 \\
&\vdots \\
\lambda_r &= \psi_r \\
\lambda_{r+1} = 0 \quad & \psi_{r+1} = 0 \\
\vdots \quad & \vdots \\
\lambda_n = 0 \quad & \psi_m = 0
\end{aligned}$$

Therefore

$$\boldsymbol{x} = \boldsymbol{A}^{\mathrm{T}}\boldsymbol{y} \qquad \boldsymbol{y} = \boldsymbol{A}\boldsymbol{x} \tag{C.4}$$

And normalizing the eigenvectors, we arrive to the following conclusion:

$$\boldsymbol{x} = \frac{\boldsymbol{A}^{\mathrm{T}}\boldsymbol{y}}{||\boldsymbol{A}^{\mathrm{T}}\boldsymbol{y}||} \quad \boldsymbol{y} = \frac{\boldsymbol{A}\boldsymbol{x}}{||\boldsymbol{A}\boldsymbol{x}||} \tag{C.5}$$

The singular values $\sigma_k$ of $\boldsymbol{A}$ are defined by

$$||\boldsymbol{A}\boldsymbol{x}_k|| = ||\boldsymbol{A}^{\mathrm{T}}\boldsymbol{y}_k|| = \sigma_k = \sqrt{\lambda_k} = \sqrt{\psi_k} \tag{C.6}$$

Then equation C.5 becomes

$$\boldsymbol{A}^{\mathrm{T}}\boldsymbol{y}_k = \sigma_k\boldsymbol{x}_k \quad \boldsymbol{A}\boldsymbol{x}_k = \sigma_k\boldsymbol{y}_k \tag{C.7}$$

Since the eigenvalues of $\lambda_k = 0$ and $\psi_k = 0$ for $k > r$, this means that

$$\boldsymbol{A}\boldsymbol{x}_k = 0 \quad \text{for } k = r+1, \ldots n$$

$$\boldsymbol{A}^{\mathrm{T}}\boldsymbol{y}_k = 0 \quad \text{for } k = r+1, \ldots m$$

If we take $\boldsymbol{A}\boldsymbol{x}_k = \sigma_k\boldsymbol{y}_k$, and multiply equation C.7 by $\boldsymbol{x}^{\mathrm{T}}$ on both sides, and use equation C.8, we see that

$$\boldsymbol{A} = \sum_{i=1}^{r} \sigma_i \boldsymbol{y}_i \boldsymbol{x}_i^{\mathrm{T}} \tag{C.8}$$

and similarly,

$$\boldsymbol{A}^{\mathrm{T}} = \sum_{i=1}^{r} \sigma_i \boldsymbol{x}_i \boldsymbol{y}_i^{\mathrm{T}} \tag{C.9}$$

The orthonormal vectors $\boldsymbol{x}$ are called right singluar vectors and $\boldsymbol{y}$ are called left singular vector. In matrix form, we can write equation C.8 as

$$\boldsymbol{A} = \begin{bmatrix} \vdots & \vdots & \vdots \\ \boldsymbol{y}_1 & \boldsymbol{y}_2 & \dots \\ \vdots & \vdots & \vdots \end{bmatrix} \begin{bmatrix} \sigma_1 & 0 & 0 \\ 0 & \sigma_2 & 0 \\ 0 & 0 & \ddots \end{bmatrix} \begin{bmatrix} \dots & \boldsymbol{x}_1 & \dots \\ \dots & \boldsymbol{x}_2 & \dots \\ \vdots & \vdots & \vdots \end{bmatrix} \tag{C.10}$$

or

$$\boldsymbol{A} = \boldsymbol{Y}\boldsymbol{S}\boldsymbol{X}^{\mathrm{T}} \tag{C.11}$$

where $\boldsymbol{S}$ is a diagonal matrix of the singular values, and $\boldsymbol{Y}$ and $\boldsymbol{X}$ are composed of the eigenvectors corresponding to those singular values.

The inverse is easily calculated by the following:

$$\boldsymbol{A}^{-1} = (\boldsymbol{Y}\boldsymbol{S}\boldsymbol{X}^{\mathrm{T}})^{-1}$$

Since $\boldsymbol{X}^{\mathrm{T}}$ and $\boldsymbol{Y}$ are orthogonal matrices due to the fact that the eigenvectors are orthogonal, we see the following:

$$\boldsymbol{A}^{-1} = (\boldsymbol{X}^{\mathrm{T}})^{-1}\boldsymbol{S}^{-1}\boldsymbol{Y}^{-1}$$

$$\boldsymbol{A}^{-1} = \boldsymbol{X}\boldsymbol{S}^{-1}\boldsymbol{Y}^{\mathrm{T}} \tag{C.12}$$

Combined with the Least Square Method, this result can be used to get us a solution to the system of equation. As you can see the inverse mapping provides us with $\frac{1}{\sigma}$ for its diagonal matrix, and this becomes a problem as the singular values get smaller and smaller. Since the non-zero eigenvalues of a Hilbert Space operator are isolated and form a sequence that converges to 0 [Ref. 28], the norm of inverse mapping $\boldsymbol{A}^{-1}$ whose singular values of $\frac{1}{\sigma}$, will increase indefinitely. Therefore, regularization methods need to be introduced to cure this effect.

THIS PAGE INTENTIONALLY LEFT BLANK

# APPENDIX D. MATLAB CODE FOR SCATTERING POINTS

```
clear;

%Parameters
nu=500e9;                          % Frequency of the wave propagation.
lambda=3.0e8/nu;                   % In terms of wave length.
%k=2*pi/lambda;                     % Magnitude of the propagation vector.
k=3000;
n=2.4;                             % Material index of refraction.
L=0.5;                             % Thickness of the wall.
z=2;                    % Measurement plane at z= constant.  Adjust accordingly.
                        % depending on position of the receiver.
A=1;                    % Amplitude of the incident plane wave.
signal=0;
noise=0;

% Defining Coordinate Systems in the spatial frequency domain.
ii=20;      % spatial frequencies for meshgrid input.
fb=ii;      % frequency band.
%fn=fb;
fn=2*fb;    % Nyquist rate.
j=1/fn;     % Separation must be at least this distance to prevent aliasing.
[fx,fy]=meshgrid(-ii:j:ii,-ii:j:ii);  % Creating coordinate system.


% Defining the Green's function.
x0=0;y0=0;z0=-3;                % Set this position accordingly to the problem.

sN=sqrt(k^2-(2*pi*fx).^2-(2*pi*fy).^2);      % Look in chapter 3 for reference.
sNm=sqrt((n*k)^2-(2*pi*fx).^2-(2*pi*fy).^2); % Look in chapter 3 for reference.
num=4*sN.*sNm*exp(-i*sN*L);                     % Numerator of the equation.

% Denominator of the equation.
den=(sNm+sN).^2.*exp(-i*sNm*L)-(sNm-sN).^2.*exp(i*sNm*L);
X0=(exp(-i*2*pi*fx*x0).*exp(-i*2*pi*fy*y0).*exp(-i*sN*z0).*exp(i*sN*z))./(2*sN);


G=(num./den).*X0; % Transmission Green's function.
```

```
%%%%%%%%%%%%%%%%%%%% Synthetic Data Generation %%%%%%%%%%%%%%%%%%%%%%%%%

% transmittance for a plane wave through a given media
t=4*n*exp(-i*k*L)./((n+1)^2*exp(-i*n*k*L)-(n-1)^2*exp(i*n*k*L));

% Scattering Points in the spatial frequency domain.
x1=-1;y1=-1;z1=-1;
x2=-1;y2=1;z2=-3;
x3=0;y3=0;z3=-5;
x4=1; y4=1;z4=-1.3;
x5=1; y5=-1;z5=-2.2;

% Incident field after the penetration of the media
E1=t*A*exp(i*k*z1);
E2=t*A*exp(i*k*z2);
E3=t*A*exp(i*k*z3);
E4=t*A*exp(i*k*z4);
E5=t*A*exp(i*k*z5);

% Positions of the scatter points in frequency domain for the given
% measurement plane at z=constant
% Since the scatter points are in terms of dirac delta functions,
% the field measurement would become the summation of the Green's function
% and the incident wave after performing the Born Approximation

X1=(exp(-i*2*pi*fy*x1).*exp(-i*2*pi*fx*y1).*exp(-i*sN*z1).*exp(i*sN*z))./(2*sN);
X2=(exp(-i*2*pi*fy*x2).*exp(-i*2*pi*fx*y2).*exp(-i*sN*z2).*exp(i*sN*z))./(2*sN);
X3=(exp(-i*2*pi*fy*x3).*exp(-i*2*pi*fx*y3).*exp(-i*sN*z3).*exp(i*sN*z))./(2*sN);
X4=(exp(-i*2*pi*fy*x4).*exp(-i*2*pi*fx*y4).*exp(-i*sN*z4).*exp(i*sN*z))./(2*sN);
X5=(exp(-i*2*pi*fy*x5).*exp(-i*2*pi*fx*y5).*exp(-i*sN*z5).*exp(i*sN*z))./(2*sN);

% Generating Data
h=(num./den).*(E1*X1+E2*X2+E3*X3+E4*X4+E5*X5);

%Setting matrix dimension
[M,N]=size(h);
h=h(1:M,1:N);         %Change matrix dimension if warranted.

%Converting bin numbers to real axis numbers in spatial domain (meters).
%Range has to be up to Nyquist frequency.
ax=linspace(-fn/2,fn/2,length(h));
```

```
n=(randn(M,N)+i*randn(M,N));  %noise in the frequency domain.

% Set the signal-to-noise (in dB)
snr=-35;

%Signal to Noise ratio

SIG=abs(h.*conj(h));
NOI=abs(n.*conj(n));
signal=sum(sum(SIG));
noise=sum(sum(NOI));
factor=sqrt((signal/noise)*10^(-snr/10));
n=n*factor;

d=h+n;                          %data in the frequency domain.



%%%%%%%%%%%%%%%%%%%%%% End of (noisy) Data Generation%%%%%%%%%%%%%%%%%%


figure(1)                       % data corrupted with noise in spatial domain.
d1=ifft2(d);                    % data in the spatial domain.
d1=ifftshift(d1);
imagesc(ax,ax,abs(d1));
colormap (1-gray);
axis([-2 2 -2 2])
title(sprintf('Noisy Data with SNR of %2.2f',snr))

% Tikhonov Regularization
alpha=3;            % Regularization parameter for Tikhonov.

R=inv(alpha*eye(size(G'*G))+G'*G)*G';

figure(2)

p=R.*d;
p=ifft2(p);           % data in the spatial domain.
p=ifftshift(p);
imagesc(ax,ax,abs(p));
axis([-2 2 -2 2])
colormap (1-gray);
```

```
title(sprintf('Tikhonov Regularization alpha=%2.3f and SNR=%2.2f',alpha,snr))



% SVD Truncation Method

alpha=.1;          % Parameter for Truncation of singular values.
[u,s,v]=svd(G);

% inverse of the singluar value matrix.
sinv=zeros(N,M);
for l=1:rank(s)
    if 1/s(l,l)<alpha
        sinv(l,l)=1/s(l,l);
    else
        sinv(l,l)=0;
    end
end


e=(v*sinv*u').*d;

e=ifft2(e);         % data in the spatial domain.
e=ifftshift(e);


figure(3)
imagesc(ax,ax,abs(e));
colormap (1-gray);
axis([-2 2 -2 2])
title(sprintf('TSVD w/ singular values cutoff at %3.2f \n SNR=%2.2f',alpha,snr))
```

# APPENDIX E. MATLAB CODE FOR MATERIAL REFLECTION

```
clear;
%Calculating the Reflection for plane waves in various surface
%Equations used from Chapter 3
%Creating various index of refraction for different materials
%Cloth, Balsa Wood, Wooden Door, Plexiglas, Paper, Dry Concrete, Diamond,
%Muscle, Blood
nm=[1.09 1.14 1.41 1.51 1.73 2.12 2.41 7.00 7.62];

%Thickness of the material
L=0.5;
c=3.0e8;   %speed of light


%Cloth, Balsa Wood, Wooden Door
figure(1)
for j=1:3
    nu=linspace(20e9,1e12,200);
    k=2*pi*nu./c;
    num=((1+nm(j))*(1-nm(j))+(nm(j)+1)*(nm(j)-1)*exp(i*2*k*nm(j)*L));
    den=((nm(j)+1)*(nm(j)+1)+(nm(j)-1)*(1-nm(j))*exp(i*2*k*nm(j)*L));
    r=num./den;
    R=r.*conj(r);
    plot(nu,R);
    text(nu(30*(j-1)+8),R(30*(j-1)+8),sprintf('n= %2.2f',nm(j)));
    hold on

end
hold off
xlabel('frequency (\nu) Hz');
ylabel('Reflection');
title('Frequency vs Reflection from the dielectric')
text(1e11,.115,sprintf('L = %1.2f m',L));
%axis([0.1e11 10e11 0 1]);
clear figure



%Plexiglass,Paper, Dry Concrete
```

```
figure(2)
for j=1:3
    nu=linspace(20e9,1e12,100);
    k=2*pi*nu./c;
    num=((1+nm(j+3))*(1-nm(j+3))+(nm(j+3)+1)*(nm(j+3)-1)*exp(i*2*k*nm(j+3)*L));
    den=((nm(j+3)+1)*(nm(j+3)+1)+(nm(j+3)-1)*(1-nm(j+3))*exp(i*2*k*nm(j+3)*L));
    r=num./den;
    R=r.*conj(r);
    plot(nu,R);
    text(nu(30*(j-1)+10),R(30*(j-1)+10),sprintf('n= %2.2f',nm(j+3)));
    hold on

end
hold off
xlabel('frequency (\nu) Hz');
ylabel('Reflection');
text(1e11,.4,sprintf('L = %1.2f m',L));
%axis([0.1e11 10e11 0 1]);

title('Frequency vs Reflection from the dielectric')



%Thickness of the material
L=0.01


%Diamond, Muscle, Blood
figure(3)
for j=1:3
    nu=linspace(20e9,1e12,100);
    k=2*pi*nu./c;
    num=((1+nm(j+6))*(1-nm(j+6))+(nm(j+6)+1)*(nm(j+6)-1)*exp(i*2*k*nm(j+6)*L));
    den=((nm(j+6)+1)*(nm(j+6)+1)+(nm(j+6)-1)*(1-nm(j+6))*exp(i*2*k*nm(j+6)*L));
    r=num./den;
    R=r.*conj(r);
    plot(nu,R);
    text(nu(30*(j-1)+10),R(30*(j-1)+10),sprintf('n= %2.2f',nm(j+6)));
    %text(nu(6*(j+2)),R((j+5)),sprintf('n= %1.2f',nm(j+6)));
    hold on

end
```

```
hold off
xlabel('frequency (\nu) Hz');
ylabel('Reflection');
title('Frequency vs Reflection from the dielectric')
text(1e11,.95,sprintf('L = %1.2f m',L));
axis([0.1e11 10e11 0 1]);
```

THIS PAGE INTENTIONALLY LEFT BLANK

# APPENDIX F. MATLAB CODE FOR TRANSMITTED WAVE FRONT

```
clear;
%This code graphs the transmission of the waves
%Observation of the fields at (0,0,3)
%Parameters
nu=500e9;                       % Frequency of the wave propagation.
lambda=3.0e8/nu;                % In terms of wave length.
k=2*pi/lambda;                  % Magnitude of the propagation vector.
%k=3000;
n=2.4;                          % Material index of refraction.
L=0.5;                          % Thickness of the wall.
z=3;                  % Measurement plane at z= constant.  Adjust accordingly.
                      % depending on position of the receiver.
signal=0;
noise=0;

% Defining Coordinate Systems in the spatial frequency domain.
ii=1000;      % spatial frequencies for meshgrid input.
j=.89;
%j=1/fn;     % Separation must be at least this distance to prevent aliasing.
[fx,fy]=meshgrid(-ii:j:ii,-ii:j:ii);  % Creating coordinate system.
[x,y]=meshgrid(-ii:j:ii,-ii:j:ii);

% Defining the Green's function.
x0=0;y0=0;z0=-3;                % Set this position accordingly to the problem.

sN=sqrt(k^2-(2*pi*fx).^2-(2*pi*fy).^2);      % Look in chapter 3 for reference.
sNm=sqrt((n*k)^2-(2*pi*fx).^2-(2*pi*fy).^2); % Look in chapter 3 for reference.
num=4*sN.*sNm*exp(-i*sN*L);                     % Numerator of the equation.

% Denominator of the equation.
den=(sNm+sN).^2.*exp(-i*sNm*L)-(sNm-sN).^2.*exp(i*sNm*L);
X0=(exp(-i*2*pi*fx*x0).*exp(-i*2*pi*fy*y0).*exp(-i*sN*z0).*exp(i*sN*z))./(2*sN);


G=(num./den).*X0; % Transmission Green's function.

figure(1)
imagesc(abs(G))
```

```
colormap(1-gray)
title(' Transmission \nu=500GHz, Observation point at z=3')
```

# APPENDIX G. GREEN'S FUNCTION POLAR COORDINATE TRANSFORMATION

If we make the following coordinate transformation:

$$f_x^2 + f_y^2 = \rho^2$$

$$f_x = \rho\cos\phi \quad f_y = \rho\sin\phi$$

$$x^2 + y^2 = r^2$$

$$x = r\cos\theta \quad y = r\sin\theta$$

Then the reflection Green's function of the Equation IV.47 can be written as

$$G(r,\theta,z,\boldsymbol{r}_0) = 2\pi\int_0^\infty \rho \mathrm{d}\rho \frac{\mathrm{J_0(2\pi\rho r)}}{2} \times \frac{\mathrm{k^2(n^2-1)(e^{i2L\sqrt{n^2k^2-4\pi^2\rho^2}}-1)e^{-i(z-z_0)\sqrt{k^2-4\pi^2\rho^2}}}}{\sqrt{\mathrm{k^-4\pi^2\rho^2}}}$$
$$\times \frac{1}{(\sqrt{n^2k^2-4\pi\rho^2}+\sqrt{k^2-4\pi^2\rho^2})^2 - (\sqrt{n^2k^2-4\pi^2\rho^2}-\sqrt{k^2-4\pi^2\rho^2})^2 e^{i2L\sqrt{n^2k^2-4\pi^2\rho^2}}}$$

Let

$$u \equiv \frac{2\pi\rho}{nk} \quad \rho = \frac{nku}{2\pi} \quad \mathrm{d}\rho = \frac{\mathrm{nkdu}}{2\pi}$$

$$G = \pi\left(\frac{nk}{2\pi}\right)^2 k^2(n^2-1)\int_0^\infty \frac{u\mathrm{du}\mathrm{J_0(nkru)}\left(\mathrm{e^{i2nkL\sqrt{1-u^2}}}-1\right)\mathrm{e^{-i(z-z_0)k\sqrt{1-n^2u^2}}}}{k\sqrt{1-n^2u^2}}$$
$$\times \frac{1}{k^2(n\sqrt{1-u^2}+\sqrt{1-n^2u^2})^2 - k^2(n\sqrt{1-u^2}-\sqrt{1-n^2u^2})^2 e^{i2Lnk\sqrt{1-u^2}}}$$

$$G = \frac{kn^2(n^2-1)}{4\pi}\int_0^\infty \frac{u\mathrm{du}\mathrm{J_0(nkru)}\left(\mathrm{e^{i2nkL\sqrt{1-u^2}}}-1\right)\mathrm{e^{-i(z-z_0)k\sqrt{1-n^2u^2}}}}{\sqrt{1-n^2u^2}}$$
$$\times \frac{1}{(n\sqrt{1-u^2}+\sqrt{1-n^2u^2})^2 - (n\sqrt{1-u^2}-\sqrt{1-n^2u^2})^2 e^{i2Lnk\sqrt{1-u^2}}}$$

let $A \equiv n\sqrt{1-u^2}$ and $B \equiv \sqrt{1-n^2u^2}$ $\Theta \equiv nkL\sqrt{1-u^2}$

Where are the zeroes of the denominator of the integrand?

where does

$$\begin{aligned}(A+B)^2 &= (A-B)^2 e^{i2\Theta} \\ A^2+B^2+2AB &= (A^2+B^2-2AB)e^{i2\Theta} \\ \frac{2AB}{A^2+B^2} &= \frac{e^{i2\Theta}-1}{e^{i2\Theta}+1} = \frac{e^{i\Theta}-e^{-i\Theta}}{e^{i\Theta}+e^{i\Theta}} \\ &= \frac{i2\sin\Theta}{2\cos\Theta} = i\tan\Theta\end{aligned}$$

Denominator vanishes when

$$\boxed{i\tan(nkL\sqrt{1-u^2}) = \tfrac{2n\sqrt{1-u^2}\sqrt{1-n^2u^2}}{n^2+1-2n^2u^2}}$$

Look at RHS Numerator is real and positive for $0 \le u \le 1/n$
it then becomes imaginary and positive for $1/n < u < 1$
it then becomes real and negative for $u > 1$
Denominator goes to zero at $u = u^* = \sqrt{\frac{n^2+1}{2n^2}}$

$$\begin{aligned}u^* < 1 \text{ for } n > 1 \\ \sqrt{\frac{n^2+1}{2n^2}} < 1 \\ \frac{n^2+1}{2n^2} < 1 \\ n^2 > 1\end{aligned}$$

Is

$$u^* > 1/n?$$

$$\frac{n^2+1}{2n} \stackrel{?}{>} \frac{1}{n^2} \rightarrow n^2+1 > 2 \rightarrow n^2 > 1$$

$$\frac{1}{n} < u^* < 1$$

So RHS, $\frac{N}{D}$

| | | |
|---|---|---|
| $0 < u < 1/n$ | $\frac{\text{real,positive}}{\text{positive}}$ | real $> 0$ |
| $1/n < u < u^*$ | $\frac{\text{imaginary,positive}}{\text{positive}}$ | imag $> 0$ |
| $u* < u < 1$ | $\frac{\text{imag,pos}}{\text{neg}}$ | imag $< 0$ |
| $u > 1$ | $\frac{\text{real,neg}}{\text{neg}}$ | real $> 0$ |

Look at the LHS $i\tan(nkL\sqrt{1-u^2})$

$$0 \le u < 1 \qquad \text{LHS imaginary, either positive or negative}$$

$$\tan(ix) = i\tanh(x)$$

$$u > 1 \qquad i \cdot i\tanh(nkL\sqrt{u^2-1}) = -\tanh(nkL\sqrt{u^2-1}) \quad \text{always negative, real}$$

The conclusion only possible to have a root for $\boxed{1/n \le u \le 1}$.
What about the end points?
Always a root at $u = 1$ $\qquad 0 = 0$
For $u = 1/n$

$$\begin{aligned} i\tan(nkL\sqrt{1-\frac{1}{n^2}}) &= i\tan(kL\sqrt{n^2-1}) \\ &= \frac{2n\sqrt{1-1/n^2}i\sqrt{n^2u^2-1}}{n^2-1} = \frac{2i\sqrt{n^2u^2-1}}{\sqrt{n^2-1}} \end{aligned}$$

as $u \to 1/n$ from above

$$\tan(kL\sqrt{n^2-1}) = 0$$

possible to have a root if $kL\sqrt{n^2-1} = m\pi$ Always a root at $u = 1$.
Root at $u = 1/n$ if $kL\sqrt{n^2-1} = m\pi$ where m is an integer.
Range of possible roots $\boxed{1/n \le u \le 1}$
How many roots are there?
The "real" equation we need to examine is

$$\tan(nkL\sqrt{1-u^2}) = \frac{2n\sqrt{1-u^2}\sqrt{n^2u^2-1}}{n^2+1-2n^2u^2}$$

To analyze this equation, lets change variables let

$$y = nkL\sqrt{1-u^2}$$

$$u^2 = 1 - \left(\frac{y}{nkL}\right)^2$$

Limits: as $u \to 1$, $y \to 0$. $u \to 1/n$, $y \to nkL\sqrt{1-\frac{1}{n^2}} = kL\sqrt{n^2-1}$
Call $\boxed{y_{\max} \equiv kL\sqrt{n^2-1}}$, $0 \le y \le y_{\max}$

$$\begin{aligned} \frac{2n\frac{y}{nkL}\sqrt{n^2(1-(\frac{y}{nkL})^2)-1}}{n^2+1-2n^2(1-(\frac{y}{nkL})^2)} &= \frac{\frac{2y}{kL}\sqrt{n^2-1-\frac{y^2}{(kL)^2}}}{-(n^2-1)+\frac{2y^2}{(kL)^2}} \\ &= \frac{2y}{(kL)^2}\frac{\sqrt{(kL)^2(n^2-1)-y^2}}{-(n^2-1)+\frac{2y^2}{(kL)^2}} \end{aligned}$$

$$\mathrm{RHS} = \frac{2\mathrm{y}\sqrt{\mathrm{y}_{\mathrm{max}}^2 - \mathrm{y}^2}}{-\mathrm{y}_{\mathrm{max}^2+2\mathrm{y}^2}}$$

Thus, we see roots of $\boxed{\tan y = \frac{2y\sqrt{y_{\mathrm{max}}^2 - y^2}}{-y_{\mathrm{max}}^2+2y^2}}$.
(Note compilation with the aid of Professor James Luscombe)

---

This transcendental equation is analogous to the same transcendental equation which solves the TE modes for the Dielectric Slabs [Ref. 32]. The intersection of the two curves between the left and right hand side of the equation are the values for which propagation in the slab is possible. The branch cuts of the integral represents the forbidden regions where propagation is not possible and where the waves begin to evanesce. Brekhovskikh and Kong work out in detail of these effects [Ref. 2] [Ref. 32]. The problem with this integral is the nature of the Bessel function. As we integrate to infinity, the Bessel function also head towards infinity, and therefore, there is no way to close the contour integral. More clever methods are required, and Brekhovskikh model provides a way to perform the contour and to implement the contour. Nevertheless, we can see that the poles are the trapped modes in the media.

# LIST OF REFERENCES


[1] George Arfken. *Mathematical Methods for Physicists*, volume Third Edition. Harcourt Brace Jovanovich, 1985.

[2] L. M Brekhovskikh. *Waves in Layered Media*. Academic Press Inc. New York, 1980.

[3] Mario Bertero and Patrizia Boccacci. *Introduction to Inverse Problems in Imaging*. Institute of Physics Publishing, 1998.

[4] Norman Bleistein. *Mathematical Methods for Wave Phenomena (Computer Science and Applied Mathematics)*. Harcourt Brace Jovanovich, 1984.

[5] Richard Haberman. *Applied Partial Differential Equation with Fourier Series and Boundary Value Problems.* Pearson Education Inc, 2004.

[6] Wolfgang K.H. Panofsky and Melba Phillips. *Classical Electrical and Magnetism*, volume Second Edition. Dover Publications Inc., 2005.

[7] Gilbert Strang. *Linear Algebra and its Applications*, volume Second Edition. Academic Press Inc, 1980.

[8] Kristin Lewotsky. *Terahertz's penetration appeal*. http://newsroom.spie.org/x2453.xml. SPIE Professional. April 2006.

[9] Moeness G. Amin, Fauzia Ahmad and Saleem A. Kassam. *Synthetic Aperture Beamformer for Imaging Through a Dielectric Wall.* IEEE TRANSACTIONS ON AEROSPACE AND ELECTRONIC SYSTEMS Vol. 41 No.1. January 2005: pp 271-283

[10] Genyuan Wang, and Moeness G. Amin, *Imaging Through Unknown Walls Using Different Standoff Distances.* IEEE TRANSACTIONS ON SIGNAL PROCESSING Vol. 54 No.10. October 2006

[11] M.S. Sherwin, C. A. Schmuttenmaer, and P.H. Bucksmaum. *Opportunities in THz Science*. Report of a DOE-NSF-NIH Workshop. Arlington, VA. February 12 14, 2004

[12] John F. Federeci, Dale Gary, Robert Barat, and David Zimdars. *THz Standoff Detection and Imaging of Explosives and Weapons*. Proc.SPIE **5781**. Vol 75. 2005

[13] H. Liu T. Yuan, J. Xu, F. Al-Douseri, Y. Hu, and X. Zhang. *Proceedings of SPIE 5070, 28 (2003).*

[14] Hans J Liebe, Donald H. Layton. *Millimeter-Wave Properties of the Atmosphere: Laboratory Studies and Propagation Modeling.* NTIA Report TR-87-224. October 1987. http://www.its.bldrdoc.gov/pub/ntia-rpt/87-224/ Chapter 3: Atmospheric Propagation Model. Jan 2007 (Last accessed).

[15] Bruce H. Wallace, *Millimeter Waves – Myths and Reality.* MMW Concepts LLC. Defense & Security Symposium. SPIE Event

[16] THZ Science and Technology Network. *History of the THZ science and technology network.* http://www.thznetwork.org/wordpress/index.php/about/history/ Aug 2006 (Last access).

[17] S. Wang, and X-C Zhang. *Pulsed terahertz tomography.* INSTITUTE OF PHYSICS PUBLISHING. J Phys. D: Appl. Phys 37. 2004: pp R1-R36

[18] N Gopalsami , A. C. Raptis, and J. Meier. *Millimeter-Wave cavity ringdown spectroscopy* REVIEW OF SCIENTIFIC INSTRUMENTS. Volume 73, No. 2. February 2002: pp 259-262.

[19] Nachappa Gopalsami, Sasan Bakhtiari, Stephen L. Dieckman, Apostolos CRaptis, and Matthew J Lepper. *Millimeter-Wave Imaging for Nondestructive Evaluation of Materials.* Materials Evaluation. March 1994: pp 412-415.

[20] N. Gopalsami, and Apostolos C Raptis. *Resonance-enhanced dielectric sensing of chemical and biological species* Unified Science & Technology for Reducing Biological Threats & Countering Terrorism. March 2003: pp 97-103

[21] N. Gopalsami, D. B. Kanareykim, V. Asanov, S. Bakhtiari, and A. C. Raptis. *Microwave Radar Detection of Gas Pipeline Leaks.* Review of Quantitative Nondestructive Evaluation. American Institute of Physics. Vol 22: pp 478-484.

[22] Y. A. Dryagin, V. V. Parshin, A. F. Krupnov, N. Gopalsami, and A.C. Raptis. *Precision Broadband Wavemeter for Millimeter and Submillimeter Range* IEEE TRANSACTIONS ON MICROWAVE THEORY AND TECHNIQUES Vol 44 No.4. September 1996: pp 1610-1613

[23] N. Gopalsami, Sasan Bakhtiari, Apostolos C Raptis, Stephen L Dieckman, and Frank C DeLucia. *Millimeter-Wave Measurements of Molecular Spectra with Application to Environmental Monitoring.* IEEE TRANSACTIONS ON INSTRUMENTATION AND MEASUREMENT. Vol 45. No. 1. February 1996: pp. 225-230.

[24] H. Weyl, *Ann. d. Physik.* **60** 1919. pg 481

[25] Born, Max and Emil Wolf. *Principles of optics*: Electromagnetic theory of propagation, interference and diffraction of light. Seventh (expanded) edition. Camberidge University Press. 1999.

[26] Tikhonov, A. N., and Arsenin. V.Y.: *Solutions of Ill-posed problems.* Winston and Sons, Washington 1977.

[27] Colton, David, Kress, Rainer. *Inverse Acoustic and Electromagnetic Scattering Theory.* Second Edition. Springer-Verlag Berlin Heidelberg 1998.

[28] Borden, Brett. *Radar Imaging of Airborne Targets: A Primer for Applied Mathematicians and Physcists* Institute of Physics Publishing Bristol and Philadelphia 1999.

[29] Leon, Steven J. *Linear Algebra with applications.* Sixth edition. Prentice-Hall Inc. 2002.

[30] Tarantola, Albert. *Inverse Problem Theory and Methods for Model Parameter Estimation.* SIAM. 2005.

[31] Image Gallery Optics http://www.phys.ufl.edu/ ãvery/course/3400/gallery/gallery_optics.html. March 2007 (Last access).

[32] Kong, J A, David H Staelin, Ann W Morgenthaler. *Electromagnetic Waves.* Prentice-Hall Inc. 1994.

[33] Sophocles J. Orfanidis. *Electromagnetic Waves and Antennas.* ECE Department Rutgers University. 94 Brett Road, Piscataway, NJ 08854-8058. orfanidi@ece.rutgers.edu. http://www.ece.rutgers.edu/õrfanidi/ewa/ (Last Accessed March 2007).

[34] Stratton, Julius A. *Electromagnetic Theory.* McGraw-Hill Book Company. New York and London 1941.

[35] Walter Fendt. *Reflection and Refraction of Waves (Explanation by Huygens' Principle)* http://www.sciencejoywagon.com/physicszone/lesson/otherpub/wfendt/huygens.htm (Last Accessed March 2007).

THIS PAGE INTENTIONALLY LEFT BLANK

# INITIAL DISTRIBUTION LIST

1. Defense Technical Information Center
   Ft. Belvoir, VA
2. Dudley Knox Library
   Naval Postgraduate School
   Monterey, CA
3. Professor Brett Borden
   Naval Postgraduate School
   Monterey, CA
4. Professor Gamani Karunasiri
   Naval Postgraduate School
   Monterey, CA
5. Professor Margaret Cheney
   Rensselaer Polytechnic Institute
   Troy, NY
6. Professor Scott Davis
   Naval Postgraduate School
   Monterey, CA
7. Professor Don Walters
   Naval Postgraduate School
   Monterey, CA
8. Professor Don Danielson
   Naval Postgraduate School
   Monterey, CA
9. Chairman, Physics Department
   Naval Postgraduate School
   Monterey, CA
10. Chairman, Mathematics Department
    Naval Postgraduate School
    Monterey, CA
11. Sami Gopalsami
    Argonne National Laboratory
    Argonne, IL
12. Professor X.C. Zhang
    Rensselaer Polytechnic Institute
    Troy, NY